MATERIAL CHARACTERIZATION OF ROLLER-COMPACTED CONCRETE PAVEMENTS

A Dissertation

by

ISSA MAHMOUD ISSA

Submitted to the Graduate and Professional School of
Texas A&M University
in partial fulfillment of the requirements for the degree of

DOCTOR OF PHILOSOPHY

Chair of Committee,	Dan G. Zollinger
Committee Members,	Robert L. Lytton
	Nasir G. Gharaibeh
	Suhasini Subba Rao
Head of Department,	Zachary Grasley

December 2021

Major Subject: Civil Engineering

ABSTRACT

Roller Compacted Concrete (RCC) pavements present an advantageous cost and construction alternative over conventional concrete pavements without sacrificing the service life and performance of the conventional concrete pavement. However, RCC pavement still faces many challenges that limit its use as a paving option due to the lack of standards to characterize the RCC mixture prior to its placement and the absence of methodologies to understand the behavior and evaluate its performance under traffic and environmental conditions. Therefore, characterizing the RCC mixture and understanding the behavior of the RCC pavement can be vital to facilitate its use in high-speed roadways.

The main objectives of this study were to characterize RCC materials in terms of moisture diffusivity and density to help future interpretation of resulting stresses as a function of the curing and climatic conditions at the time of construction; model the workability and evaluate density prior to placement; model the transport properties of RCC specimens to facilitate the evaluation of RCC durability; develop new methodologies to quickly measure density and moisture in the field as well as evaluate the short- and long- term performance of RCC pavements under traffic loading.

In this study, a new testing configuration and interpretation method was developed for the well-known Time Domain Reflectometer (TDR) as a tool to estimate the electrical properties of RCC specimens in the lab. The developed method was used i) to establish the moisture and density profile of RCC mixtures with different aggregate gradation and curing conditions in the lab and ii) to characterize the diffusivity and

permeability of RCC by suggesting a change in the rapid chloride permeability (RCPT) test procedure. This dissertation also recommends using the compactibility of RCC as a metric to evaluate the workability and compaction energy required for RCC mixtures before placement. Furthermore, a PaveScan methodology was introduced to assess the on-site density of RCC surface conditions after placement. Lastly, a framework to evaluate the short- and long-term performance of RCC pavement under environmental conditions and traffic loading was proposed.

The procedures developed in this dissertation are envisioned to impact the understanding of RCC mixture before and after placement as well as the short and long-term RCC pavement performance. Although RCC material and pavement are concerned in this dissertation, developed procedures can be used for other infrastructures and composite materials.

DEDICATION

To The God, the Most Beneficent, the Most Merciful

ACKNOWLEDGEMENTS

I would like to express my sincere gratitude to my committee chair, Dr. Dan G. Zollinger, for his consistent encouragement, patience, and limitless support. His outstanding scholarly inputs helped me throughout the research journey and writing of this dissertation. I could not imagine having such impactful research outcomes without his advisory and mentorship.

My appreciation also goes to Dr. Robert L. Lytton, Dr. Nasir G. Gharaibeh, and Dr. Suhasini Subba Rao for serving as my committee members. I would like to thank Dr. Lytton for all his scholarly inputs in the graduate-level courses and research. I admire his scientific impact and willingness to share his research knowledge. Thanks much, Dr. Gharaibeh, for supporting my admission application to the Civil Engineering Department. Dr. Rao, I really thank you for your openness to participate in my committee despite your commitments. I acknowledge the support I received from the RCC Pavement Council through three years of Fellowships. I hope this research provides a significant advancement in the RCC pavement field. I also appreciate the fund from the Texas Department of Transportation and Oklahoma Department of Transportation

My sincere thanks go to all of my colleagues at the civil engineering department, especially Ibrahim Onifade, for his scholarly support, as well as David Dillon and Thomas Cunningham, for their prominent support during the lab work. Thanks to Rick

Canatella and Tony Barbosa from the Texas A&M Transportation Institute for their valuable help in the laboratory.

Last but not least, I would like to thank my parents, Mahmoud Issa and Jamelah Issa, for their support and patience. I am thankful and grateful to my lovely wife, Rawan Hasan. This journey would not be possible without her encouragement, support and patience. My daughter Sabeen Issa and my son Adam Issa, I am lucky to have you on this journey. Many thanks to my friends Haitham Shtieh and Faisal Al Dhalmawi for their consistent support.

CONTRIBUTORS AND FUNDING SOURCES

Contributors

This work was supervised by a dissertation committee consisting of Professor Dan G. Zollinger (advisor) and Professor(s) Robert L. Lytton, Nasir G. Gharaibeh, and Suhasini Subba Rao of the Department of Statistics.

All work conducted for the dissertation was completed by the student independently.

Funding Sources

Graduate study was supported by a fellowship from The RCC Pavement Council. Its contents are solely the responsibility of the authors and do not necessarily represent the official views of the RCC Pavement Council.

NOMENCLATURE

RCC	Roller Compacted Concrete
GPR	Ground Penetrating Radar
ACI	American Concrete Institute
TDR	Time Domain Reflectometry
RCPT	Rapid Chloride Permeability Test
ASTM	American Society for Testing Materials
ESAL	Equivalent Single Axle Load
TxDOT	Texas Department of Transportation
AASHTO	American Association of State Highway and Transportation Officials
LL	Specified Lower Limit Aggregate Gradation
UL	Specified Upper Limit Aggregate Gradation
USB	Universal Serial Bus
TL	Transmission Line
SID	System Identification Method
Θ	Volumetric content
ε	Relative Dielectric
α	Degree of Hydration
γ	Unit weight
ρ	Density

TABLE OF CONTENTS

Page

ABSTRACT i

DEDICATION iii

ACKNOWLEDGEMENTS iv

CONTRIBUTORS AND FUNDING SOURCES vi

NOMENCLATURE vii

TABLE OF CONTENTS viii

LIST OF FIGURES xii

LIST OF TABLES xv

1. INTRODUCTION 1

1.1. Research Objectives and Methodology 1
1.2. The History of Using RCC in Pavements 4
1.3. Dissertation Significance and Impact 6
1.4. Dissertation Organization 7
1.5. References 11

2. A LABORATORY APPROACH TO DETERMINE RCC MIXTURE ELECTRICAL CHARACTERISTICS USING A NEW TDR INTERPRETATION METHOD 12

2.1. Introduction 12
2.2. Background and Literature Review 13
2.3. Test Program 17
2.3.1. Instrumentation 17
2.3.2. Mix Design 20
2.3.3. Specimen Preparation and Test Setup 22
2.3.4. Dielectric Measurements 23
2.4. Research Methodology and Results 25
2.4.1. Transmission Line Equation 25
2.4.2. Fitting TDR Traces 29

2.4.3. Effect of Reflectivity 34
2.4.4. Electrical properties of RCC 34
2.5. Conclusions 38
2.6. References 41

3. ESTABLISH MOISTURE AND DENSITY PROFILES IN RCC SPECIMENS AT EARLY AGE USING TDR MEASUREMENTS 44

3.1. Introduction 44
3.2. Experimental Program 45
3.2.1. Materials and Specimen Preparation 46
3.3. Research Approach 50
3.3.1. Composite Dielectric Constant 51
3.3.2. Solid, Water and Air of RCC Mixes 52
3.3.3. Calibrating Water and Air Content 54
3.3.4. Finding RCC material density 57
3.4. Results and Discussion 57
3.5. Conclusions 64
3.6. References 67

4. MODELLING COMPACTIBILITY OF RCC SPECIMENS USING THE ASPHALT GYRATORY COMPACTOR 69

4.1. Introduction 69
4.2. Background and Literature Review 70
4.3. Research Approach 71
4.4. Experimental Program 72
4.4.1. Instrumentation 73
4.4.2. Mix Design 74
4.5. Model Compactibility of RCC Specimens 77
4.6. Results and Discussion 83
4.6.1. SGC Data Interpretation 83
4.6.2. Computation of Energy Applied by the SGC 86
4.6.3. Assessment of density and energy of thicker RCC specimens 91
4.7. Conclusions 95
4.8. References 97
Issa IM, Zollinger DG. Modelling compactibility of RCC specimens using the asphalt gyratory compactor. Construction and Building Materials. 2021 Dec 6;310:125271 97

5. CHARACTERIZATION OF TRANSPORT PROPERTIES IN ROLLER COMPACTED CONCRETE BY INCORPORATING RCPT AND TDR 100

5.1. Introduction 100
5.2. Research Significance 102

5.3. Research Approach 103
5.3.1. Fitting TDR traces 104
5.3.2. Composite Dielectric Solution 105
5.4. Experimental program 109
5.4.1. Mix design 109
5.4.2. Specimen preparation and test setup 112
5.5. Results and Discussion 114
5.5.1. Diffusion of NaCl solution 115
5.5.2. The permeability coefficient of the RCC mix 117
5.5.3. Charge Passed vs. Volumetric Content of Solution 121
5.6. Conclusions 122
5.7. References 123

6. USING PAVESCAN GPR DATA TO ASSESS FRESH AND HARDENED AIRFIELD CONCRETE PAVEMENTS 126

6.1. Introduction 126
6.2. Research Approach 127
6.2.1. Fresh Concrete Surface Solution 128
6.2.2. Dry Concrete Surface Solution 130
6.3. Results and Discussion 132
6.3.1. Fresh Concrete Surface- Dielectric Solution 132
6.3.2. Dry Concrete Surface-Dielectric Solution 135
6.4. Conclusions 140
6.5. References 142

7. A FRAMEWORK TO EVALUATE SHORT- AND LONG-TERM PERFORMANCE OF RCC PAVEMENTS UNDER TRAFFIC LOADS 145

7.1. Introduction 145
7.2. Research Approach 147
7.3. Traffic Model 150
7.4. Neural Network for Stress Calculations 154
7.5. Tensile Strength of RCC Specimens 157
7.5.1. Material and specimen preparation 158
7.5.2. Specimen's testing 159
7.6. Case study 162
7.6.1. Effect of pavement thickness and aggregate gradation 166
7.6.2. Effect of Compaction level 168
7.6.3. Effect of environmental stresses 170
7.6.4. The combined effect of compaction level and residual stress 173
7.7. Conclusions 176
7.8. References 177

8. CONCLUSIONS AND FUTURE RESEARCH 180

8.1. Overview 180
8.2. Conclusions 182
8.3. Future Research 186
8.4. References 187

LIST OF FIGURES

Page

Figure 1.1 Research methodology illustration 4

Figure 2.1 Typical TDR traces and different methods to estimate t1 (Adapted from Baker and Allmaras 1990) 16

Figure 2.2 Typical TDR 200 schematic for voltage trace measurement- the schematic is not to scale (Reprinted from Issa et al. 2021). 19

Figure 2.3 Upper limit and lower limit aggregate gradation specification of RCC (Reprinted from Issa et al. 2021). 21

Figure 2.4 The proposed test setup (Reprinted from Issa et al. 2021). 23

Figure 2.5 Electromagnetic wave voltage in a lossless medium (Reprinted from Issa et al. 2021). 27

Figure 2.6 Voltage vs. Time measurements at 1.5 inches from surface for different aggregate gradation and curing (Reprinted from Issa et al. 2021). 32

Figure 2.7 Voltage vs. Time measurements and fitting of lower limit aggregate gradation specimens at 38.1 mm from the exposed surface - Specimen 1 (Reprinted from Issa et al. 2021). 33

Figure 2.8 Dielectric constant of specimens with a lower limit and upper limit aggregate gradation (Reprinted from Issa et al. 2021). 37

Figure 2.9 Material conductivity of specimens with a lower limit and upper limit aggregate gradation (Reprinted from Issa et al. 2021). 38

Figure 3.1 Specimen Preparation 49

Figure 3.2 Total water content with time 59

Figure 3.3 Profile of the degree of hydration with time 60

Figure 3.4 Profiles of free water and calibrated air content with time 63

Figure 3.5 Profiles of wet unit weight with time 64

Figure 4.1 Upper and lower limit of aggregate gradation specification of RCC (Reprinted from Issa and Zollinger 2021). 76

Figure 4.2 Model Free Body Diagram (Reprinted from Issa and Zollinger 2021). 80

Figure 4.3 SGC data and density calculation with height change (Reprinted from Issa and Zollinger 2021). 86

Figure 4.4 Displacement equation fitting of the SGC data (Reprinted from Issa and Zollinger 2021). 87

Figure 4.5 Compaction energy with time representation (Reprinted from Issa and Zollinger 2021). 89

Figure 4.6 Compaction energy with thickness comparison (Reprinted from Issa and Zollinger 2021). 94

Figure 5.1 Difference in dielectric vs. Solution volumetric content 109

Figure 5.2 Upper and lower limit of aggregate gradation specification of RCC 111

Figure 5.3 Test setup 114

Figure 5.4 Volumetric content of NaCl solution with time for LL and UL aggregate gradation 115

Figure 5.5 Diffusion coefficient with time for LL and UL aggregate gradation 117

Figure 5.6 Velocity vs. Time relationship for control LL and UL aggregate gradation samples 120

Figure 5.7 Permeability coefficient for LL and UL aggregate gradation.....121

Figure 5.8 Volumetric content of NaCL solution vs. charge passed relationship for LL and UL aggregate gradation- Control Specimens.....121

Figure 6.1 Measured GPR dielectric and related characteristics in the wet concrete surface.....134

Figure 6.2 Measured GPR dielectric and related characteristics- dry concrete surface.137

Figure 6.3 Water volumetrics in the dry concrete surface 140

Figure 7.1 Traffic distribution model (Reprinted from Issa and Zollinger 2021).....151

Figure 7.2 ISLAB 2000- pavement structure cross-section 155

Figure 7.3 Typical ISLAB 2000 stress outputs.....157

Figure 7.4 Splitting tensile strength test setup 160

Figure 7.5 Splitting tensile strength of LL and UL aggregate gradation RCC specimens. 161

Figure 7.6 Pavement cross-section and general inputs 163

Figure 7.7 Defaulted traffic distribution 164

Figure 7.8 ESALs calculations at critical stress locations- upper limit aggregate gradation mix 165

Figure 7.9 Long term damage calculations for pavements with UL and LL aggregate gradation, 5-inch thickness, 100% compaction level, and zero built-in curling stress 166

Figure 7.10 Short- and long-term damage calculations for LL and UL aggregate gradation, 100% compaction level, and zero built-in curling stress 168

Figure 7.11 Damage associated with the level of compaction at an early age- LL RCC pavement 170

LIST OF TABLES

Page

Table 2.1 RCC mix design (Reprinted from Issa et al. 2021) 21

Table 2.2 Test matrix (Reprinted from Issa et al. 2021) 24

Table 2.3 Electrical properties of RCC specimens from fitting V vs. T traces- LL gradation (Reprinted from Issa et al. 2021). 35

Table 3.1 Specified LL and UL limit and developed blends 47

Table 3.2 RCC mix design 48

Table 3.3 Test matrix 50

Table 4.1 RCC mix design (Reprinted from Issa and Zollinger 2021). 76

Table 4.2 Displacement Equation-Fitting coefficients and R-squared (Reprinted from Issa and Zollinger 2021). 87

Table 4.3 Studied thicknesses and associated mass (Reprinted from Issa and Zollinger 2021). 92

Table 5.1 Concrete permeability classification of ASTM C1202 101

Table 5.2 RCC mix design 111

Table 5.3 Linear fitting parameters for charge passed vs. volumetric content of solution relationship 122

Table 7.1 Number and (%AT_k) of Different Axles per Truck. 154

Table 7.2 PCC slab and CTB materials properties 155

Table 7.3 Traffic Equivalency Factors (Adapted from Issa and Zollinger 2021) 157

Table 7.4 Model fitting coefficients for splitting tensile strength calculations 162

Table 7.5 Damages associated with different residual tensile stresses 173

Table 7.6 Damage Calculations considering mechanical properties, environmental and traffic stresses- LL aggregate gradation 175

Table 7.7 Damage Calculations considering mechanical properties, environmental and traffic stresses- UL aggregate gradation 176

1. INTRODUCTION

Roller Compacted Concrete (RCC) pavements present a sustainable alternative for asphalt and conventional concrete pavements. However, RCC pavements are prone to issues related to workability, density, and built-in set because of the absence of standards that adequately characterize the mixture consistency before placement operations take place. Issues such as built-in set, in-place density, joint stiffness, and the potential for pavement blow-up can limit the applicability of RCC pavements in a high-speed roadway. Multiple factors affect RCC durability either directly and/or indirectly. The major factors are inherently related to the properties of the RCC mix design and its properties. Therefore, it is significant to research the RCC mixture and characterize its behavior under different environments to propose adequate recommendations that can be used in newly designed and constructed RCC pavements. This understanding of RCC pavement behavior can be vital for the popularity and applicability of RCC mixtures in a wider range of routes. This thesis contributes to this understanding through the material characterization of RCC pavements in the lab and in the field.

1.1. Research Objectives and Methodology

The primary objectives of this dissertation are to (i) Investigate the Roller Compacted Concrete (RCC) moisture diffusivity to help future characterization and interpretation of resulting stresses as a function of the curing and climatic conditions at the time of construction. (ii) Model the workability and evaluate density development in terms of aggregate gradation and admixtures. (iii) Model the transport properties of RCC specimens to facilitate the evaluation of RCC durability, (iv) Develop new

methodologies to quickly measure density and moisture in the field. (v) Evaluate the short- and long-term performance of RCC pavements under traffic loading.

The graduate research program involved the characterization of RCC mixtures relative to their use in roadway paving. The research involved studying the effects that the consistency of RCC mixtures (in terms of density and workability) have on the key transport properties of moisture diffusivity of the mixture. Factors such as the aggregate gradation and curing conditions were considered to evaluate their effect on moisture and density profiles. Several key items necessary to accomplish the primary research objectives are highlighted below:

1. Design, fabricate and test small-scale specimens to establish the moisture and density profiles, especially during the 1st drying cycle. This aspect of slab behavior also has future implications that involve the set profile of the pavement, the associated curling and warping stress development, and the potential for pavement blow-up. Due to the unavailability of an established procedure, the concentration of this step was to develop a new methodology to evaluate the mentioned properties
2. Design, fabricate, and small-scale test specimens to develop a relationship between workability of RCC mixtures to aggregate type, texture, amount, and gradation; the resulting density of an RCC mixture. To initiate this relation, the research investigated the effect of admixtures, aggregate gradation, and characteristics on the workability and density of the RCC mixture.

3. Develop a methodology to assess the fresh and hardened concrete surface characteristics using the PaveScan RDM 2.0 GPR dielectric. The data was collected from an airport located in El Paso to develop a methodology that can be used to assess the fresh and hardened concrete conditions in the field. This step implies characterizing the fresh and wet density of concrete (RCC is included) pavement and the effectiveness of curing for the freshly placed pavements.
4. Analyze the laboratory data to model the development of a methodology to evaluate the short- and long-term performance of RCC pavements under traffic loading. The thesis proposes a traffic model that can help evaluate the short- and long-term performance of RCC pavement by incorporating the stress calculations at different critical slab locations and using a neural network to automate the stress calculations as well as using the detailed traffic characteristics to calculate the ESALs and hence the damage. A study for the effect of compaction level, aggregate gradation, and RCC pavement thickness, as well as the existence of set residual stress, was evaluated.

The research plan can be summarized by the flowchart below:

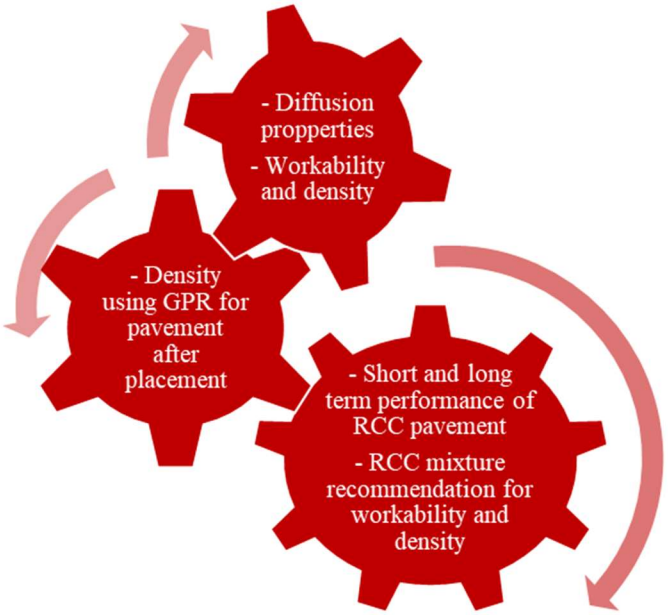

Figure 1.1 Research methodology illustration

1.2. The History of Using RCC in Pavements

The Roller-Compacted Concrete (RCC) consists of the same basic content as conventional concrete. However, RCC much denser material than conventional concrete because of the low water/ cement ratio as well as the dense graded aggregate gradation. These proportions, therefore, give the RCC high compressive strength, stiffness, and zero slumps that require heavy equipment to be placed and rolled. Thus, using RCC is common in infrastructures such as airplane terminal pavements, trucking terminals, parking lots, and mass concrete construction. As indicated by the ACI 325.10R, the use of RCC has been advantageous for use in two general areas of construction: pavements and dams.

The first RCC form was introduced in Sweden as early as 1930 (ACI 325.10R). The RCC pavements were first introduced to the North America pavement construction in 1942 by the U.S. Army Corps of Engineers- Seattle office, where a runway at Yakima, Washington was constructed. The real start of using the RCC was held until the beginning of the 1980s when the US army corps of engineers-initiated interest in using the RCC in the pavement of military facilities. The use of RCC in the pavement was first tested by the US army corps of engineers by constructing small test roads for specific vehicles. Test roads were built in Ft. Stewart and Ft. Gordon, Georgia, in 1983. These road tests were continued in 1984 when the US army corps built a pavement of tank trail at Ft. Lewis, Washington, with a total area of 1870 yd^2 with 8.5 in. thickness. In 1984, the first design of RCC pavement was constructed at Ft. Hood, Texas. The project was a tactical equipment hardstand with a total area of 18150 yd^2 and a thickness of 10 inches. This project was valuable for the US Corps of Engineers because it provided information about the compressive strength that can be achieved using the RCC as well as the aggregate gradation, compaction method, curing, and sampling of RCC material pavement.

By the mid-80s, the interest of RCC had expanded beyond the logging and mining projects. In 1985, 53000 yd^2 of pavement of new intermodal facility at Houston, Texas for the Burlington Northern Railroad was the first use of RCC in other industries. The RCC then have been used extensively in ports such as Tacoma, Washington in 1985, and parking areas such as Spring Hill, Tennessee, and Ft. Drum, NY between 1988 and 1989. However, the only example of using RCC in airports was in the Portland

International Airport in 1985. In the 90s, many other developments on using RCC for streets with moderate traffic, secondary highway, and municipality streets were also introduced in Canada and USA. Although RCC paving has been initiated and developed for years, many issues of RCC paving still need to be addressed before it can be considered as a pavement option for major high-speed roadways.

1.3. Dissertation Significance and Impact

Developing an RCC pavement system will allow the construction of high-speed roadways effectively in terms of time and cost. RCC pavements have a plausible load-carrying capacity to bear occasional small vehicles such as cars immediately following the placement. This load-bearing capacity is gained from the initial compaction process through asphalt-type paver, creating enough aggregate interlock to allow light traffic to be running on the freshly placed pavement without inducing any damages. Moreover, RCC is more cost-effective than conventional concrete pavements and comparable to asphalt pavements. Cost records show that the RCC has a lower unit cost than similar sections of conventional concrete pavements or asphalt pavements (Adaksa 2006). However, recent developments in RCC paving operations focused on improving finishability/durability and density during placement. A need also exists for developing a better understanding of the climatic and material density-related factors affecting the development of noisy joints shortly after RCC placement and, later on, in some circumstances, the development of pavement blow-ups. Taking these items into account, along with the related material aspects of RCC mixtures, should lead to an improved

understanding of the behavior of RCC pavement, which is essential to the successful future implementation of the RCC as a paving option for new constructions.

The RCC Pavement Council has initiated the effort to study the in-situ RCC pavement behavior by studying the effect of moisture permeability of RCC pavement, especially during the 1st drying cycle. This initiative was extended to study the density and workability of the RCC mixture prior to and upon RCC placement. Therefore, investigation of these two components through material characterization of RCC mixtures was significant for the development of the long-performance RCC pavement. The research findings in this dissertation provide new ideas and methodologies to evaluate the RCC materials in the lab and the field. The research findings can be further used to evaluate the RCC materials in the lab before placement and predict the in-situ short- and long-term behavior of RCC pavements.

1.4. Dissertation Organization

This dissertation consists of eight chapters. Chapter 1 (the present chapter) describes the research objectives and methodology, the significance of the research topic, and the dissertation outline.

Chapter 2 develops a new test setup and interpretation methodology of using Time Domain Reflectometry (TDR) in concrete. Using TDR has been practically limited in soil materials to measure the moisture content, where probes can be inserted whenever a measurement is required. The data interpretation is designed around the concept of the apparent length of the reflected voltage reflection. The apparent length has a significant connection to the geometry and material of the designed probes. The developed

methodology can replace the current practice by i) fitting the voltage trace using a physically sound approach that reflects the electromagnetic knowledge. This eliminates the need to use specific material and geometry for the probe and facilitates the use of TDR in other materials, including concrete, ii) using the transmission line equation to estimate the dielectric constant, material conductivity, and reflectivity to evaluate RCC electrical properties and hence estimate the moisture content. This replaces the apparent length methodology that has been used since the beginning of the 1980s in calculating the dielectric constant. The contents are reprinted with minor revisions from a paper published in Transportation Research Record: Journal of the Transportation Research Board (2021)

Chapter 3 uses the newly developed TDR methodology to evaluate the moisture and density profiles of different RCC mixes. The RCC mixes were cast into a plastic mold with an exposed surface to initiate one-dimensional diffusion of moisture. The TDR measurements were taken at three depths from the exposed surface to help establish i) the moisture profile with depth, which can be used to estimate the moisture gradient and associated stresses, ii) the density profile, which can be used to evaluate the effect of density change on the mechanical properties of RCC specimens. The contents are reprinted with minor revisions from a paper submitted to the Transportation Research Record: Journal of the Transportation Research Board (2021)

Chapter 4 studies the compactibility of RCC mix using the Superpave Asphalt Gyratory Compactor. The current practice uses the Vee bee test that uses a vibrating table to evaluate the consistency of the RCC specimens. However, RCC does not have

consistency because it usually crumbles once a vibration is introduced. This part of the dissertation provides two main contributions to the understanding of RCC workability, i) develops a new methodology to evaluate the workability using the compactibility of RCC mix instead of the consistency of the mix, ii) introduces a model to evaluate the energy required to compact RCC samples with different thicknesses. The contents are reprinted with minor revisions from a paper submitted to the Journal of Construction and Building Materials (2021)

Chapter 5 presents a new methodology to evaluate the permeability and diffusivity of the RCC sample in the lab. The new method incorporates the TDR measurements along with the well-known Rapid Chloride Permeability Test (RCPT) to actually evaluate the NaCl ingress with time and model the diffusivity and permeability. The current practice of RCPT, which is mainly used in bridge engineering, actually measures the ion transport instead of solution ingress, it has a qualitative measure for the permeability, it can be used to measure conductance instead of the conductivity, and finally, it is sensitive to concrete with chemical additives because they have a non-understandable effect on the test results. The new test setup helps i) evaluate the solution ingress with time, ii) quantitively estimate the permeability and diffusivity coefficients, iii) measure conductivity (i.e., a material property) from the TDR measurements, iv) eliminate the sensitivity of concrete sample to the chemical admixtures. This paper has a potential impact on the current ASTM standard for the RCPT along with its applicability on different infrastructures. The contents are reprinted with minor revisions from a paper

submitted to the Transportation Research Record: Journal of the Transportation Research Board (2021).

Chapter 6 presents a solution for the Ground Penetrating Radar, a GPR to evaluate the density and volumetrics in fresh and hardened concrete pavements. The methodology basically evaluates the volumetrics of the fresh concrete to evaluate the moisture loss and effectiveness of curing at an early age of the pavement. It also evaluates the volumetrics of the hardened concrete surface and relates it to the distress found. The fresh concrete solution can be used to evaluate the compaction of the RCC pavement after placement and predict early-age behavior due to the loss of moisture, while the hardened concrete surface solution provides information about the long-term performance of RCC pavement. The developed methodology is not limited to RCC pavement but also can be used in different infrastructures as a measure for potential problems. The contents are reprinted with minor revisions from a paper submitted to the Journal of Construction and Building Materials (2021)

Chapter 7 presents a methodology to evaluate the short- and long-term performance of RCC under traffic loading. This methodology incorporates the mechanical properties of the RCC to evaluate the short-term and long-term pavement performance through calculating the Equivalent Single Axle Load (ESAL) and associated damage at critical pavement slab locations. The contents are reprinted with minor revisions from a paper intended to be submitted to the International Journal of Pavement Engineering (2021).

Chapter 8 summarizes the main findings and conclusions of this study as well as the recommendation for future research.

1.5. References

ACI Committee 325, 1995, “Report on Roller-Compacted Concrete Pavements (ACI 325.10R),”. American Concrete Institute, Farmington Hills, MI, 32 pages.

Adaska, W. 2006. “Roller-Compacted Concrete (RCC).” PCA Research & Development Information Serial No. 2975. Skokie, IL: Portland Cement Association.

2. A LABORATORY APPROACH TO DETERMINE RCC MIXTURE ELECTRICAL CHARACTERISTICS USING A NEW TDR INTERPRETATION METHOD[1]

2.1. Introduction

Roller Compacted Concrete (RCC) pavements provide an advantageous cost alternative over conventional concrete pavements. One of the main differences between RCC and conventional concrete pavement is the dryness of RCC mix, which requires placement with asphalt-type pavers to achieve the density required for mechanical properties, while conventional concrete is placed with slip-form concrete machines or vibrating screeds. The absence of a complete understanding of RCC slab behavior, especially at an early age, limits it as a paving option on heavily trafficked roadways. Furthermore, using the current practice measurements of preplaced moisture and temperature sensors to investigate early aged behavior is not practical because of the method of construction used to place RCC pavement. Therefore, exploring a new approach to estimate the moisture profile of RCC can be vital to understanding the RCC pavement behavior.

Time-domain reflectometry (TDR) provides a non-destructive procedure that has been used in the estimation of the bulk electrical conductivity as well as the water content of soil materials (Topp et al., 1980; Robinson et al. 2003).

---

[1] Reprinted (with minor revisions) with permission from "A Laboratory Approach to Determine RCC Mixture Electrical Characteristics Using a New TDR Interpretation Method" by Issa M. Issa, Dan G. Zollinger, Ibrahim Onifade, and Robert L. Lytton, 2021, Transportation Research Record: Journal of the Transportation Research Board (TRB), Copyright [2021] by TRB.

TDR measurements are usually analyzed in two main steps; the first step is performed to estimate the electrical permittivity (dielectric constant), while the second step is performed to link the dielectric constant to the equivalent parameters such as water content. The estimation of the dielectric constant and the water content in soil has typically relied on empirical relationships based on an estimate of the apparent length of the TDR trace (Topp et al. 1983). To accurately estimate the apparent length, the probes and the coaxial cable are calibrated following manufacturer guidelines. This eliminates the systematic errors from probe orientation, length, and diameter, thereby improving the estimation of the apparent length. In order to utilize TDR technology with different probe configurations (length, diameter, and materials), it is desirable to develop a new TDR methodology with disposable probes to obtain the TDR reflection as well as to analyze and estimate the electrical properties of the RCC. This methodology provides a reliable and practical way to measure the electrical properties of any composite material in the lab. Studying the electrical properties of the RCC will facilitate the way to measure other properties of RCC mixes such as water content, density, and hydration rate.

2.2. Background and Literature Review

The utility of TDR measurements has often been associated with the detection of water in soil materials, which has the highest dielectric constant than any other constituents of soil (Topp et al. 1983; Robinson et al. 2003; Greco 2006*)*. The characterization of a TDR trace has been done with respect to a transmission circuit development and calculation based on the propagation velocity of the voltage signal.

This voltage signal is generally a step function with a frequency range of either 1.5GHz or 20 kHz (Robinson et al., 2003). The volumetric water content (θ_V - in cm^3 per cm^3 of soil) has been calculated based on Eq. (2-1) in terms of the apparent dielectric constant (K_a), which is the ratio of the apparent probe length to the actual probe length *(*Topp et al. 1983*)*.

$$\theta_v = -5.3 * 10^{-2} + 2.92 * 10^{-2} K_a - 5.5 * 10^{-4} K_a^2 + 4.3 * 10^{-6} K_a^3 \qquad (2\text{-}1)$$

The apparent dielectric constant in Eq.(2-1) depends on the calculation of the apparent length, which can be determined in terms of the reflection coefficient and the time required for the signal to travel through the length of the probes (i.e., the propagation time) (Topp et al. 1983). Figure 2.1 shows typical TDR traces that are typically used to determine the travel time using Eq. (2-2). The travel time consists of the start time t_1 and the end time t_2 of when the step signal enters and departs from the TDR sensor. The start and end times are associated with the first and second reflection positions numbered 1 and 2 in

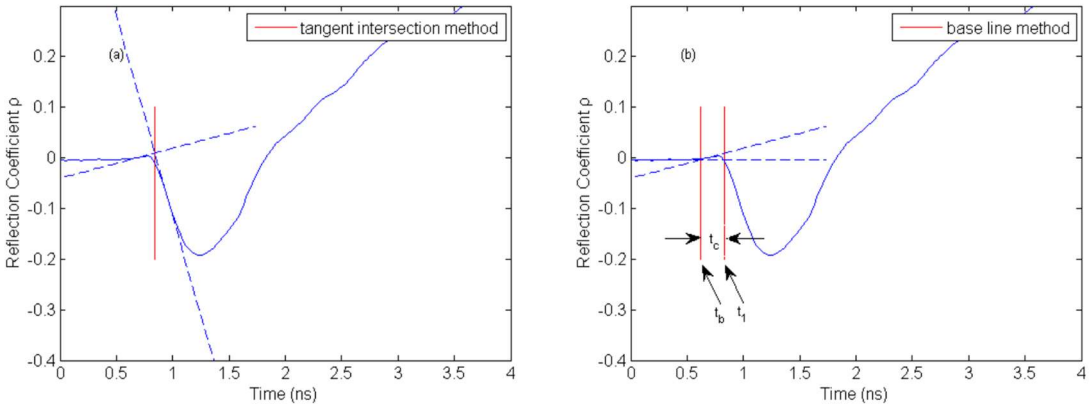

a) Tangent intersection method

b) Baseline method

, respectively. In previous research, t_1 is linked with the spike and variation in the slope where a steep reduction occurs in the waveform at the first maximum voltage, and t_2 is linked with the point where a sudden increase occurs in the waveform at the valley (Heimovaara 1993; Baker and Allmaras 1990; Evett 2000). The difference between t_1 and t_2 represents the travel time (Δt - sec) of the signal, which can be expressed in terms of the apparent dielectric constant, the velocity of the electromagnetic signal in free space (c- m/sec), and the apparent waveguide length L (m) as follows:

$$\Delta t = \frac{2L\sqrt{K_a}}{c} \qquad (2\text{-}2)$$

The physical properties of the TDR sensor are prime factors influencing the location of t_1 on the TDR trace. As the TDR physical properties such as length and diameter are typically known, t_1 should be constant for repeated measurements. Figure 2.1 shows two methods to determine the value of t_1. Figure 2.1 (a) shows the tangent intersection method. This method determines t_1 by drawing a tangent line for the highest increasing point before the spike and the highest decreasing point after the spike and evaluating the t_1 value based on the intersection of the two tangent lines (Baker and Allmaras 1990; Evett 2000). Figure 2.1 (b) shows the baseline method, which uses the intersection of the tangent line before the highest increasing point with the baseline constructed by the horizontal part at the left end of the TDR waveform (t_b) plus adding a certain off-set time t_c to yield $t_1 = t_b + t_c$ (Heimovaara 1993; Evett 2000). For t_2, the same procedure can be used or newly developed procedures such as the adaptive waveform clarification using the Gaussian Filters (AWIGF) described in reference (Schwartz et al. 2014). However, using the empirical method developed in reference (Topp et al. 1983) provides an

effective and easy way to calculate all required parameters along with soil properties from TDR traces.

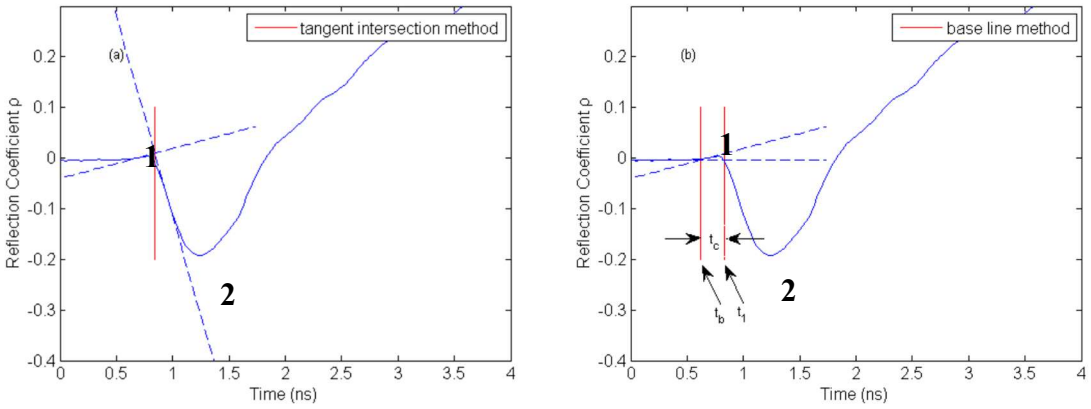

c) Tangent intersection method d) Baseline method

Figure 2.1 Typical TDR traces and different methods to estimate t1 (Adapted from Baker and Allmaras 1990)

In this paper, the Campbell Scientific TDR 200 system with an output impedance of 50 ohms ±1% was used to obtain voltage traces. This system uses the concepts discussed earlier to determine the volumetric water content and the bulk electrical conductivity from the measured data. The relation between the volumetric water content and the dielectric constant has been explained in references (Topp et al. 1980; Ledieu et al. 1986) in terms of both the linear and polynomial forms. The use of these expressions was automated by the output from the TDR 200, making these equations suitable for many applications. Eq. (2-1) shows the calculation for volumetric water content in reference (Topp et al. 1980), while Eq. (2-3) shows the calculation of the same parameter from reference (Ledieu et al. 1986):

$$\theta_{va} = 0.1138\sqrt{K_a} - 0.1758 \qquad (2\text{-}3)$$

Previous research indicated that, stay in place, disposable TDR probes can be used after the concrete has hardened to obtain the TDR traces (Liu 2011; Cataldo et al. 2017; Drnevich and Yu 2007). In these efforts, the design of probes met manufacturer requirements in terms of length, diameter, and spacing to facilitate accurate estimation of the apparent length and, subsequently, the associated dielectric constant. In this paper, the transmission line concept is employed to fit the TDR trace of any probe configuration to directly estimate the dielectric constant, electrical conductivity, and reflection coefficient. This will eliminate the need to calculate the apparent length and the travel time as well as the calibration of the probe.

2.3. Test Program

The application of the TDR 200 is limited to materials or media, which permits the insertion of the probes. Any change in the dimensions or orientation of these probes results in uninterpretable TDR traces. Therefore, it was important to recalibrate the transmission line equation solution provided in reference (Lee et al. 2008) to adopt it for the determination of electrical properties of any material using stay in place and/or non-standard probes. The main objectives of this test program were i) to provide preliminary data to evaluate the applicability of the proposed transmission line equation and ii) to evaluate TDR traces of RCC specimens using disposable probes to determine the feasibility of obtaining suitable estimates of the electrical properties of RCC specimens with different aggregate gradation and curing conditions using the transmission line equation.

2.3.1. Instrumentation

The TDR 200 instrument by Campbell Scientific uses a pulse generator to apply an electromagnetic signal through a TDR sensor that is designed to detect a reflected response in order to determine the volumetric water content or/and electrical conductivity (Campbell Scientific 2017). The TDR measurements are usually obtained by inserting the TDR probes in the material medium of interest. These probes are a waveguided extension of the coaxial cable where reflections result from an impedance variation. Impedance variability occurs due to the geometry of the probe, which is also inversely associated with the dielectric constant of the material medium. The dielectric constant in porous media is highly sensitive to the volume of water in the media since water has a high dielectric constant. Applying a signal through a coaxial cable and into the embedded probes results in a reflection as a function of the impedance of the probe. As water has a large effect on the probe impedance, the shape of the reflection over the length of the probe is an indication of the amount of water present in the surrounding material and its bulk electrical conductivity. Figure 2.2 shows the TDR 200 measurement system in soil or similar materials.

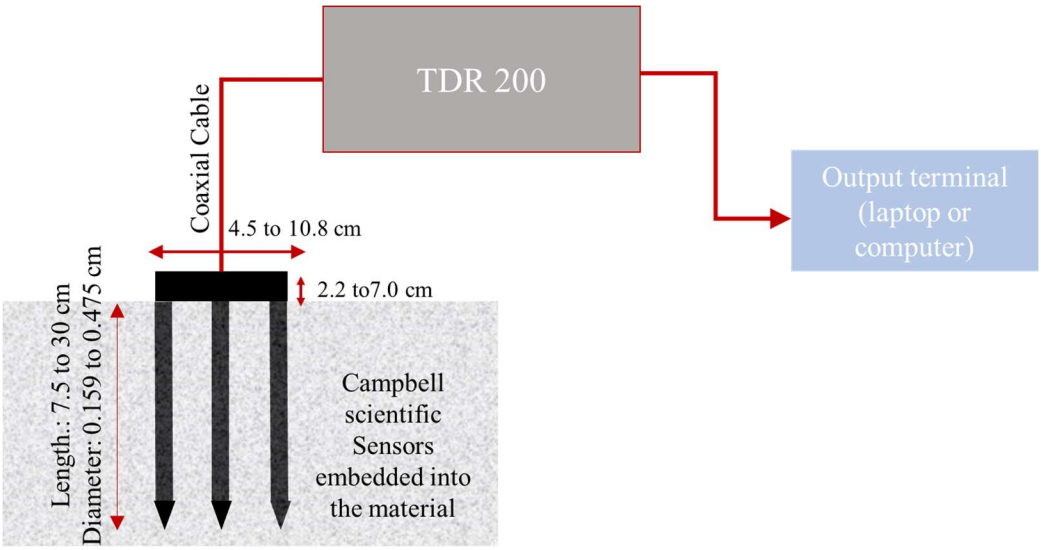

Figure 2.2 Typical TDR 200 schematic for voltage trace measurement- the schematic is not to scale (Reprinted from Issa et al. 2021).

TDR probes presented in Figure 2.2 are typically only useable in materials such as soil or fresh concrete, where they can be removed and reused. This same approach can be used to collect measurements for the electrical properties of RCC mixtures. However, if the mixtures begin to harden, the probe will become non-removable, and it is neither effective nor economical to use the commercially available probes provided by the manufacturer for measuring the reflection response. Therefore, carbon steel probes were inserted at multiple depths from the surface to collect TDR traces. At each depth, two disposable metal probes were horizontally spaced at 25.4 mm to record a voltage vs. time trace. One of the probes was used as a waveguide, while the other was used for the reflected signal. The PC-TDR software was used to obtain the reflection trace. In usual cases, TDR measurements are obtained using a calibrated probe to accurately identify the apparent length required for the empirical calculations of dielectric constant and

electrical conductivity. In this study, the electrical properties of the RCC were determined by fitting the voltage vs. time trace using the transmission line equation. Therefore, the calibration of the disposable metal probes was not required. Consulting the TDR 200 manual (Campbell Scientific 2017), the use of 7.5 cm embedded probes was considered appropriate.

2.3.2. Mix Design

The soil compaction design method was employed for the mix design of RCC mixtures studied in this research. Four aggregate grades were used: ASTM C 33 No. 56 limestones, TxDOT Surface Aggregate Classification C and F rocks, as well as river sand. Coarse and intermediate aggregate types were sieved into their specific sieve size except for the river sand. Two aggregate gradations were then formed from these aggregate grades. The aggregate gradations were representatives of the specified lower limit (LL) and upper limit (UL) aggregate gradation established in the soil compaction mix design, Figure 2.3. The blended aggregate gradations were optimized with the lower and upper specifications considering a maximum aggregate size of 25.4 mm for both gradations. The initial RCC mix designs were developed to establish the required moisture-density relationships for both aggregate gradations. Based on commonplace practice, an initial cement content was assumed as 267 Kg/m^3, while the specific gravities for cement and combined aggregate were assumed as 3.15 and 2.63, respectively (based on typical mineralogy of the aggregate sources). The initial mix designs to establish the moisture-density curve are shown in Table 2.1

The Tex-113-E proctor test procedure, using the 152.4 mm diameter mold, was followed to determine the optimum moisture content at the maximum dry density of the mix. For the lower limit aggregate blend, a range of moisture of 4%, 6%, 8%, 9% of the dry material weight was used to determine that the optimum moisture content is 6.1%, and the associated maximum dry density is 2284.2 Kg/m^3. On the other hand, a range of moisture, 4%, 5.5%, 7%, and 8.5 %, was used for the upper limit aggregate gradation to determine that the optimum moisture content is 7.2% and the associated dry density is 2329.1 Kg/m^3. Based on the optimum moisture content found from the proctor test, the initial material quantities were re-proportioned for one cubic yard (0.765 m^3), as shown in Table 2.1

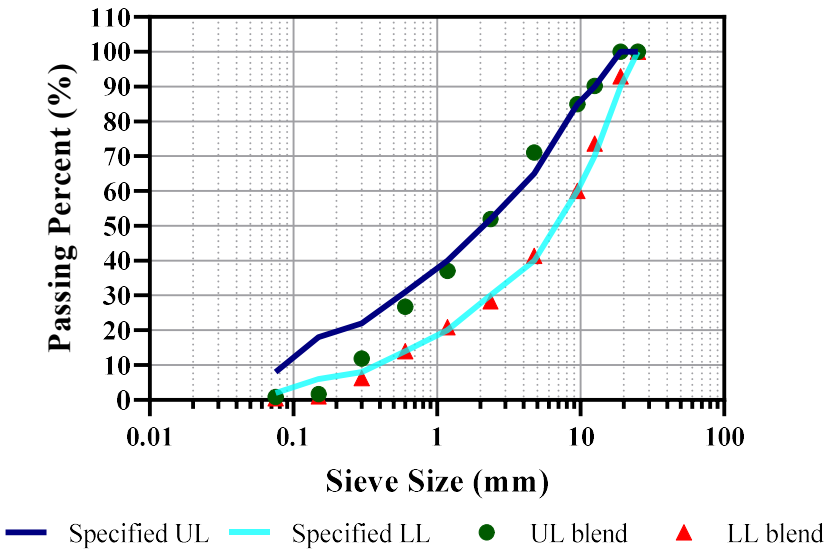

Figure 2.3 Upper limit and lower limit aggregate gradation specification of RCC (Reprinted from Issa et al. 2021).

Table 2.1 RCC mix design (Reprinted from Issa et al. 2021)

RCC Constituents	Initial Mix Design -Kg/m^3		Final Mix Design- Kg/m^3	
	Lower limit	Upper limit	Lower limit	Upper limit
Cement	267	267	284.2	273.5
Combined Dry Aggregate wt.	1957.8	1957.8	2084.2	1990.4
Mixing water	122.1	160.2	130	169.7

2.3.3. Specimen Preparation and Test Setup

ASTM C1435 was employed to prepare four RCC cylinder specimens. 152.4 mm by 304.8 mm cylinders were cast and compacted into four layers of RCC mix using a vibrating compaction hammer that matches ASTM C1435 requirements. The plastic cylinders were previously prepared for insertion of the two probes at 25.4 mm spacing by drilling holes into the plastic cylinders at 38.1 mm, 120.65 mm, and 222.25 mm from the exposed surface. The holes were duct-taped prior to compaction of the RCC specimens to prevent water leakage during compaction. After compacting the RCC specimens, two 88.9 mm probes were inserted through the taped holes in the plastic specimens. It was expected to have a very high electrical conductivity measurement for the RCC mix. Therefore, it was more accurate to keep probe lengths between 76.2 mm and 152.4 mm inside of RCC specimens (Campbell Scientific 2017). Economical and disposable metal probes were used to satisfy the requirements of probe length, being widely available, and stiff enough to withstand insertion into the dry RCC mix. The main obstacle was to secure a parallel insertion of probes. Therefore, a drill with a small

bit size was used to make an insertion path prior to the placement of the metal probes. The material was re-compacted after the insertion of all metallic probes to ensure the material-probe contact. A length (i.e., 19mm) of the metal probes at the end was kept exposed for connection (via alligator clips) to the coaxial cables for taking measurements. Figure 2.4 shows a schematic representation of the specimen preparation. First-day measurements (1 day) were taken at different depths from the exposed surface within one hr. after mixing and compacting the RCC specimens.

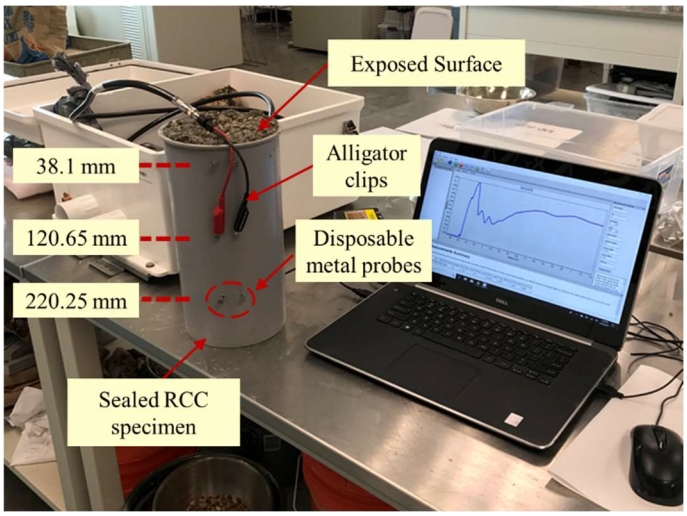

Figure 2.4 The proposed test setup (Reprinted from Issa et al. 2021).

2.3.4. Dielectric Measurements

The dielectric determination was investigated with respect to the aggregate gradation and the curing of the RCC specimens. The test specimen matrix is shown in Table 2.2. To investigate the time-dependent dielectric at different specimen depths, each aggregate gradation was subjected to two curing methods, which were air curing and moisture room curing. The one-dimensional water diffusion in RCC was modeled by

exposing only the top face of the cylindrical specimen to the given method of curing. This one-dimensional diffusion process was preserved throughout the time of measurement by casting the concrete into 152.4 x 304.8 mm plastic cylinders and preventing water evaporation from the specimen's sides and bottom. Two of the specimens were placed at a room temperature of 20ºC and relative humidity of 35 ± 5 % to air dry, while the other two specimens were placed in the moisture room with 95% relative humidity and 20ºC.

Table 2.2 Test matrix (Reprinted from Issa et al. 2021)

Test Type	Parameter	Purpose (s)	Variables	No. specimens
RCC electrical properties	Curing methods	Effect of curing on dielectric constant	- Air curing - Moisture curing	2
	Aggregate gradation	Effect of aggregate gradation on dielectric constant	- Lower limit - Upper limit	2
	Total Number of Specimens			4

Concrete is considered a dielectric material that resists electrical transmission through its components. Dielectric has been defined as the ratio of the composite material's electrical permittivity to the air electrical permittivity (Ledieu et al. 1986). Therefore, the dielectric constant measurement can also provide information about the electrical properties of the concrete material, such as reflectivity and conductivity. As

mentioned in references (Lezama 2007, Davis and Annan 1989) and many others, water has the highest dielectric constant compared to other concrete constituents. Therefore, it has the highest impact on the dielectric measurements in concrete materials. The dielectric constant of fresh concrete should result in a high dielectric constant compared to its value after a few hours. This is because free water in concrete initiates a chemical reaction (hydration) with the other components of the mixture to form the hardened concrete phase. As the hydration process continues, the free water content becomes lower, and hence the dielectric constant becomes lower for the concrete material.

2.4. Research Methodology and Results

The basic approach proposed for determining the dielectric constant at different depths of hardened RCC is based on fitting the TDR voltage trace with the transmission line equation (Lee et al. 2008). The main features of this approach require:

1. Capture the trace of voltage vs. time from the TDR measurements.
2. Fit the transmission line equation and determine the reflectivity Γ, conductivity σ, and composite dielectric constant ε parameters.

2.4.1. Transmission Line Equation

TDR voltage measures are analyzed for the material dielectric parameters such as dielectric constant, conductivity, and reflectivity calculated using the transmission line equation (Lee et al. 2008). Because this research uses non-manufactured probes to capture the voltage trace, it was important to use a method that considers all the noise that might affect the dielectric constant measurements. The expected noise can be any systematic errors such as probe orientation, probe length, probe spacing, or assumption

of the unity of the RCC mixture magnetic permeability. To reduce such noise affecting TDR dielectric determination, the electrical properties of the conducting medium are vital. Therefore, the transmission line equation, shown below, was employed to fit the voltage trace calculated by the transmission line equation to the voltage trace measured from the TDR equipment in order to calculate the dielectric constant, electrical conductivity, and reflectivity of the material. This equation accurately reflects the actual physics of wave transmission through a dielectric medium and determines the conductivity and reflectivity as well as the dielectric constant of the surrounding medium. The equation to calculate the relative voltage in terms of travel time can be expressed as (Lee et al. 2008):

$$v(t) = \left(e^{-\frac{\sigma t}{2\varepsilon\sqrt{\varepsilon_0}}} + \Gamma_L e^{+\frac{\sigma t}{2\varepsilon\sqrt{\varepsilon_0}}} \right) \cdot cos\left(\omega \frac{t}{\sqrt{\varepsilon_0}} \right) \qquad (2\text{-}4)$$

Where $v(t)$ is the relative instantaneous voltage in terms of time travel of microwave, σ is the material conductivity (Siemens/meter), t is time in seconds, ε is the dielectric constant of the composite material (i.e., RCC), ε_0 is the electric permittivity of free space and equals to $\frac{1}{36\pi} \times 10^{-9}$ in Farad/meter, Γ_L is the amplitude of the reflected wave to the incident wave or reflection coefficient, and ω is the angular frequency (Hz) of the voltage signal.

The above equation represents the relative instantaneous voltage on the transmission line for a lossless standing-wave pattern that includes multiple wave cycles, as shown in Figure 2.5. In the case of time-domain reflectometer measurements, probe

length is relatively short, and the medium is not lossless, which means that the maximum and minimum voltage is captured whenever the electromagnetic field enters and exits the metal probe. Afterward, the trace starts to decay due to the impedance presented in the RCC mix. Because the equation above is meant to calculate the electrical conductivity, electrical reflectivity, and dielectric constant, an additional component is required to be known, which is the angular frequency. In this study, the relative instantaneous voltage was converted into a relative voltage by omitting the cosine term that includes the angular frequency and introducing the voltage decay in a lossy medium as discussed subsequently.

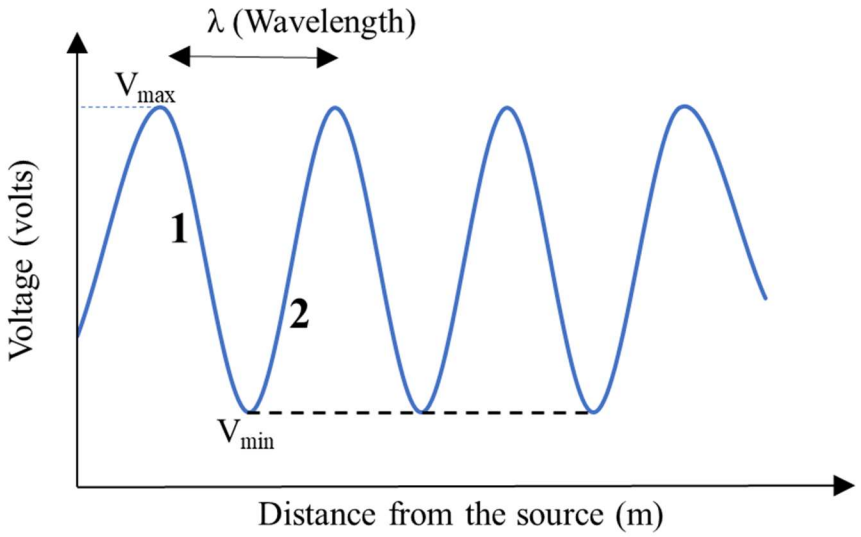

Figure 2.5 Electromagnetic wave voltage in a lossless medium (Reprinted from Issa et al. 2021).

In Figure 2.5, the portion of the wave labeled 1 represents the first term in the equation, which is the curve from the maximum voltage value to the minimum voltage. The portion labeled 2 starts after the first minimum voltage and is controlled by the

reflection part of the transmission line equation, which can be evaluated using the reflection coefficient. The reflection coefficient in materials can be defined as the amount of reflected electromagnetic wave due to the impedance discontinuities of the transmission medium, and it usually ranges from -1 for a short circuit to +1 for an open circuit (Shen and Kong 1987). Eq. (2-4) solves for both parts as a continuous equation, which suggests considering the reflectivity coefficient in both parts of the curve. However, this equation must be modified to allow for the reflection coefficient to be a function of the distance or time. Therefore, a generalization for the reflection coefficient as a function of distance was introduced in reference (Shen and Kong 1987). This generalization is significant to evaluate the reflection that occurred due to the impedance discontinuities throughout the voltage travel time. Based on this generalization, the amplitude of the relative voltage as a function of distance can be expressed as:

$$v(t) = \left(e^{-\frac{\sigma t}{2\varepsilon\sqrt{\varepsilon_0}}} + \Gamma(t) * e^{-\frac{\sigma t}{2\varepsilon\sqrt{\varepsilon_0}}} \right) \qquad (2\text{-}5)$$

The nature of the reflection wave depends mainly on the reflection coefficient. The resistor-capacitor circuit, formed by the existence of aggregate, cement, and water, suggests that the voltage will decay exponentially directly after the minimum voltage is achieved. This decay can be explained by the resistance of the aggregate and the hydrated cement, which reflects most of the electromagnetic waves. As concrete hardens, more reflection (i.e., resistance) is expected. Therefore, it is acceptable to represent the second part of the equation as a complement to the first term. Using the

maximum voltage case described in reference (Shen and Kong 1987), the previous equation can be represented as:

$$v(t) = \left(e^{-\frac{\sigma t}{2\varepsilon\sqrt{\varepsilon_0}}} + \Gamma_L * (1 - e^{-\frac{\sigma t}{2\varepsilon\sqrt{\varepsilon_0}}}) \right) \qquad (2\text{-}6)$$

In the above equation, the first term is used to estimate the dielectric constant and electrical conductivity of the incident wave (wave initiated from the source), while the reflection coefficient is measured from the second term, which represents the reflected wave affecting the propagation constant ($i.e. \sigma/2\varepsilon\sqrt{\varepsilon_0}$) of the voltage wave. Therefore, there is a slight difference in the estimated value of electrical conductivity and dielectric constant between the first and second terms of Eq. (2-6). The main purpose of the transmission line equation is to estimate the electrical conductivity and dielectric constant of the incident wave whilst considering the reflectivity of the material. Therefore, the propagation constant in the second term can be rewritten as a calibration coefficient c. The final form of the modified transmission line equation can be expressed as follows:

$$v(t) = \left(e^{-\frac{\sigma t}{2\varepsilon\sqrt{\varepsilon_0}}} + \Gamma_L * (1 - e^{-ct}) \right) \qquad (2\text{-}7)$$

2.4.2. Fitting TDR Traces

The TDR voltage measurements were taken using the BNC female alligator test clips attached to the exposed metal probes. The BNC female alligator clips were attached to a 3.05 m coaxial cable connected to the TDR 200 instrument. The TDR instrument was connected through a USB port to a laptop. The measurements were taken

at three different depths for three days. The voltage vs. time responses were extracted and cleaned to evaluate the effect of aggregate gradation and curing on the electrical properties of the RCC mixture. Two aggregate gradations were used to cast RCC cylinders. These aggregate gradations were used to represent the lower and upper limits of the dense graded aggregate specification for an RCC mixture.

Figure 2.6 shows the effect of the aggregate gradation and curing on the voltage trace at a depth of 38.1 mm from the exposed surface. Specimen 1 refers to a specimen with no curing, and specimen 2 refers to a specimen with curing. The cured specimens were placed throughout the testing time in a chamber room with humidity of 95 % and a temperature of 20^{o} C. As shown in Figure 2.6; the aggregate gradation has a plausible effect on the voltage reflection with time. The following observations can be drawn about the aggregate gradation from Figure 2.6:

1. The initial maximum voltage in upper limit aggregate gradation is higher than the initial maximum in LL aggregate gradation.
2. The minimum voltage increases gradually with time in specimens with upper limit aggregate gradation, while minimum voltages are almost the same for all time measurements in specimens with lower limit aggregate gradation.
3. The maximum voltage in the reflection part is gradually increasing with time for specimens with UL aggregate gradation, reaching the initial maximum voltage after three days. On the other hand, the maximum voltage after reflection for the specimen with LL aggregate gradation is higher than the initial maximum voltage starting the second day. Also, no significant differences are noticed in the

reflection between the second and third days for specimens with LL aggregate gradation.

Moreover, curing seems to have a significant impact on the voltage traces. The effect of the curing is clear specifically in Figure 2.6 (b), the lower limit aggregate gradation mix. Although the maximum and minimum voltages in the first part seem equal regardless of the curing, a big difference in the voltage after reflection is presented, especially on the first and second day, between cured and non-cured specimens. In contrast, voltage reflections are not significantly affected in specimens with upper limit aggregate gradation, where the voltage after reflection of the cured specimen is slightly lower than the non-cured specimen. In this case, the effectiveness of curing is related mainly to the depth of the measurement. As depth increases, the effect of curing decreases and vice versa. This can be noticed in the first-day voltage traces in Figure 2.6 (a). In general, curing showed a higher impact on specimens with lower limit aggregate gradation than specimens with upper limit aggregate gradation.

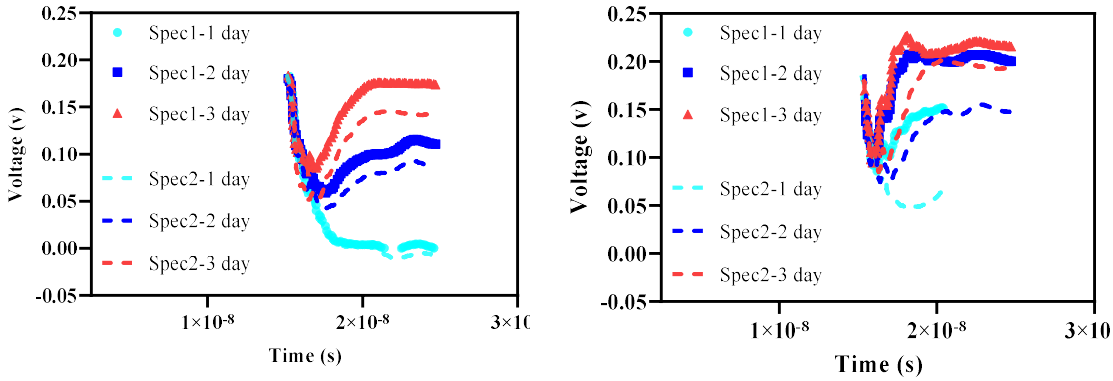

a) Upper limit aggregate gradation b) Lower limit aggregate gradation

Figure 2.6 Voltage vs. Time measurements at 1.5 inches from surface for different aggregate gradation and curing (Reprinted from Issa et al. 2021).

Figure 2.7 shows the typical voltage vs. time traces and their transmission line (TL) equation fitting for three days at 38.1 mm from the exposed top surface. The presented measurements are taken from the RCC cylinder of the lower limit aggregate gradation with no curing (i.e., Specimen 1). The nonlinear least square method was employed using MATLAB code. The values of R-squared are 0.94, 0.96, and 0.91 for the first day (i.e., 1-hour after compacting the RCC), second-and third-day measurements, respectively.

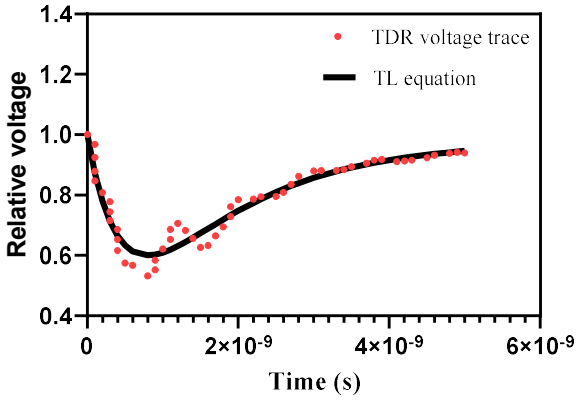

(a) First-day measurement (within 1 hour)

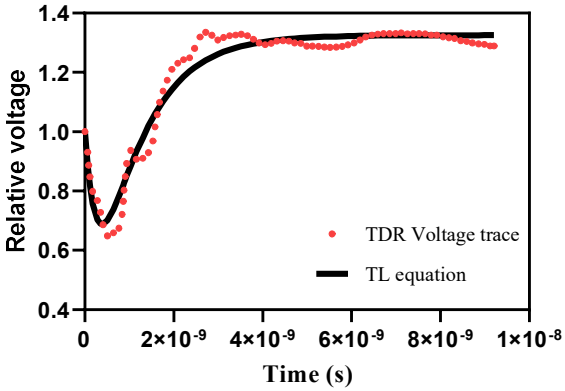

(b) Second-day measurement

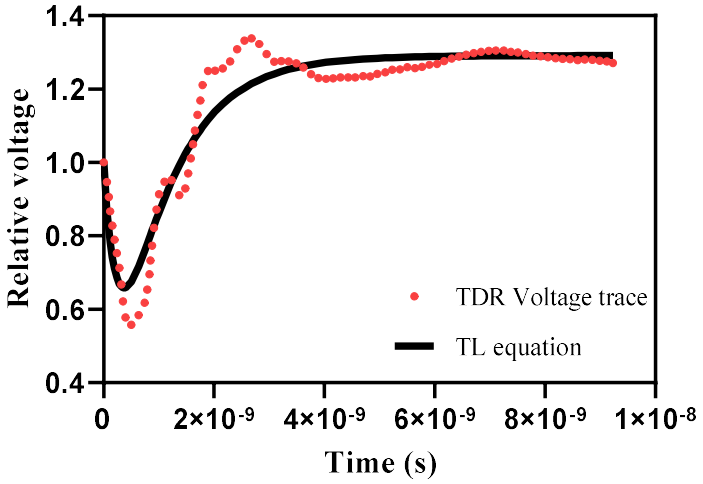

(c) Third-day measurement

Figure 2.7 Voltage vs. Time measurements and fitting of lower limit aggregate gradation specimens at 38.1 mm from the exposed surface - Specimen 1 (Reprinted from Issa et al. 2021).

As shown in Figure 2.7, the voltage traces exhibit the same behavior, and the lowest minimum voltage is recorded on the first day. Similar traces were also captured for measurements at 120.65 and 220.25 mm. After the first day, the difference between the maximum and minimum voltage records significantly decreases, which indicates a decrease in the dielectric constant. Another significant effect is observed in the second part of the chart, which indicates the reflectivity of the RCC mixture. As shown in the figure, the maximum voltage in the reflection part on the first day is lower than the initial maximum voltage. In the second and third days, the maximum reflection voltage is higher than the initial maximum voltage, which can be related to the continuous hardening of the RCC specimen. The TDR traces of the RCC samples with upper limit aggregate gradation exhibit the same behavior. However, the voltage vs. time

relationship shows a gradual difference with age. Only the third-day measurement showed equal or slightly higher maximum reflection voltage than the initial maximum voltage. In general, the difference between the maximum and minimum voltage is the lowest for measurement at 38.1 mm from the surface compared to measurements at 120.65 and 220.25 mm. This indicates that the rate of hydration and the loss of free water is much higher at 38.1 mm than at 120.65 mm and 220.25 mm.

2.4.3. Effect of Reflectivity

Figure 2.7 (a) shows that the relative voltage of the second portion of the curve is lower than the initial relative voltage. However, it becomes higher than the initial relative voltage on the second and third days, as shown in Figure 2.7 (b) and (c). This may be connected to the reflectivity of the aggregate content, density of the layer, and cement hydration. The aggregate and density affect the reflectivity on the first day. However, as the hydration process continues, an insulating layer usually forms around the pore water within the cement paste (Wilson 1986), which consequently increases the reflectivity of the RCC mix. This can explain the TDR traces in Figure 2.7. The first-day reflection shows a lower voltage than the initial maximum voltage, which means that the insulating layer has not been established yet. On the second and third-day, reflection voltages are higher than the initial maximum voltage, which can be explained by the formation of the isolation layer around the pore water along with the presence of a high percentage of coarse aggregate and the material density.

2.4.4. Electrical properties of RCC

The fitting process was conducted on all UL and LL aggregate gradation specimens. Table 2.3 shows the measurements of the LL aggregate gradation specimens with age and depth. The table shows the dielectric, material conductivity, and reflectivity, as well as the R-squared for each measurement. In the table, specimen 1 refers to the specimen with no curing, while specimen 2 refers to the specimen with curing. It is worth reminding that first-day measurements were taken 1 hour after compacting the specimen.

Table 2.3 Electrical properties of RCC specimens from fitting V vs. T traces- LL gradation (Reprinted from Issa et al. 2021).

Specimen	Age (days)	Depth (mm)	Dielectric	Material Conductivity (S/m)	Reflectivity	R-squared
1	1	38.1	4.09	5.74×10^4	0.93	0.94
	1	120.65	9.30	5.54×10^4	0.74	0.82
	1	220.25	6.48	4.68×10^4	0.46	0.96
	2	38.1	2.7	5.68×10^4	1	0.96
	2	120.65	5.73	5.34×10^4	1	0.95
	2	220.25	4.84	5.10×10^4	1	0.94
	3	38.1	2.45	5.66×10^4	1	0.91
	3	120.65	4.77	5.22×10^4	1	0.93
	3	220.25	4.74	5.87×10^4	1	0.93
2	1	38.1	6.28	3.75×10^4	0.32	0.97
	1	120.65	7.20	4.54×10^4	0.48	0.95
	1	220.25	6.37	3.61×10^4	0.32	0.97

Specimen	Age (days)	Depth (mm)	Dielectric	Material Conductivity (S/m)	Reflectivity	R-squared
	2	38.1	3.89	5.08×10^4	0.84	0.93
	2	120.65	3.76	5.20×10^4	0.92	0.95
	2	220.25	4.35	4.94×10^4	0.83	0.96
	3	38.1	4.12	5.06×10^4	1.00	0.92
	3	120.65	3.87	5.11×10^4	1.00	0.98
	3	220.25	4.82	5.21×10^4	1.00	0.93

The overall trend of the dielectric is decreasing with time, as shown in Figure 2.8. The rate of decrease in the dielectric constant with time is dictated by the ability of the RCC mix to retain moisture after casting. Retaining the moisture may be affected by the aggregate gradation, the presence of curing, and the depth of the measurement. As shown in Figure 2.8 (a) and (b) for LL aggregate gradation, specimen 1 with no curing shows the lowest dielectric constant values at 38.1 mm from the surface compared to dielectric at 120.65 mm and 220.25 mm. Specimen 2 with curing shows a decrease in the dielectric constant on the second day but not on the third day regardless of the depth of the measurement, which might express limited moisture loss compared to specimen 1. In Figure 2.8 (c) and (d), which represent the dielectric of the upper limit aggregate gradation, the dielectric constant changes significantly after three days. In Figure 2.8 (c), the decrease in dielectric constant at depth 220.25 mm is the steepest compared to the other two depth measurements. In Figure 2.8 (d), all depth measurements show almost the same rate of decrease in the dielectric constant.

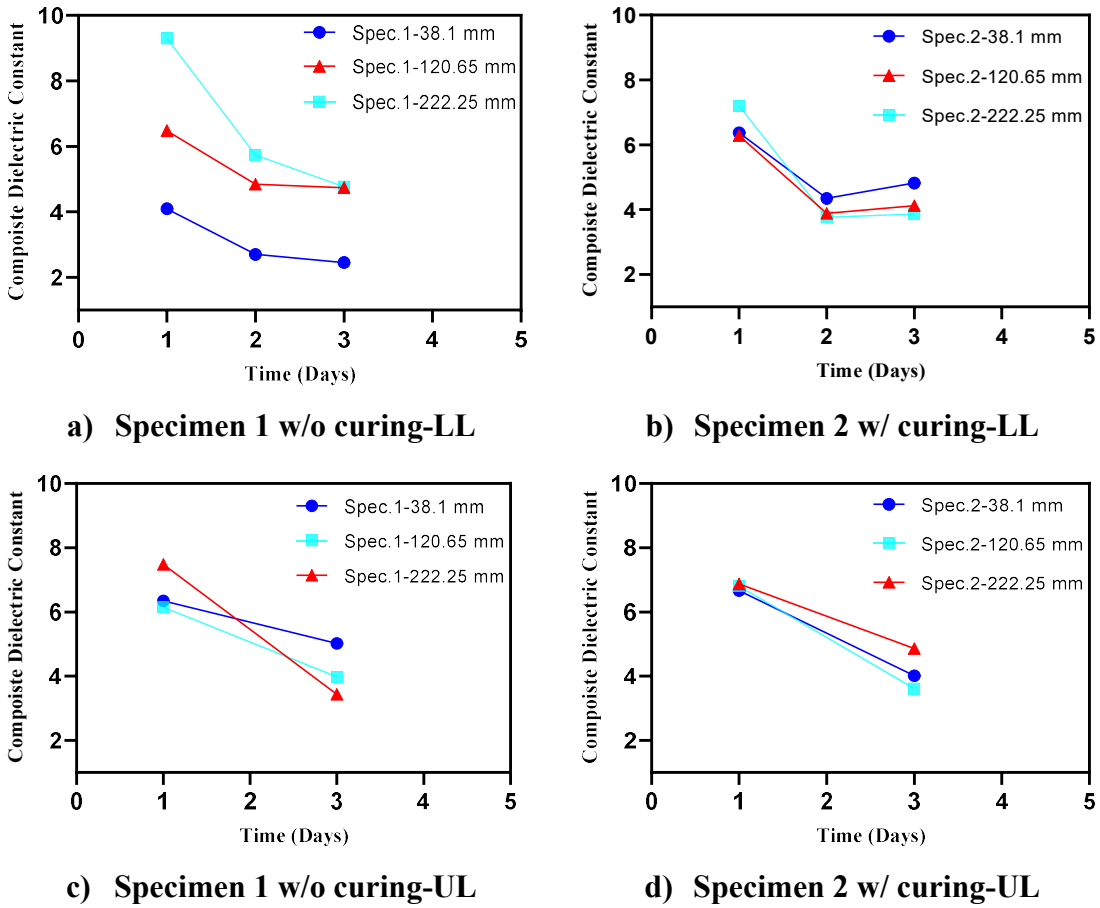

Figure 2.8 Dielectric constant of specimens with a lower limit and upper limit aggregate gradation (Reprinted from Issa et al. 2021).

Material conductivity shows an inverse proportion with dielectric constant. As the dielectric constant increases, the conductivity decreases. This relationship is important because it indicates the accuracy of the measured dielectric constant, which is directly related to the moisture content. Figure 2.9 shows the trend of the material conductivity of the LL and UL aggregate gradation. Unlike dielectric constant, conductivity was calculated with respect to the age only by taking the average of

measured conductivities at all depths at each age. Figure 2.9 (a) shows that the specimen with no curing (i.e., specimen 1) has a steep increase of conductivity, especially after the first day, which is relevant to the decrease in the dielectric constant shown in Figure 2.8 (a). On the other hand, the specimen with curing shows no significant increase in the average conductivity over the three-day period. Figure 2.9 (b) shows linear relationships between conductivity and age in both specimens, which emulate the linear decrease of the dielectric constant in Figure 2.8 (c) and (d). Figure 2.9 (b) also shows no large differences between specimens 1 and 2. However, the specimen with curing (i.e., specimen 2) starts with lower conductivity on the first day and ends with higher conductivity on the third day than the specimen with no curing (i.e., specimen 1).

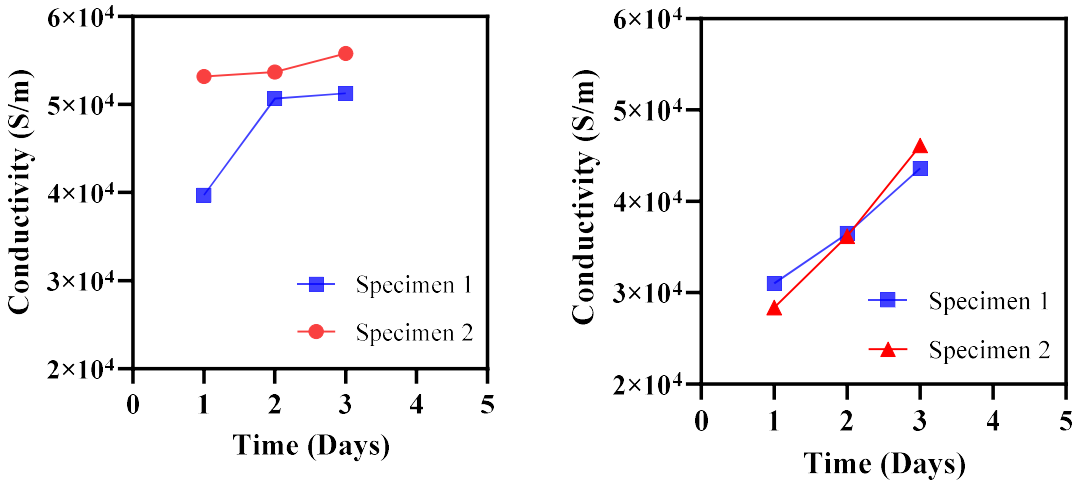

a) LL specimens **b) UL specimens**

Figure 2.9 Material conductivity of specimens with a lower limit and upper limit aggregate gradation (Reprinted from Issa et al. 2021).

2.5. Conclusions

A new methodology to measure voltage trace from the TDR and a modified transmission line equation for determining the electrical properties of RCC specimens is developed and proposed in this paper. The proposed methodology revealed the following points about the electrical properties of RCC specimens:

1. The new methodology depends on fitting the voltage trace from the TDR by the transmission line equation in terms of conductivity, reflectivity, and dielectric constant, which does not require probe calibration. This allows for a wide range of materials to serve as disposable TDR probes without inducing systematic errors related to probes calibration and materials.
2. The transmission line equation presents an accurate and practical way to determine the dielectric constant at different depths from the surface. Instead of using empirical equations to estimate it, other electrical properties such as electrical conductivity and reflectivity serve as a determinant for the dielectric constant.
3. The voltage traces from the TDR are highly affected by the aggregate gradation and the curing method. The upper limit aggregate gradation shows a much more gradual change of voltage traces with time compared to the lower limit aggregate gradation. Also, the curing method has a high impact on the TDR voltage trace, especially in the lower limit aggregate gradation, which indicates the importance of curing for RCC pavements. Lower limit aggregate gradation contains a higher percent of coarse aggregate, which allows faster water loss than upper limit

aggregate gradation. This result suggests applying an efficient technique of curing as well as maintaining aggregate gradation close to the upper limit.

4. The overall trend of the dielectric is decreasing with time, while conductivity increases with time. Dielectric values are affected by the compaction effort (in the case of RCC mix) or/and the hydration of cement. Conductivity is affected by the presence of ions in the pores, which can be used as indications for the accuracy of the dielectric values. Due to the dryness of fresh RCC mix, the investigation of the RCC dielectric and conductivity on the first day is important and should be studied.
5. In general, high dielectric and low conductivity mean the RCC is holding the moisture and limiting movement – typical of the uncured concrete and the high-water content due to bleeding. As the water begins to move, the dielectric drops and the conductivity goes up. The coarser the aggregate gradation, the more readily the RCC will allow water to move through it due to less surface area (type of aggregate would affect this as well due to the effect of surface energy). A finer aggregate and more surface area hold the moisture for a longer period of time and keep the dielectric higher and the conductivity lower.

Using the transmission line equation to fit the voltage traces obtained from the TDR 200 was found appropriate and applicable for different RCC mixes and curing methods. Improvements in the collection and cleaning of the TDR traces will increase the accuracy of the modified transmission line equation. The current study does not address

the variability of the results from the proposed test setup and RCC mixing. Future work will include additional testing of materials to evaluate the proposed methodology further.

2.6. References

Issa IM, Zollinger DG, Onifade I, Lytton RL. Laboratory Approach to Determine Roller Compacted Concrete Mixture Electrical Characteristics Using a New Time-Domain Reflectometry Interpretation Method. Transportation Research Record. 2021 Aug 30:03611981211036370.

Topp GC, Davis JL, Annan AP. Electromagnetic determination of soil water content: Measurements in coaxial transmission lines. Water resources research. 1980 Jun;16(3):574-82.

Robinson DA, Schaap M, Jones SB, Friedman SP, Gardner CM. Considerations for improving the accuracy of permittivity measurement using TDR: Air/water calibration, effects of cable length. Soil Sci. Soc. Am. J. 2003(67):62.

Greco R. Soil water content inverse profiling from single TDR waveforms. Journal of hydrology. 2006 Feb 20;317(3-4):325-39.

Heimovaara TJ. Design of triple-wire time domain reflectometry probes in practice and theory. Soil Science Society of America Journal. 1993 Nov;57(6):1410-7.

Baker JM, Allmaras RR. System for automating and multiplexing soil moisture measurement by time-domain reflectometry. Soil Science Society of America Journal. 1990 Jan;54(1):1-6.

Evett SR. The TACQ computer program for automatic time domain reflectometry measurements: II. Waveform interpretation methods. Transactions of the ASAE. 2000;43(6):1947.

Wang Z, Kojima Y, Lu S, Chen Y, Horton R, Schwartz RC. Time domain reflectometry waveform analysis with second order bounded mean oscillation. Soil Science Society of America Journal. 2014 Jul;78(4):1146-52.

Schwartz RC, Casanova JJ, Bell JM, Evett SR. A reevaluation of time domain reflectometry propagation time determination in soils. Vadose Zone Journal. 2014 Jan;13(1):1-3.

Ledieu J, De Ridder P, De Clerck P, Dautrebande S. A method of measuring soil moisture by time-domain reflectometry. Journal of Hydrology. 1986 Nov 30;88(3-4):319-28.

Liu Y. *Innovative Non-destructive Testing Technologies for QA/QC of Fresh and Early-Stage Concrete* (Doctoral dissertation, Case Western Reserve University).

Cataldo A, De Benedetto E, Cannazza G, Piuzzi E, Pittella E. TDR-based measurements of water content in construction materials for in-the-field use and calibration. IEEE Transactions on Instrumentation and Measurement. 2017 Nov 24;67(5):1230-7.

Drnevich VP, Yu X, inventors; Purdue Research Foundation, assignee. Method and apparatus for measuring properties of concrete. United States patent US 7,289,916. 2007 Oct 30.

Lee SI, Zollinger DG, Lytton RL. Determining moisture content of soil layers with time domain reflectometry and micromechanics. Transportation research record. 2008 Jan;2053(1):30-8.

Campbell Scientific Inc. TDR200-Based Time-Domain Reflectometry System. Rev.: 4/17, Edmonton: Campbell Scientific (Canada) Corp.; 2017.

Avelar Lezama I. Preliminary non-destructive assessment of moisture content, hydration and dielectric properties of Portland cement concrete (Doctoral dissertation, Texas A&M University).

Davis JL, ANNAN AP. Ground-penetrating radar for high-resolution mapping of soil and rock stratigraphy 1. Geophysical prospecting. 1989 Jul;37(5):531-51.

Shen LC, Kong JA. Applied electromagnetism. PWS Publishing Company; 1987.

Wilson JG. The electrical properties of concrete (Doctoral dissertation, University of Edinburgh).

3. ESTABLISH MOISTURE AND DENSITY PROFILES IN RCC SPECIMENS AT EARLY AGE USING TDR MEASUREMENTS

3.1. Introduction

RCC mixes have lower cement and water content than conventional concrete and require compaction using the asphalt-type paver due to its dryness. High compaction effort creates enough aggregate interlock to allow light traffic to be running on the freshly placed RCC pavement without inducing any damages. Therefore, understanding the behavior of the RCC pavement is significant to facilitate its use in high-speed roadways. To achieve this goal, the fresh RCC mix characteristics such as the volumetric content of free water and the wet and dry unit weight is vital for formulating the set profile of RCC pavement and the associated curling and warping stresses. It is well known that studying curling and warping stresses in the concrete pavement can be performed by establishing the moisture and temperature gradient through instrumenting the concrete mix by a preplaced relative humidity sensor before casting. However, this practice is not applicable in RCC mix due to the use of vibratory compactor in RCC specimen fabrication as a requirement to achieve the specified density and associated mechanical properties. Therefore, measuring the dielectric constant of RCC specimens can provide means to establish the moisture and density profiles to be used for RCC behavior analysis.

Using the dielectric constant to measure the volume fractions of conventional concrete constituents has been investigated in many studies (Camp et al. 1989; Korhonen et al. 1997; Chen et al. 2012; Jamil et al. 2012). However, most of these activities used

empirical models to relate the dielectric constant with the water content and other mechanical properties. Lezama 2005 and Lee et al. 2012 proposed microanalytical approaches to analyze the composite nature of concrete mixes. In Lee et al. 2012, the composite dielectric constant of the composite material was assumed to vary with the dielectric and the volumetric fraction of the individual component, which meant using a linear combination of the material constituents in terms of dielectric constant and volume fractions of each component. The paper also proposed a detailed procedure to estimate the individual dielectric constant of the components based on a range of pre-determined individual dielectric constants. Upon determining the individual dielectric constants, time-dependent volume fractions of concrete constituents were determined using the system identification (SID) solution (Lytton 1989).

Issa et al. 2021 developed a new methodology to obtain the TDR traces and use a modified transmission line equation to fit the TDR traces obtained from disposable probes at different depths to estimate key properties of RCC specimens such as composite dielectric constant, material conductivity, and reflection coefficient. The new methodology increased the practicality of using the TDR to obtain dielectric constant and associated composite material fractions using economic and disposable metal probes. The main objective of this paper is to use the composite dielectric found from the new TDR approach and present a new approach to practically estimate the free water and fresh RCC properties.

3.2. Experimental Program

The main objective of the experimental program is to determine the free water content and density of fresh RCC specimens at different depths from an exposed surface. The measurements were taken using the TDR for different aggregate gradation and curing conditions. The use of TDR is facilitated by using disposable metal probes to obtain voltage traces and then using the transmission line equation to estimate the dielectric constant considering other electrical properties of the RCC mix, such as the reflection coefficient and the material conductivity (Issa et al. 2021; Lee et al. 2008). In this work, the TDR 200 instrument by Campbell scientific was used. This instrument is designed to detect the reflection response of the electromagnetic signal of the soil and use it to empirically estimate the volumetric water content or/and electrical conductivity. In this paper, disposable metal probes were inserted and kept in the RCC specimens to take measurements at 1.5, 4.75, and 8.75 inches from an exposed surface. TDR traces were collected at 1, 2, 4, 6, 8, 24 hours to study the early age properties of RCC mixes.

3.2.1. Materials and Specimen Preparation

In this study, three aggregate sizes were used: coarse limestone with a maximum size of ¾ inch, intermediate limestone, and river sand. Two aggregate gradations were formed from these aggregate grades. The aggregate gradations were representative of the specified lower and upper limits of aggregate gradation established in the soil compaction mix design shown in Table 1. In Table 1, the lower limit blend consisted of 54.16 % coarse limestone, 12.3% intermediate limestone, and 33.55% river sand, while the upper limit blend consisted of 20.08% coarse limestone, 15.13% intermediate limestone, and 64.79% river sand. Based on the common practice in RCC mix design,

initial cement content was assumed as 450 Ib/yd3, while the specific gravities for cement and combined aggregate were estimated as 3.15 and 2.63, respectively. The initial mix designs to establish the moisture-density curve are shown in Table 2. The ASTM D1557 method-procedure C for determining the optimum moisture content and maximum dry density was used to form the final mix design. For the lower limit aggregate blend, the optimum moisture content is 5.4 %, and the associated maximum dry density is 137.2 Ib/ft3. For the upper limit aggregate gradation to determine the optimum moisture content of 6.3 % and the associated dry density is 146.1 Ib/ft3. Based on the optimum moisture content found from the proctor test, the initial material quantities were re-proportioned for one yard or 27 ft^3, as shown in Table 3.2.

Table 3.1 Specified LL and UL limit and developed blends

Sieves	Sizes (mm)	Lower bound (passing %)	Upper bound (passing %)	Lower Limit blend (Passing%)	Upper limit blend (Passing%)
1"	25	100	100	100.00	100.00
3/4"	19	90	100	93.00	100.00
1/2"	12.5	70	90	73.62	90.22
3/8"	9.5	60	85	60.00	85.00
No. 4	4.75	40	65	41.42	71.01
No. 8	2.36	30	52	28.26	52.00
No. 16	1.18	20	40	20.90	37.08
No. 30	0.6	14	31	14.00	26.72
No. 50	0.3	8	22	6.31	11.92

Sieves	Sizes (mm)	Lower bound (passing %)	Upper bound (passing %)	Lower Limit blend (Passing%)	Upper limit blend (Passing%)
No. 100	0.15	6	18	1.01	1.74
No. 200	0.075	2	8	0.48	0.83

Table 3.2 RCC mix design

RCC Constituents	Initial Mix Design (lb/yd^3)		Final Mix Design (lb/yd^3)	
	Lower limit	Upper limit	Lower limit	Upper limit
Cement	450	450	450	431
Combined Dry Aggregate wt.	3511	3587	3497	3432
Mixing water	214	254	213	243

ASTM C1435 was followed to prepare four 6-inch by 12-inch RCC cylinder specimens. ASTM C1435 was followed to compact RCC specimens using a vibrating compaction hammer. The plastic cylinders were previously prepared for insertion of the two disposable metal probes at 1.0 inches horizontal spacing by drilling holes into the plastic cylinders at 1.5 inches, 4.75 inches, and 8.75 inches from the exposed surface. After compacting the RCC material specimens, two 3.5 inches of metal probes were inserted through the duck taped holes in the plastic samples. The length of probes was kept between 3 inches (7.5 cm) to 6 inches (15 cm) to follow the manufacturer's

requirements (Campbell Scientific 2017). An insertion path was drilled into the RCC specimen before the placement of metal probes. 0.5 to 0.75 inches of the inserted metal probes were kept exposed to allow a female alligator clip attached to a coaxial cable to take measurements. Figure 3.1 shows a schematic representation of the specimen preparation. First measurements were taken at different depths from the exposed surface within 1 hour after mixing the RCC specimens

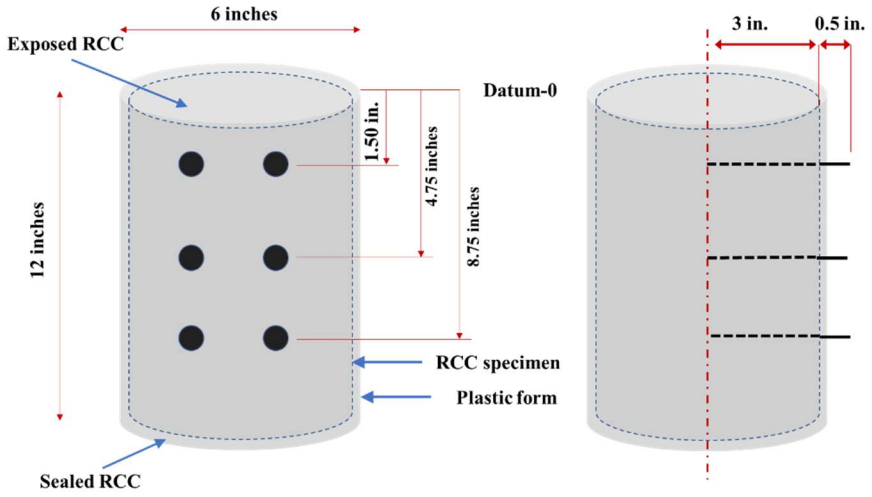

Figure 3.1 Specimen Preparation

To investigate time-dependent moisture distributions in the early age of RCC specimens, two specimens with each aggregate gradation were subjected to two curing methods: air curing and moisture room curing. The one-dimensional water diffusion in concrete was modeled by exposing only the top surface of the cylindrical specimen to the curing method. This one-dimensional diffusion process was conserved throughout the test time by casting the concrete into 6 x 12 inches plastic cylinders and preventing water evaporation from the sides and bottom of the specimen. One specimen of each

aggregate gradation was placed at a room temperature of 20°C to air dry, and one specimen of each aggregate gradation was placed in the moisture room with 100% relative humidity and 20°C. The specimen matrix is shown in Table 3.3.

Table 3.3 Test matrix

Test Type	Parameter	Purpose (s)	Variables	No. specimens
RCC electrical properties	Curing methods	Effect of curing on moisture distribution	- Air curing - Moisture curing	2
	Aggregate gradation	Effect of aggregate gradation on moisture distribution	- Lower limit - Upper limit	2
	Total Number of Specimens			**4**

3.3. Research Approach

In this paper, Material characteristics such as the volumetrics of free water content, air content, reacted and unreacted cement of RCC specimens at a different depth from the surface is estimated using the composite dielectric constant. These characteristics can then be used to estimate the wet unit weight and the degree of hydration at different depths from the surface. To estimate the mentioned characteristics, the following steps are required:

I. Fit the TDR voltage trace with the transmission line equation to find the dielectric constant at different depths with time

II. Use the dielectric constant to find the volumetric solids, water, and air contents using System Identification (SID) solution

III. Calibrate material characteristics to estimate the volumetric content of reacted and unreacted cement, the free water content, and the calibrated air content

IV. Estimate wet unit weight and degree of hydration using the calibrated characteristics volumetric content in step III

3.3.1. Composite Dielectric Constant

The composite dielectric constant is determined by fitting the transmission line equation to the voltage vs. time trace response obtained from the TDR. Fitting the TDR traces using the transmission line equation removes systematic errors such as assuming the unity of RCC mixture magnetic permeability or the noise produced from the probe orientation, length, and spacing. This equation accurately reflects the actual physics of wave transmission through a dielectric medium and determines conductivity and reflectivity, and the dielectric constant of the surrounding medium. The equation to calculate the relative voltage in time travel was developed by Issa et al. 2021. The equation can be expressed as:

$$v(t) = \left(e^{-\frac{\sigma t}{2\varepsilon\sqrt{\varepsilon_0}}} + \Gamma_L * (1 - e^{-ct}) \right) \qquad (3\text{-}1)$$

Where v(t) is the relative instantaneous voltage in terms of the time of travel of microwave, σ is the material conductivity (S/m), t is time in seconds, ε is the dielectric constant of the composite material (i.e., RCC), ε_0 is the electric permittivity of free space and equals to $\frac{1}{36} \times 10^{-9}\mathrm{F/m}$, Γ_L is the reflection coefficient, and c is a calibration coefficient.

3.3.2. Solid, Water and Air of RCC Mixes

To investigate the RCC mix characteristics with time as well as establish the moisture profile, the volumetric water content should be estimated. The self-consistent model described in Lee et al. 2012 was used. A generalization for the self-consistent model is presented in Eq.(3-2). Lee et al. 2012 estimated the water content by calculating the dielectric constant of individual concrete constituents (i.e., aggregate, hydrated cement, and unreacted cement). In this paper, the same concept is employed to identify the volumetric content of RCC constituents. However, the solution was further simplified by assuming that the fresh RCC constituents include solids (i.e., aggregate, hydrated, and unreacted cement), water, and air. Therefore, Eq. (3-2) can be explained in terms of volumetric contents and dielectric, as shown in Eq.(3-3), which is aligned with the original form of the equation presented in Lee et al. 2008.

$$\sum_{i=1}^{n} v_i \left(\frac{\varepsilon_i - \varepsilon}{\varepsilon_i + 2\varepsilon} \right) = 0 \qquad (3\text{-}2)$$

Where n is the number of components in a composite material, v_i is the volume fraction of component i ($\sum v_i = 1.0$), ε_i is the dielectric constant of component i, ε is the measured composite dielectric constant

$$\theta_s \frac{\varepsilon_s - \varepsilon}{\varepsilon_s + 2\varepsilon} + \theta_w \frac{\varepsilon_w - \varepsilon}{\varepsilon_w + 2\varepsilon} + +\theta_{Air} \frac{\varepsilon_{air} - \varepsilon}{\varepsilon_{air} + 2\varepsilon} = 0 \qquad (3\text{-}3)$$

Where, θ_s, θ_w, θ_{Air} the volume fractions of solids, water, and air, respectively. ε is the measured composite dielectric constant, ε_s, ε_w, ε_{air} are the dielectric constants of solids, water, and air, respectively. The dielectric constant of air can be taken as 1.0, while the dielectric of water can be assumed at 80. The volume fractions of RCC constituents are either time dependents such as water and air voids or fixed as aggregate. The unknowns in Eq. (3-3) are θ_w, θ_{Air}, ε_s . The θ_{Air} can be omitted by incorporating the fact that $\sum \theta_i = 1$. Hence, Eq. (3-3) can be further simplified as:

$$\theta_s \frac{\varepsilon_s - \varepsilon}{\varepsilon_s + 2\varepsilon} + \theta_w \frac{\varepsilon_w - \varepsilon}{\varepsilon_w + 2\varepsilon} + (1 - \theta_s - \theta_w) \frac{\varepsilon_{air} - \varepsilon}{\varepsilon_{air} + 2\varepsilon} = 0 \qquad (3\text{-}4)$$

The above equation can be solved by the System Identification (SID) method detailed in (Lee et al. 2008; Lee et al. 2012). The central concept of the SID method is the iteration around the composite dielectric constant (ε_c) to produce the unknown values (θ_w, ε_s) and the measured volume fractions at each iteration are compared with the measured dielectric constant (ε). The measured dielectric constant here corresponds to the dielectric constant found from the line transmission equation fitting, while the composite dielectric constant is the dielectric produced at each iteration. In that sense, the SID method conducts the least square method for two parameters at once. Therefore, it used matrix analysis for iteration until it stops whenever the change vector [β] is less than 0.05. The detailed procedure of the matrix analysis and related equations are discussed in (Lee et al. 2008). In this paper, once the change vector reaches less than 0.05, another restraint is checked as follow:

$$\theta_s + \theta_w + \theta_{Air} = 1.0 \qquad (3\text{-}5)$$

3.3.3. Calibrating Water and Air Content

The volumetric water content found from the system identification (SID) solution represents the total amount of water, which includes the free water as well as the chemically and physically bounded water. Moreover, the solid volumetric content and dielectric consist of the aggregate as well as the reacted and unreacted cement. To solve for the free water, reacted and unreacted cement, the volumetric content of aggregate ($\theta_{agg.}$) as a fixed value should be incorporated into the calculation. Knowing θ_{agg} and ε_s, Eq.(3-6) can be used to estimate the dielectric of the aggregate and dielectric of the combined reacted and unreacted cement. In the equation, the composite dielectric equals the dielectric of the solids found from the solution of solids, water, and air. It is worth noting that aggregate dielectric is constant and can be measured in the lab. In this case, however, the dielectric of aggregate includes the unreacted and reacted cement covering the aggregate particles. Therefore, it was assumed unknown.

$$\theta_{agg}\frac{\varepsilon_{agg} - \varepsilon_s}{\varepsilon_{agg} + 2\varepsilon_s} + \theta_{ruc}\frac{\varepsilon_{ruc} - \varepsilon_s}{\varepsilon_{ruc} + 2\varepsilon_s} = 0 \qquad (3\text{-}6)$$

Where, θ_{agg}, θ_{ruc} are the known aggregate and combined reacted and unreacted cement volumetric contents, respectively. ε_{agg} is the unknown dielectric of aggregate and ε_{ruc} is the unknown reacted and unreacted cement dielectric, and ε_s is the dielectric of solids. Using the SID method, the two unknowns ε_{agg} and ε_{ruc} can be found by iteration.

Finding the dielectric constant of reacted and unreacted cement ε_{ruc} can then be used to solve for the volumetric content of unreacted cement and reacted cement and the dielectric of the reacted cement using Eq. (3-7) below. In the equation, the composite dielectric is ε_{ruc} while the dielectric of the type III cement can be measured in the lab.

$$\theta_{uc}\frac{\varepsilon_{uc}-\varepsilon_{ruc}}{\varepsilon_{uc}+2\varepsilon_{ruc}}+\theta_{rc}\frac{\varepsilon_{rc}-\varepsilon_{ruc}}{\varepsilon_{rc}+2\varepsilon_{ruc}}=0 \qquad (3\text{-}7)$$

Where, θ_{uc}, θ_{rc} are the unknown volumetric content of unreacted cement and reacted cement, respectively, ε_{rc} is the unknown dielectric of the reacted cement, ε_{uc} is the known dielectric of the unreacted type III cement and equals 4.35, and ε_{ruc} is the composite dielectric of unreacted and reacted cement found in the previous step. Assuming that a 1-unit volume of water is required to thoroughly hydrate a 1-unit volume of cement, the calibrated free water content and air content can be found using the following equations.

$$\theta_{freewater} = \theta_w - \theta_{rc} \qquad (3\text{-}8)$$

$$\theta_{cal.air} = \theta_{Air} - (\theta_{rc} - \theta_{uc}) - \theta_{freewater} \qquad (3\text{-}9)$$

Where, $\theta_{freewater}$ is the volumetric content of free water in the mix, θ_w is the volumetric content of water found from solid, air, and water solution, θ_{rc} is the volumetric content of the reacted cement, $\theta_{cal.air}$ is the calibrated air content, θ_{Air} is the volumetric content of air found from the solid, air, and water solution, and θ_{uc} is volumetric content of the unreacted cement.

After finding the volumetric content of reacted and unreacted cement, the degree of hydration can be calculated by using the following equation (Lee et al. 2012):

$$\alpha\,(t) = \frac{\theta_{hc}(t)}{\theta_c} \qquad (3\text{-}10)$$

Where θ_{hc} is a time-dependent volumetric content of hydrated cement, θ_c is the original cement amount considering both have the same specific gravity.

In RCC specimens, a modification in the degree of the hydration equation is required. The RCC specimens are compacted using vibratory compaction, which can lead to a significant loss in the originally mixed cement paste. This loss can be represented by adding the cement loss to the original cement content in Eq.(3-10). The loss can be calculated by taking the difference between the original mixing water volumetric content and the first total water volumetric content measurement at any depth. To consider the time dependence of the hydration process, the evaporable water can also be considered by taking the difference between the first total water volumetric content measurement and the afterward total water volumetric content measurements. In both calculations, the difference in water content volumetrics is equivalent to the cement content volumetrics under the 1-1 water-cement assumption. Taking these two factors into account, Eq. (3-10) becomes:

$$\alpha\,(t) = \frac{\theta_{rc}(t)}{\theta_c + (\theta_{w0} - \theta_w(t) - (\theta_{w1} - \theta_w(t))} \qquad (3\text{-}11)$$

Where θ_{w0} is the original volumetric of mixed water content, $\theta_w(t)$ is the total water content at time t, θ_{w1} is the first total water content measurement after the specimen compaction.

3.3.4. Finding RCC material density

After determining the water content at different depths from the surface, the fresh unit weight (density) of the RCC specimen can be calculated using the following equation.

$$\gamma_{RCC} = (\theta_s + \theta_w) * G_s * \gamma_w \qquad (3\text{-}12)$$

Where, γ_{RCC} is the wet unit weight of RCC, θ_s is the volumetric content of the solid, θ_w is the volumetric content of the total water at any depth and time, G_s is the specific gravity of the RCC mix measured in the lab using ASTM C 127, and γ_w is the unit weight of water and equals 62.4 Ib/ft^3.

3.4. Results and Discussion

Dielectric constant measurements and its associated volumetric water content of two LL aggregate gradation (coarser gradation) and two UL aggregate gradation (finer gradation) specimens were taken with time at three depths from an exposed surface. The measurements were taken at 1,2,4,6,8, and 24 hours. One specimen of each aggregate gradation was air-dried, and one was placed in a 100% moisture room to investigate the effect of curing on moisture content profile and associated free water and wet unit weight. Figure 3.2 shows the moisture content for the four specimens with time. It is worth noting that these measurements do not account for the moisture loss that happened during the compaction of RCC specimens, which can be shown in the difference between the first-hour water content measurement and the mixing water. As shown in the figure, the overall volumetric water content measurements are trending down with time while exhibiting fluctuation in values relative to the depth of the measurements.

This can be related to the fluctuation of the composite dielectric constant measurements, which depend on the water content as well as the density at the measurement location. As mentioned earlier, the RCC specimens were cast into five layers using a vibratory compactor, where achieving adequate compaction effort is dictated by many subjective factors. Therefore, the volumetric water content at deeper depths (i.e., at 4.75 inches and 8.75 inches) in some cases shows a higher falling rate for the first 8 hours than the volumetric water content near the surface (i.e., at 1.5 inches). However, the volumetric water content at 1.5 inches shows a lower value throughout the testing period, which indicates the presence of a drying front in all cases except for the UL aggregate gradation with curing. In the LL aggregate gradation case, the specimen with no curing exhibits a higher falling rate than the specimen with curing within the first 8 hours. In the UL aggregate gradation, the same is noticed, but in this case, the sample with curing shows a linear decrease with time. Comparing the LL and UL aggregate gradation specimens, the following points are noticed i) the falling rate within the first 8 hours is higher in the LL aggregate gradation specimens than in the UL aggregate gradation specimens regardless of the curing, ii) curing helps the moisture-time curve to become close to linearity, this is especially noticed in the UL aggregate gradation with curing and, iii) the UL aggregate gradation seems to enhance the ability of the mix to retain moisture for a more extended period, which can impact the properties of RCC specimens.

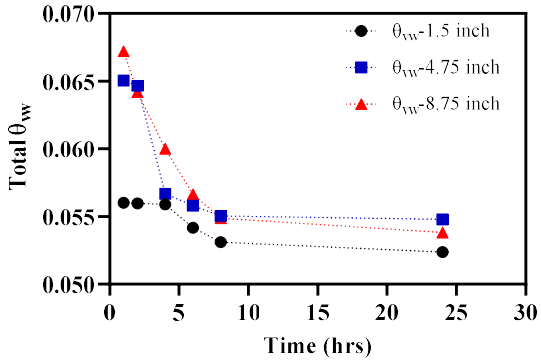

(a) LL aggregate with no curing

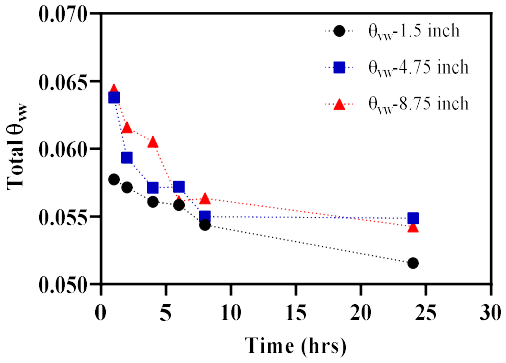

(b) LL aggregate with curing

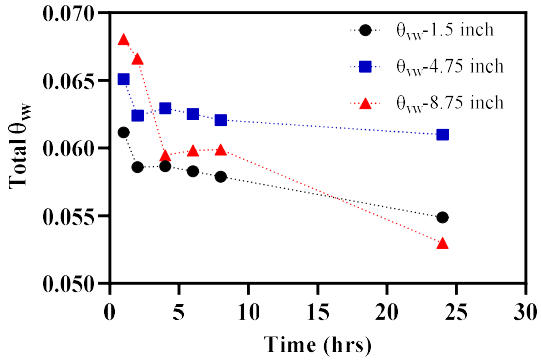

(c) UL aggregate with no curing

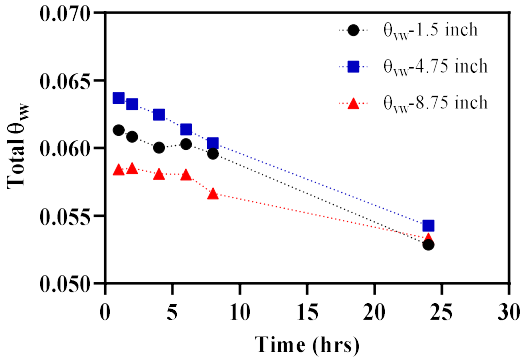

(d) UL aggregate with curing

Figure 3.2 Total water content with time

After determining the solid, air, and water of the RCC mix, the constant aggregate fraction was used to calculate the combined reacted and unreacted cement. The solution of volumetric contents of aggregate reacted and unreacted cement was performed to find the volumetric content of unreacted cement. Using the values obtained from this solution, the degree of hydration at a different depth from the exposed surface was established. Figure 3.3 shows the degree of hydration profile for both aggregate gradations with curing and no curing conditions.

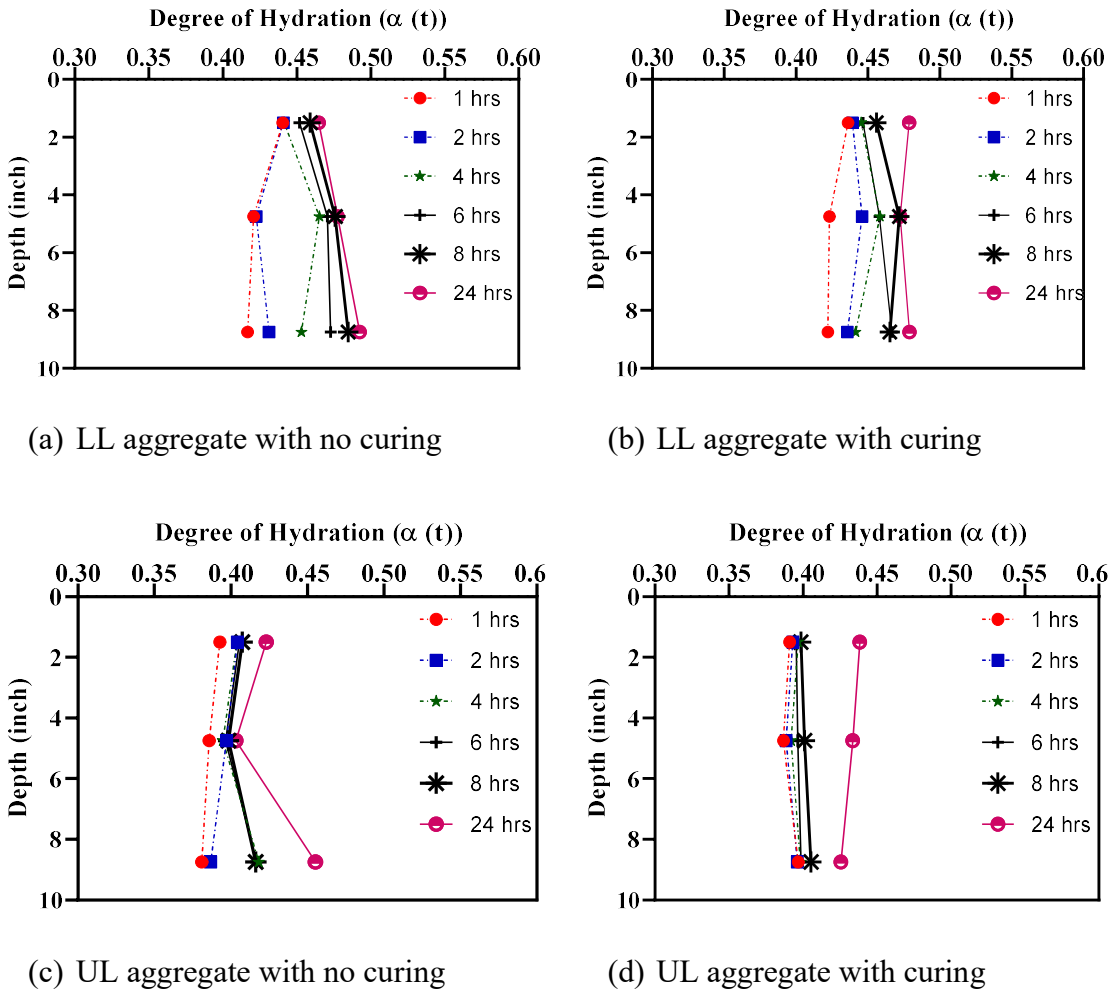

Figure 3.3 Profile of the degree of hydration with time

As shown in Figure 3.3, the degree of hydration for both aggregate gradations range between 0.40 and 0.50, and this reflects the strength of RCC specimens gained from low cement and water content as well as the compaction effort used to compact the specimens. In the UL aggregate gradation specimens, a uniform degree of hydration profile for the first 8 hours is shown, which indicates no significant volume change with depth during the first 8 hours. In the LL aggregate gradations, specimens show a gradual

change in the degree of hydration at each depth from the exposed surface. In the LL aggregate gradation specimens, curing shows an impact on the uniformity of the degree of hydration profile. In the UL aggregate gradation, the curing effect is shown in the degree of hydration after 24 hours at each depth from the exposed surface, indicating the development of higher strength than in the UL aggregate gradation specimen with no curing.

The volumetric water content at different times was used to establish the free water and calibrated air content profile. Figure 3.4 shows the free water for all specimens. Figure 3.4 (a) and (b) show a free water profile for LL aggregate gradation specimens where free water only exists at 4.75 inches and 8.75 inches from the exposed surface in the first and second hours but not later. On the other hand, Figure 3.4 (c) and (d) show the free water profile in the UL aggregate gradation specimens. Figure 3.4 (c) shows that free water is presented in all depths during the first- and second-hour measurements, but after that, the free water exists only at 4.75 inches from the surface before reaching 0 after 24 hours. On the other hand, free water in the UL aggregate gradation with curing exists in all depths and all measurement time until 0 free water content after 24 hrs. This shows how curing helps increase the moisture retention in the RCC mix, enhancing the overall properties of the mix. In both cases, the RCC mixture is considered an unsaturated mix where free water is not enough to fill the voids. Figure 3.4(e) and (f) show the calibrated volumetric air content of the UL aggregate gradation specimens at different depths. In both cases, the volumetric air content is inversely related to the volumetric of free water. Air content is the highest at 1.5 inches and the

lowest at 4.75 inches from the exposed surface except for the specimen with no curing during the first two hours. It is evident that the variation in the volumetric air content is more gradual and consistent in the sample with curing than the specimen with no curing.

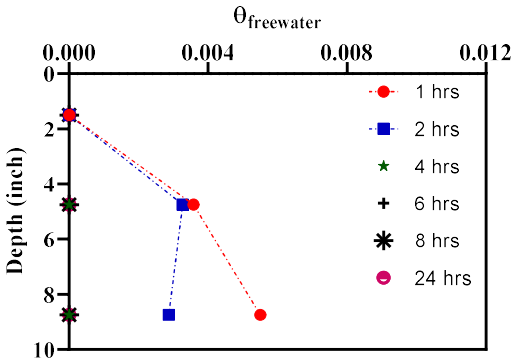

(a) LL aggregate w/o curing

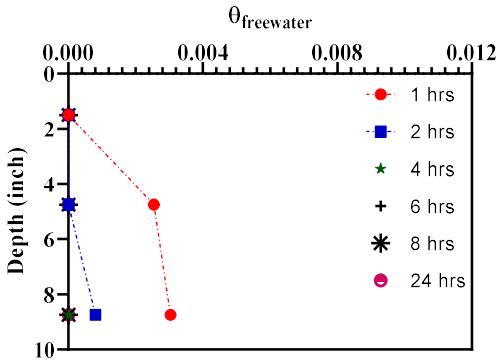

(b) LL aggregate w/ curing

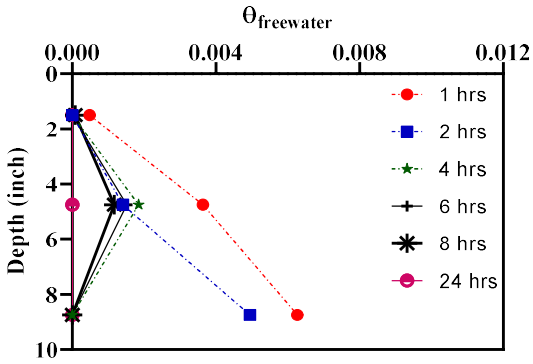

(c) UL aggregate w/o curing

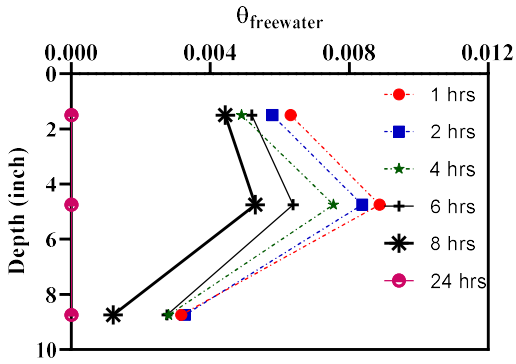

(d) UL aggregate w/ curing

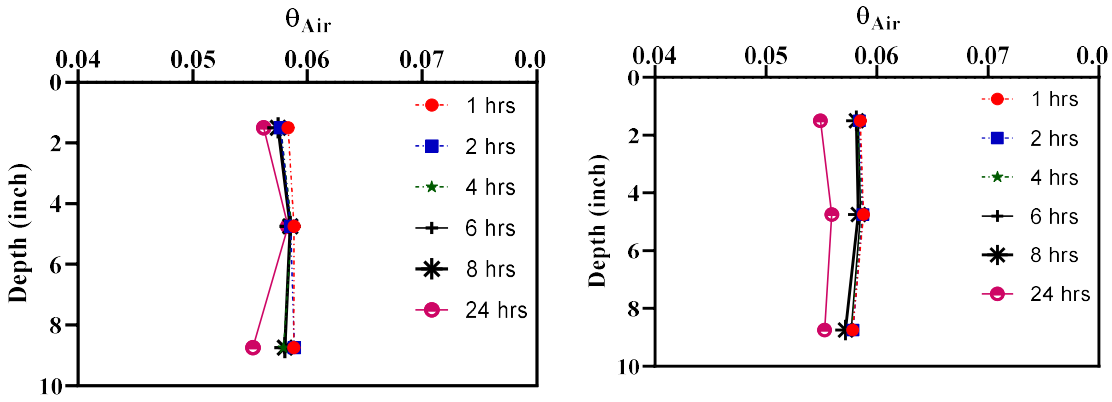

(e) UL aggregate w/o curing-Air content

(f) UL aggregate w/ curing-Air content

Figure 3.4 Profiles of free water and calibrated air content with time

The wet unit weight (density) of RCC specimens was also established relative to the composite dielectric constant and its associated water content. Figure 3.5 shows the wet unit weight profile for the tested samples. The specific gravity for the LL aggregate gradation mix was measured to be 2.47, while the specific gravity for the UL aggregate gradation was 2.44. The wet unit weight of the RCC specimens depends mainly on the water loss during compaction and the applied compaction effort. Therefore, two observations can be made from the wet unit weight profiles in Figure 3.5. First, as depth increases, the variation in wet unit weight decreases indicating a higher compaction effort at deeper depths, especially in the LL aggregate gradation mix. Second, the curing facilitates the development of uniform wet unit weight density profiles, especially in the case of the UL aggregate gradation mix.

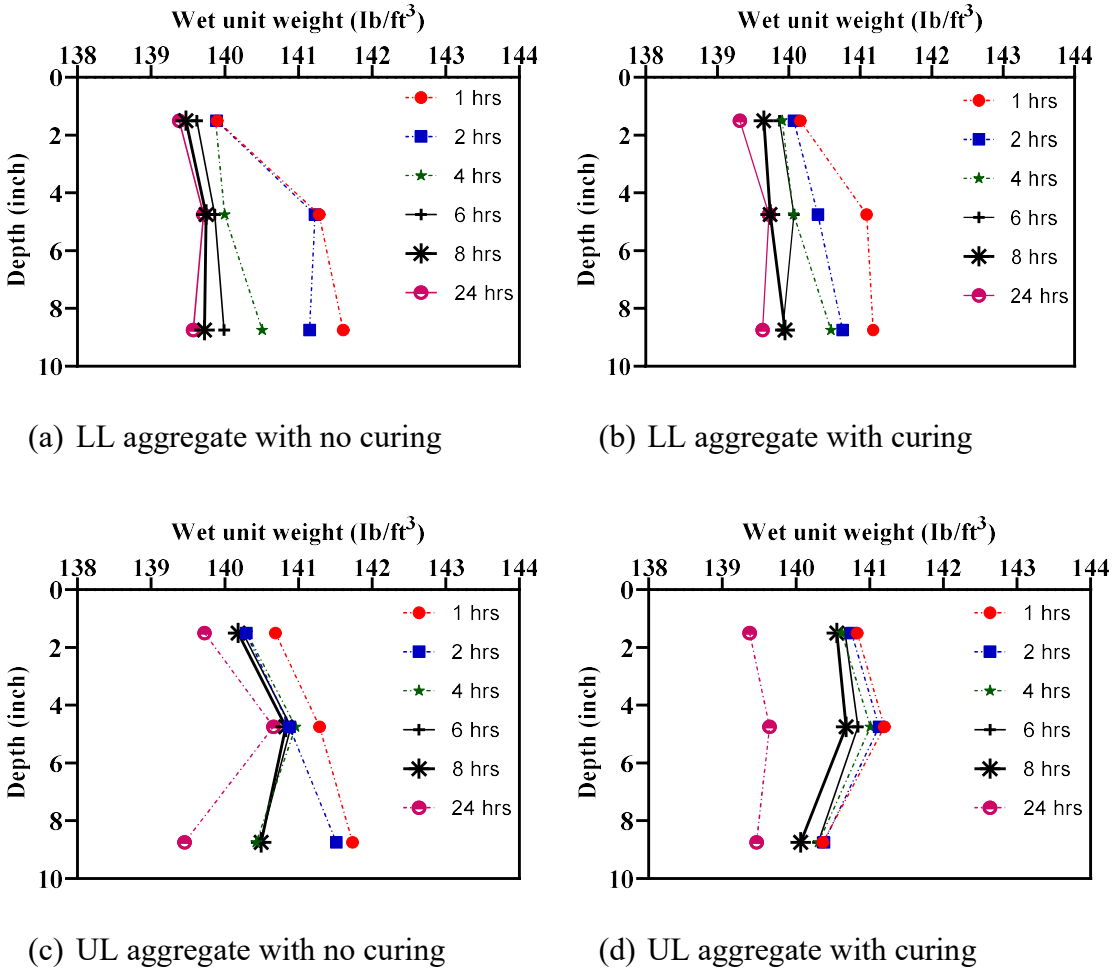

(a) LL aggregate with no curing (b) LL aggregate with curing

(c) UL aggregate with no curing (d) UL aggregate with curing

Figure 3.5 Profiles of wet unit weight with time

3.5. Conclusions

A new approach to estimate material properties of RCC specimens using a modified transmission line equation for TDR voltage traces and system identification solution for water content, air voids, and wet unit weight is developed and proposed in this paper. The proposed approach shows the following remarks about the material properties of RCC specimens:

1. The new approach estimated an accurate dielectric constant by fitting the voltage trace obtained from disposable metal probes using the transmission line equation considering other electrical factors such as material conductivity and reflection coefficient. The dielectric constant was then used in the system identification solution to calculate material properties such as volumetric of water content, air, solids, and the free water content, and the wet unit weight at different depths. This approach can be applied not only for RCC but also for any other composite material in which voltage traces can be obtained using disposable metal probes for a TDR instrument.
2. The volumetric content of total water shows that the RCC specimens have a drying front, meaning that water content is the lowest near the exposed surface at all measurement times. One exception is noticed in the sample with UL aggregate gradation with curing. The UL RCC specimens with UL aggregate gradation showed the ability to retain the moisture for a more extended period than the LL aggregate gradation. The same remark applies when comparing curing presence at each aggregate gradation. Curing reduces falling moisture rate during the first 8 hours for the LL aggregate gradation while it eliminates the rapid moisture falling in the first 8 hours in the UL aggregate gradation, which can be significant to the RCC's early age mechanical properties. Although curing has an apparent effect on moisture retention in both aggregate gradations, it has a more substantial impact on the UL aggregate gradation mix than LL aggregate gradation specimens.

3. The RCC specimens are unsaturated concrete mixes because a minimal amount of free water exists at all depths of the specimen. All free water obsoletes by the 24 hours measurements. In the LL aggregate gradation, free water exists only within two hours after casting. In UL aggregate gradation, free water exists only at 4.75 inches from the exposed surface after the first two hours. Curing preserves the free water in the UL aggregate gradation but not in the LL aggregate gradation. Knowing the free water allowed calibrating the volumetric air content, which showed an inverse relationship with the total water content and free water content. Also, the volumetric air content increases as the hydration process continue.
4. The wet unit weight in all specimens increases with the depth as an indication of better compaction and higher total water content. On the other hand, the variation of the wet unit weight decreases as depth increases, which means that the wet unit weight at greater depths is closer to the maximum wet unit weight than the wet unit weight near the exposed surface. The wet unit weight variation with time is more remarkable in specimens with the LL aggregate gradation than samples with the UL aggregate gradation. In both aggregate gradations, curing facilitated uniform wet unit weight profile, but it better impacted specimens with UL aggregate gradation.

Estimating the material properties of RCC specimens will facilitate the way to relate them to the mechanical properties of the RCC mix as well as understanding the RCC pavement behavior, especially the curling and warping behavior, placement density, and

development of long-term distresses. Using the new approach was found applicable for different RCC mixes under various curing conditions, and the same technique can also be used to estimate moisture, solids, and air content for many other composite materials. Advancement can be made in automating the process to calculate moisture, solids, and air directly from TDR voltage trace inputs.

3.6. References

Camp, P. R. and S. Bilotta. Dielectric Properties of Portland Cement Paste as a Function of Time Since Mixing. Journal of Applied Physics, Vol. 66, No. 12, 1989, pp. 6007-6013.

Korhonen, C. J., V. C. Janoo, and C. M. Berini. Time-Domain Reflectometry of Water Content in Portland Cement Concrete. Special Report 97-27, CRREL, US Army Corps of Engineers, 1997.

Chen,W., P. Shen , Z. Shui. Determination of water content in fresh concrete mix based on relative dielectric constant measurement. Journal of Construction and Building Materials, No. 34, 2012, pp. 306–312.

Jamil, M., M. K. Hassan, H. M. A. Al-Mattarneh , M. F. M. Zain. Concrete dielectric properties investigation using microwave nondestructive techniques. Journal of Materials and Structures. No. 46, 2013, pp. 77–87.

Lee, S., D. G. Zollinger, and R. L. Lytton. Determining Moisture Content of Soil Layers with Time Domain Reflectometry and Micromechanics. In Transportation Research Record: Journal of the Transportation Research Board, No. 2053,

Transportation Research Board of the National Academies, Washington D.C., 2008, pp. 30-38.

Lee, S.,I., and D. G. Zollinger. Estimating Volume Fraction of Free Water in Hardening Concrete by Interpretation of Dielectric Constant. Journal of Materials in Civil Engineering, American Society of Civil Engineers, Vol. 24, No. 2, 2012, pp. 159–167

Avelar Lezama I. Preliminary Non-Destructive Assessment of Moisture Content, Hydration and Dielectric Properties of Portland Cement Concrete. MS thesis, Texas A&M University, College Station, 2005.

Lytton, R. L. Backcalculation of Pavement Layer Properties. In Symposium on Nondestructive Testing of Pavements and Backcalculation of Moduli, Special Technical Publication 1026 (A. J. Bush III and G. Y. Baladi, eds.), ASTM, Philadelphia, Pa., 1989, pp. 7–38

Issa, M.I., Zollinger, D.G., Onifadi, I., Lytton, R. A Laboratory Approach to Determine RCC Mixture Electrical Characteristics Using a New TDR Interpretation Method. Transportation Research Record: Journal of the Transportation Research Board (TRR). 2021, (Accepted for publication)

4. MODELLING COMPACTIBILITY OF RCC SPECIMENS USING THE ASPHALT GYRATORY COMPACTOR[2]

4.1. Introduction

Roller Compacted Concrete (RCC) pavements provide an advantageous cost alternative over conventional concrete pavements due to the material used and the construction procedure. Also, RCC pavements have a plausible load-carrying capacity to bear occasional small vehicles such as cars a few hours following the placement, which can be vital in constructing high-speed roadways. However, density and workability are issues of durability present in RCC pavement construction. Unlike the conventional concrete, the RCC mix requires a High-Density Asphalt paver to place and a vibratory roller compactor to achieve density due to the dryness of the mix. To facilitate placement and compaction, the mix design starts by forming the aggregate 0.45 power gradation to compose a dense graded aggregate blend. Following the common practice, this blend can be used in the soil compaction test method, which follows the modified proctor compaction test, ASTM D 1557, to determine the optimum moisture content and maximum dry density for a range of cementitious material contents. The possibility of achieving uniform density over the thickness during the construction of RCC pavements is questionable due to the lack of a methodology to predict density, especially at higher RCC thicknesses prior to placement. The density of the RCC during placement depends

[2] Reprinted (with minor revisions) with permission from "Modelling compactibility of RCC specimens using the asphalt gyratory compactor" by Issa M. Issa, Dan G. Zollinger, 2021, published by the Journal of Construction and Building Materials, Copyright [2021] by Construction and Building Materials.

on the compactibility of the fresh RCC mix, which is dictated by the water and cement content, the aggregate gradation and types, as well as usage of additives. The optimum water content in RCC mixtures is limited to the modification, while the effects of aggregate gradation and usage of additives can still provide essential insight into the compactibility of RCC mixes. Multiple research efforts used slump-based tests to evaluate the consistency and compactibility of fresh RCC mixes. However, achieving the specified density on-site is directly related to the compaction effort, the mixture constituents, and the thickness of the RCC mix during placement. Therefore, estimating the energy effort required to compact different thicknesses of RCC mixes can be beneficial to enhance RCC placement. The hot mix asphalt Superpave Gyratory Compactor (SGC) can be used to simulate the compaction effort in the field as it provides a consistent loading effort during compaction. This constant loading can be used to evaluate the energy levels of different RCC mixes for a specific thickness and consequently estimate the energy required for greater thicknesses.

4.2. Background and Literature Review

Tests such as Vebe and Cabrera slump tests are commonly used to estimate the consistency as well as the compactibility of the RCC mixes (Hazaree et al. 2010; Khayat et al. 2019; LaHucik et al. 2018). These tests use a conventional concrete slump cone to record the time required for an RCC mix to change its shape from conical to a bulging cylindrical shape under vibration. Although the test setup and procedure between these tests may differ, they have the same concept of determining the ability of an RCC mix to change from one form to another. Such tests have been widely used in RCC for dam

construction (Hazaree et al. 2010). Using RCC as a paving alternative has reinitiated the concept of using the Vebe test to measure the compactibility of RCC mix (Hazaree et al. 2010; Khayat et al. 2019). However, based on research (Juvas 1990; Kappi and Nordenswan 2007), using such an approach to estimate the compactibility of the RCC mix is considerably subjective as well as it cannot be used to detect accurate compactibility differences between RCC mixes or provide sound technical performance. Therefore, researchers have investigated the use of a gyration compactor to facilitate fabricating specimens to emulate the field placement and study its performance (Juvas 1990; Kappi and Nordenswan 2007; Paakkinen 1986; Amer et al. 2003). The gyration compactor is used in hot mix asphalt sample preparation to predict the performance of asphalt pavement in the field, but it was validated in previous studies because of its accuracy and consistency in applying compaction effort. In previous research efforts, a gyratory compactor was mainly used to analyze sample density with the number of gyrations that allow for the determination of the number of gyrations sufficient to compact different sample thicknesses or different RCC mixes as well as study the mechanical properties of hardened RCC specimens (Hazaree et al. 2010, Amer et al. 2003). In this effort, the SGC effort is modeled using vibrational mechanics to determine the damping coefficient of specified upper and lower limit aggregate gradation mixes and determine the energy required to compact them. For each aggregate gradation, the effect of fly ash and water reducers on compactibility is also investigated in terms of density and energy.

4.3. Research Approach

The main objective of this effort is to develop a methodology for evaluating the required energy to compact RCC specimens using the SGC in the lab and the field. The RCC specimens were mainly divided into lower limit aggregate and upper limit aggregate gradations. For each aggregate gradation, the effect of replacing 25% of type I cement with fly ash and adding a water reducer to the optimum water content was investigated. To estimate the compaction energy required to compact RCC specimens, the following steps were followed:

1. Configure the RCC mix design for both aggregate gradation and compact specimens using the SGC to obtain displacement readings vs. gyratory numbers.
2. Develop a vibrational mechanic model to estimate the energy applied by the SGC
3. Estimate the behavior and energy associated with the compaction of thicker RCC specimens using the damping coefficients found for the original material and weight.

4.4. Experimental Program

Achieving a specified density during RCC placement requires an assessment of the RCC mix capacity to absorb energy during compaction to produce a well compacted RCC pavement through the entire layer thickness. To evaluate the density of an RCC mix, an instrument that outputs load vs. displacement along with a consistent test setup is needed. Given the previous experience in using the asphalt compaction procedure to determine the mechanical properties of RCC mixes *(*Kappi and Nordenswan 2007*,* Amer et al. 2003*,* Amer et al. 2007), adopting the use of an SGC was incorporated into the test program. The main objective of the program was to study the compaction behavior of

different aggregate gradation mixes and mineral and chemical admixtures under the use of gyratory compaction.

4.4.1. Instrumentation

In this work, a Pine AFG1 SGC was used. The SGC technology was developed during the Strategic Highway Research Program as part of the Superpave mix design system, which aimed at stimulating the compaction of hot mix asphalt (HMA) in the field (Cominsky 1994*;* Prowell 2003). Based on the study, the SGC should meet the specifications in the AASHTO T312, which can be summarized as:

(i) The axis of the ram should be perpendicular to the plate of the compactor

(ii) The ram should maintain a perpendicular pressure of 600± 18 KPa to the axis of the cylindrical specimen during the compaction

(iii) The compactor should apply a tilt angle of 22 ± 0.35 rad/m (1.25 ± 0.02°) and,

(iv) Specimens should be gyrated at a rate of 30 ± 0.5 gyrations per minute during the compaction (AASHTO 2001; Prowell 2003).

The consistency and accuracy of these compactors come from the automation of the compaction process, where the specimen is placed into a cylinder and compacted under constant ram pressure. The constant pressure is applied to a bottom plate inside the cylinder that contains the asphalt mix. This plate is constantly rotating at a specific gyration angle and frequency to provide a kneading pressure, which can be represented by the resultant force produced from the constant pressure and the plate angle. After each gyration, the sample is compacted, and the height change is recorded. Height

change can be used to calculate the volume change as well as the rate of compaction (volume change rate). Using the specified density, the compaction level (% density) after each gyration can be calculated by:

i) Determining the density of the specimen using the volume at each gyration and then,

ii) Dividing the density at each gyration by the specified density.

The Pine AFG1 compactor was found to meet all these specifications and criteria. Additionally, it provides the ability to obtain an accurate displacement measurement in millimeters after each gyration, which is the main component in modeling the compaction of the RCC specimen. Although the SGC was designed to simulate field compaction of asphalt concrete mixes, which is a viscoelastic material, using a similar machine and specifications for compacting RCC is much more efficient than developing a new methodology, especially when it is basically used to obtain displacements vs. time to model the amount of energy required to compact an RCC material.

4.4.2. Mix Design

The soil compaction design method was employed for the design of RCC mixtures. Three aggregate fractions were used in this study: a coarse fraction consisting of limestone with the maximum size of ¾ inch, an intermediate fraction consisting of a limestone aggregate, and a fine fraction consisting of river sand. For the coarse fraction, the aggregate was sieved on the 1 inch and #200 sieves to remove aggregate material larger than 3/4 inch and any minus #200 sieve size material. Two aggregate gradations were manufactured from these aggregate gradations. The blended aggregate gradations

were developed by comparison to specified lower and upper gradation limits for a maximum aggregate size of 3/4 inch. The lower limit blend consisted of 54.16 % coarse limestone, 12.3% intermediate limestone, and 33.55% river sand, while the upper limit blend consisted of 20.08% coarse limestone, 15.13% intermediate limestone, and 64.79% river sand. Figure 4.1 shows the blended aggregate gradations compared to the specified lower and upper limit aggregate gradations. The initial RCC mix designs were developed to establish the required moisture-density relationships for both aggregate gradations. Based on established practice, a cement content of 450 lb/yd^3 (267 Kg/m^3) was adopted, assuming specific gravities for cement and combined aggregate as 3.15 and 2.63, respectively. The initial mix designs to establish the moisture-density curve are shown in Table 4.1.

The ASTM D1557 C procedure, using the 6-inch diameter mold and material passing 3⁄4-in sieve, was followed to determine the optimum moisture content at the maximum dry density of the mixtures. For the lower limit aggregate blend, a range of moisture of 4.5%, 5.5%, 7.5%, 8.5% of the dry material weight was used to determine that the optimum moisture content as 5.4 %, and the associated maximum dry density is 137.2 lb/ft^3 (2197.73 Kg/m^3). The same water percentages were also used for the upper limit aggregate gradation to determine the optimum moisture content of 6.3 % and an associated dry density of 146.1 lb/ft^3 (2340.30 Kg/m^3). Based on the optimum moisture content found from the proctor test, the initial material quantities were re-proportioned for one yard or 27 ft^{3,} as shown in Table 4.1.

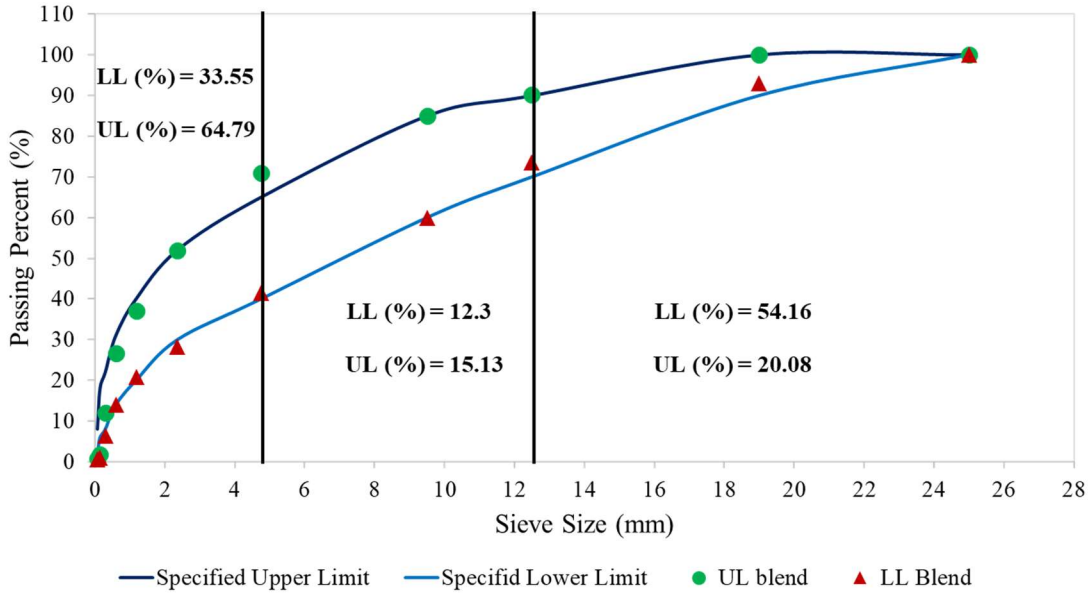

Figure 4.1 Upper and lower limit of aggregate gradation specification of RCC (Reprinted from Issa and Zollinger 2021).

Table 4.1 RCC mix design (Reprinted from Issa and Zollinger 2021).

RCC Constituents	Initial Mix Design- lb/yd^3 (Kg/m^3)		Final Mix Design- lb/yd^3 (Kg/m^3)	
	Lower limit	Upper limit	Lower limit	Upper limit
Cement	450 (267)	450 (267)	450 (267)	431(255.7)
Combined Dry Aggregate wt.	3511 (2083)	3587 (2128)	3497 (2074.7)	3432 (2036.1)
Mixing water	214 (127)	254 (150.7)	213 (126.4)	243 (144.2)

After determining the mix design of the lower and upper limit aggregate gradations, a test matrix was developed to determine the number of specimens required. In this paper, the compactibility of mixes with upper and lower limit aggregate gradation

was first investigated. For each aggregate gradation mix, one specimen was mixed by replacing 25% of the type I cement with a Class F fly ash. Another specimen was mixed with a Type F water reducer at a dosage of 390 ml/100 Kg of cement. These variations were used to investigate their effects on the compactibility of RCC mixes while keeping the original or control LL and UL mix proportions. For each sample, 4500 grams (9.92 Ibs) of the mixed material was used to fill out the compaction cylinder in order to get a sample thickness of around 4 inches. A total of six samples (three samples per aggregate gradation) were mixed and compacted for 25 gyrations, which was selected by trial whenever the UL and LL specimens' height records show less than 0.1 mm change during compaction for at least three consecutive gyrations.

4.5. Model Compactibility of RCC Specimens

The compactibility of RCC specimens with different aggregate gradation and additives was modeled using vibrational mechanics (Kleppner and Kolenkow 1973). The definition of vibration is the cyclic motion of a component or a structure. In the general case, vibration is undesirable, especially in structures, because it promotes damaging instability within the structure. However, it is desirable in many other cases, such as in non-destructive testing using ultrasonic pulses. Measurement of vibration is a function of the frequency level. In low-frequency applications such as the SGC, vibration is measured by the displacement transducer, which output displacement measurements proportional to an electrical signal. In order to study the vibrational mechanics of any component, the vibrational signal should be periodic by means that the vibrational signal (i.e., displacement) should repeat itself at fixed time intervals. This fixed time or period

(T) is defined as the time required for one cycle of vibration to complete. The number of vibrational signals in a specific time is dictated by the frequency (f) of applied vibration, which is equal to the reciprocal of period T. As mentioned before, the SGC is designed to provide 30 gyration per minute, which means that T is equal to 2 seconds. This frequency can be angular in radians/sec, as in the case of the SGC, and can be expressed as:

$$\omega = 2\pi \mathrm{f} = \frac{2\pi}{T} \qquad (4\text{-}1)$$

Where ω is the angular frequency in rad/sec, f is the frequency in $sec^{-1,}$ and T is the period in seconds.

The frequency amplitude is another important factor to characterize vibrational action. Amplitude in physics is defined as the mean half of the signal's peak to peak amplitude. In engineering, however, the amplitude is the peak-to-peak displacements. In both cases, the peak is referred to as the loading and unloading of the periodic vibration signal. In the case of the SGC machine, there is only one directional and vertical loading action, which suggests taking amplitude as the maximum displacement at first gyration. This is an accurate assumption because the pressure in a Pine AFG1 compactor raises to a level of 600 KPa before starting the first gyration and then repeatedly thereafter at 2-second intervals. The displacement at the first gyration is given and can be used to estimate the amplitude of the system.

Vibration motion is usually analyzed using simple harmonic oscillations. One of the well-known and simple examples of this oscillation is the mass-spring system, which meets the following criteria (Kleppner and Kolenkow 1973):

I. The system has one degree of freedom, which means that the system can be described by one scalar value (i.e., displacement).

II. The system is linear where the equation of motion is linear by obeying Hooke's law, and the system will react with a restoring force (k) proportional to the displacement whenever the system is displaced from equilibrium, as shown in Eq. (4-2) below. However, the simple mass-spring system is a free vibration where the mass oscillates in an infinite constant displacement interval. Therefore, the damping coefficient c is usually added to the previous system to form the spring-mass dashpot system, which depends on the energy dissipation of the system that leads to the end of the free vibration, as shown in Figure 4.2.

$$F = -k * d \qquad (4\text{-}2)$$

Where F is the force from the restoring reaction due to displacement, k is the restoring reaction in the spring, and d is the displacement in the spring.

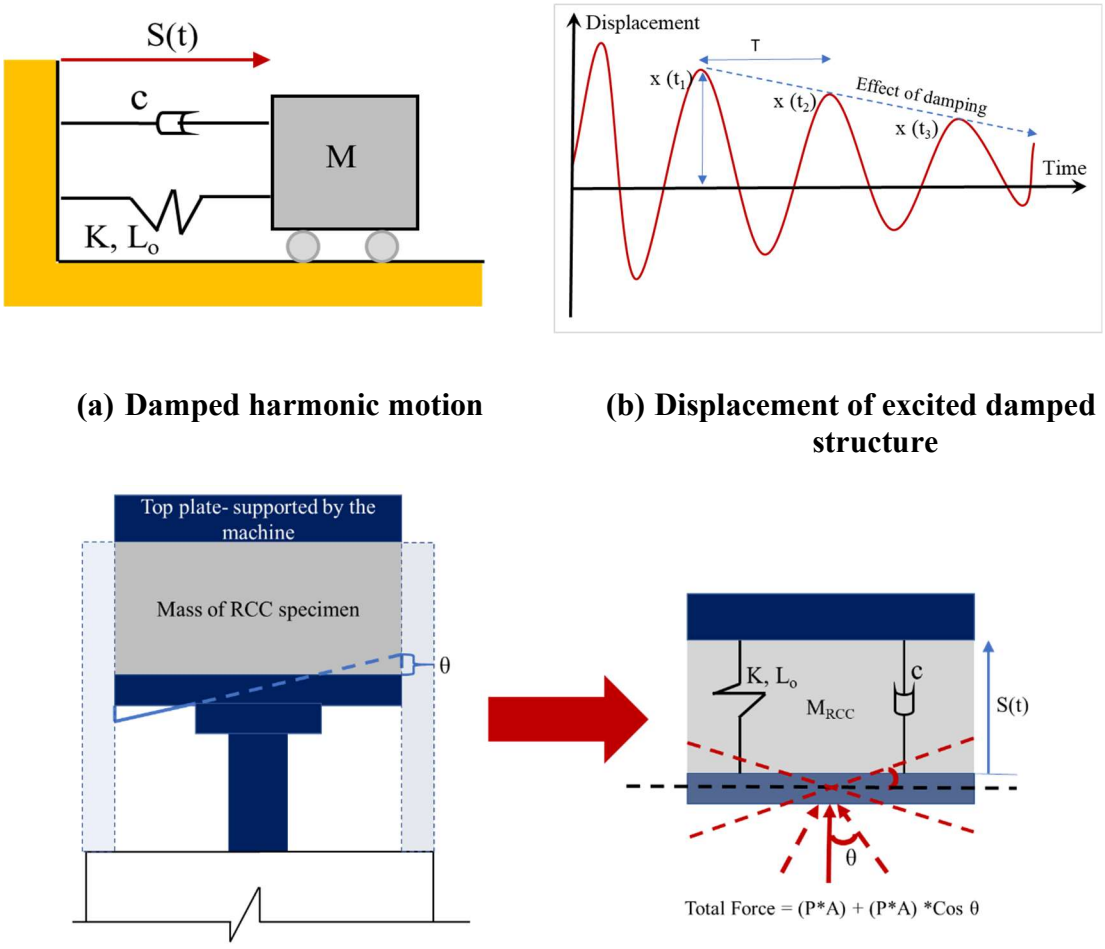

(a) Damped harmonic motion

(b) Displacement of excited damped structure

(c) Damped harmonic motion

Figure 4.2 Model Free Body Diagram (Reprinted from Issa and Zollinger 2021).

The material compactibility can be modeled using the forced vibration of a damped linear spring-mass system with one degree of freedom. However, two main changes are required to facilitate the use of this model in the compactibility of the RCC specimens. The first one is adding an external force into the damped spring-mass system shown in Figure 4.2 to replicate the pressure provided by the SGC ram. This constant pressure should be in a vertical, one-directional displacement throughout the gyration

period, which can eliminate the mass of the bottom plate held by the ram as well as omit the unloading part of the vibration system. The second change is simulating the damping coefficient and restoring reaction by the RCC material while considering the mass of the RCC material itself. Incorporating these two changes, the energy-based compactibility model can be configured as shown in Figure 4.2 (c). In this system, the constant vertical force is included along with the resultant force produced by the gyration angle. As shown in Figure 4.2(c), the gyration angle is constantly applied to the specimen while rotating. This action happens within 2 seconds, which is the period of each gyration. Therefore, the resultant force can be assumed to be constant throughout the SGC operation and can be added to the vertical force. Using the free body diagram presented in Figure 4.2 (c), the equation of motion can be formulated as follows:

$$F * (1 + cos\,\theta) = k * \big(Lo - s(t)\big) + m * \frac{d^2 s}{dt^2} + c * \frac{ds}{dt} \qquad (4\text{-}3)$$

Where F is the corresponding force from the applied pressure and the resultant force in KN, k is a time related restoring force in KN/m; L_o is the initial height before the first gyration, s(t) is the displacement at each gyration, m is the mass of the RCC specimen in Kg and c is the damping coefficient of the RCC specimen in N.s/m.

In the above equation, the unknowns are k and c. The displacement equation s(t) and damping coefficient are related and can be combined to find the damping coefficient. Therefore, the main unknown is k because it is changing with time or/and the number of gyrations. By taking these observations into account, the above equation can be rearranged to find k at each gyration or time.

$$\mathrm{k(t)} = \frac{F * (1 + \cos\theta) - \mathrm{m} * \frac{\mathrm{d}^2\mathrm{s}}{\mathrm{dt}^2} - \mathrm{c} * \frac{\mathrm{ds}}{\mathrm{dt}}}{(Lo - s(t))} \quad (4\text{-}4)$$

To evaluate the displacement at each gyration, the displacement equation of damped harmonic oscillation is used. This equation is usually used to determine the displacement in a mass-spring situation of a surface with friction or to evaluate the oscillation of a pendulum movement inside a viscous liquid. It was proven that the damped oscillation exhibits an exponential decay in the amplitude, which leads to the stopping of the initial oscillation effort (Kleppner and Kolenkow 1973). This equation can be applied to model the compactibility of RCC specimens by considering the mass, damping coefficient, and time. This equation can be articulated as follows:

$$s(t) = A * e^{\frac{-c*t}{2*m}} * cos\ (\omega t + \Phi) \qquad (4\text{-}5)$$

Where s(t) is the displacement at time t in seconds, A is the amplitude in mm, c is the damping coefficient in N.s/m or Kg/sec, m is the mass of the RCC specimen in Kg, ω is the angular frequency of the load and Φ is the phase lag between the applied force and the response of the material which depends on the frequency as well as the properties of a mass-spring system. In a constantly forced system, the lag phase is approximately zero and can be neglected. In addition, Eq.(4-5) represents the loading and unloading vibration, which can be depicted by the cosine term. However, the response of the SGC shows the damping effect on the SGC displacement readings under the constant applied load. Therefore, the cosine term can be eliminated, and the equation can be further simplified as:

$$s(t) = A * e^{\frac{-c*t}{2*m}} \qquad (4\text{-}6)$$

This equation provides two important inputs that can be used in the equation to find k at different displacements. The first input is the damping coefficient of different RCC mixes, which can be determined by fitting the equation to the displacement vs. time data obtained from the SGC. The second input is the displacement in terms of time, which can be used to calculate the distance (L_o-s(t)) in the denominator of Eq. (4-4).

4.6. Results and Discussion

As discussed previously, estimating the energy required to compact RCC specimens can be a reliable representation of the compactibility of RCC mixes prior to placement. To evaluate the energy required to compact different RCC specimens, four main steps were performed in this part:

1. Analyze the SGC data and calculate the density of the RCC specimens
2. Fitting the displacement vs. time data to find the damping coefficient (c)
3. Apply the new model to calculate the energy applied by the SGC during the test
4. Evaluate the compactibility in terms of density and energy of thicker RCC specimens using the damping coefficient found from step 2

4.6.1. SGC Data Interpretation

The Pine AFG1 compactor provides the gyration number and displacement in mm at each gyration for each specimen. The first step after obtaining these data is to evaluate the density acquired during the 25 gyration cycles. Figure 4.3 below shows the number of gyrations with displacement for all six samples. This figure shows that specimens with an upper limit aggregate gradation have a lower displacement range than

specimens with lower limit aggregate gradation. The upper limit gradation range was 0 to 15 mm, while the lower limit gradation range was 0 to 25 mm, which means that the initial displacement in the UL aggregate gradation specimens is closer to the maximum dry density than specimens with LL aggregate gradation specimens. However, additional analysis to determine the density percentage at each gyration is required.

To estimate the density, the volume change was calculated from the displacement outputs at each gyration. The density percentage was then calculated in terms of volume by dividing the volume at each gyration by the volume associated with the maximum dry density obtained from the moisture density curve for each aggregate gradation. To calculate the volume of the maximum dry density, Eq. (4-7) was used. In this equation, the mass remains constant at 4500 g for all RCC mixes while density is equal to the maximum dry unit weight for each gradation, which is 146.1 Ib/ft^3 (2340.29 Kg/m^3) for the UL aggregate gradation and 137.2 Ib/ ft^3 (2197.7 Kg/m^3) for the LL aggregate gradation. By using the equation, the volume at a maximum density of UL aggregate gradation is 0.068 ft^3 (0.00192 m^3), and for LL, aggregate gradation is 0.0723 ft^3 (0.002 m^3). The same equation is used at each gyration, where mass and volume are known to calculate the density. Figure 4.3 shows the percent of density in terms of height change during the gyration process. In both cases, the control specimens show lower density percent throughout the SGC gyrations. In both cases, the control specimens achieve a high density of 98% after 25 gyrations. In comparison, specimens with additives showed higher initial and final densities than the control specimens. In the case of LL aggregate

gradation, the density reached 99.9% for the specimen with 25% fly ash and 99.4% for the specimen with the water reducer. On the other hand, the density of specimens with UL aggregate gradations reached 97.5% and 98.6% for the 25% fly ash and water reducer additives, respectively. Overall, specimens with UL aggregate gradation show higher initial density than specimens with LL aggregate gradation, while the latter achieved a higher final density.

$$\rho = \frac{m}{v} \qquad (4\text{-}7)$$

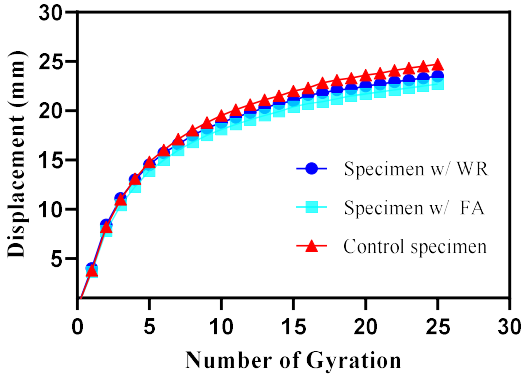

(a) RCC with Lower Limit gradation

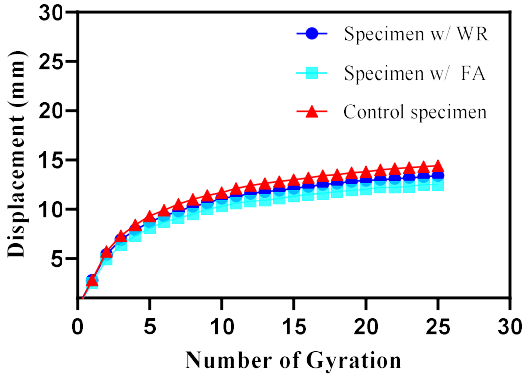

(b) RCC with Upper Limit gradation

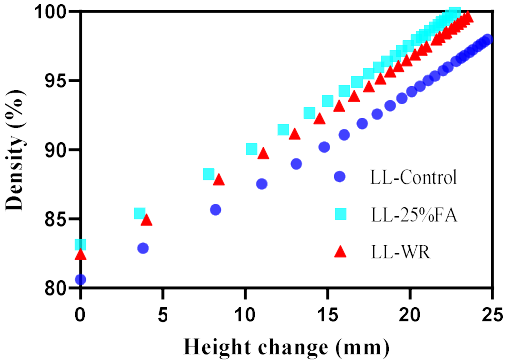

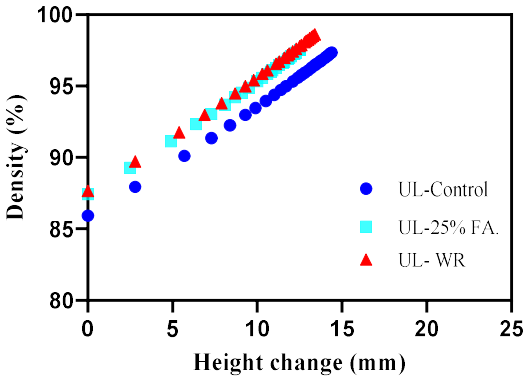

(c) RCC with Lower Limit gradation (d) RCC with Upper Limit gradation

Figure 4.3 SGC data and density calculation with height change (Reprinted from Issa and Zollinger 2021).

4.6.2. Computation of Energy Applied by the SGC

After determining the density of the compacted specimens, the model developed earlier was used to calculate the restoring reaction at each gyration, as well as the energy applied by the SGC to achieve the calculated densities. Therefore, the first step was to find the damping coefficient and amplitude of each mix by fitting the displacement Eq.(4-6) to the SGC obtained data. Finding the damping coefficient is significant in facilitating the use of the displacement equation to calculate the restoring reaction at each gyration using Eq. (4-4). Figure 4.4 shows the fitting of the displacement equation to the SGC data for the control specimens. Other specimens exhibited the same fitting curve. Therefore, Table 4.2 shows the amplitude and damping coefficient for each specimen with different aggregate gradations and additives. As shown in the table, the amplitude for the LL aggregate gradation mixes is 1 mm higher than the amplitude for the UL aggregate gradation mixes. As seen in the table, although the overall damping coefficient for both mixes is low, it is higher for specimens with the UL aggregate gradation than for the specimen with LL aggregate gradation. This is a very important note because it means that RCC mixes do not efficiently dissipate energy. On the other hand, energy dissipation is higher in specimens with UL aggregate gradations than in specimens with LL aggregate gradations, and this can be validated by the energy calculations in the next step. In both aggregate gradations, the damping coefficient

increase with the presence of additives. In LL aggregate gradation, the damping coefficient is the highest with adding 25% fly ash, while it is the highest when using water reducers in the UL aggregate gradation mix.

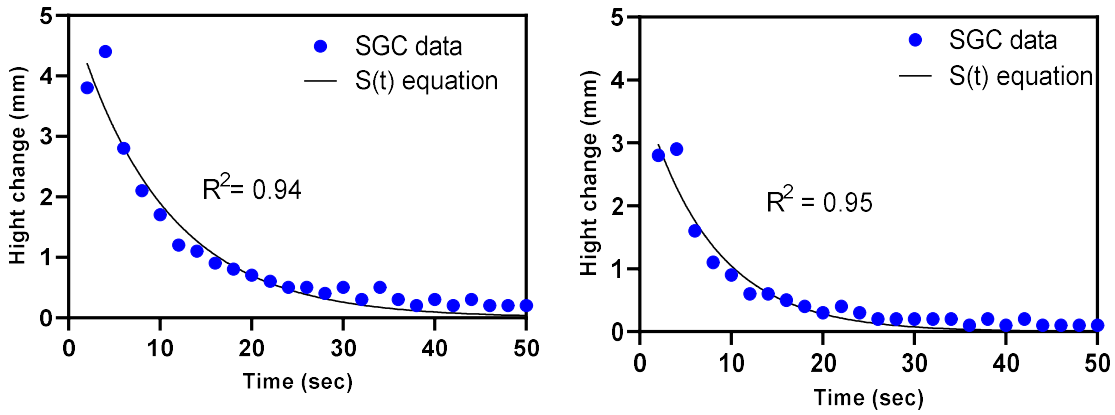

(a) LL aggregate gradation- no additives specimen

(b) UL aggregate gradation- no additives specimen

Figure 4.4 Displacement equation fitting of the SGC data (Reprinted from Issa and Zollinger 2021).

Table 4.2 Displacement Equation-Fitting coefficients and R-squared (Reprinted from Issa and Zollinger 2021).

Aggregate Gradation	Specimen	Amplitude (mm)	Damping coefficient c (N.m/sec)	R-squared
Lower limit	Control	5.145	0.899	0.94
	25% fly ash	4.955	0.942	0.94
	Type F water reducer	4.753	0.931	0.97

Upper limit	Control	3.883	1.181	0.95
	25% fly ash	3.406	1.191	0.95
	Type F water reducer	3.808	1.250	0.96

After determining the amplitude and damping coefficient for each specimen, the model developed earlier was used to determine the energy at each gyration, as well as the cumulative energy required to achieve the calculated final densities. Using the SGC data to calculate the energy, the displacement equation can be used to obtain the damping coefficient while the displacement at each gyration is already given by the SGC. Therefore, Eq.(4-8) below is used to calculate the total mechanical energy. Using the equation below, along with the time-related restoring force (K), the cumulative energy for specimens with LL and UL aggregate gradation is presented in Figure 4.5.

$$E = \frac{1}{2} * K * \left(L_o - s(t)\right) + \frac{1}{2} * m * v \quad (4\text{-}8)$$

Where E is the mechanical energy in KN.m; K is the restoring force in KN/m; L_o is the length of the specimen at zero gyration; s(t) is the displacement in the specimen at each gyration;m is the mass of specimen in Kg; v is the velocity in m/sec which is the derivative of the displacement equation (ds/dt).

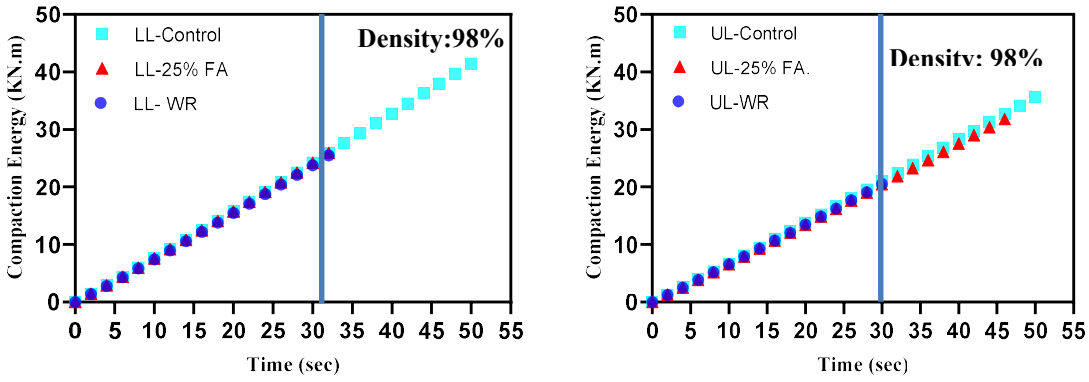

(a) RCC with Lower Limit gradation (b) RCC with Upper Limit gradation

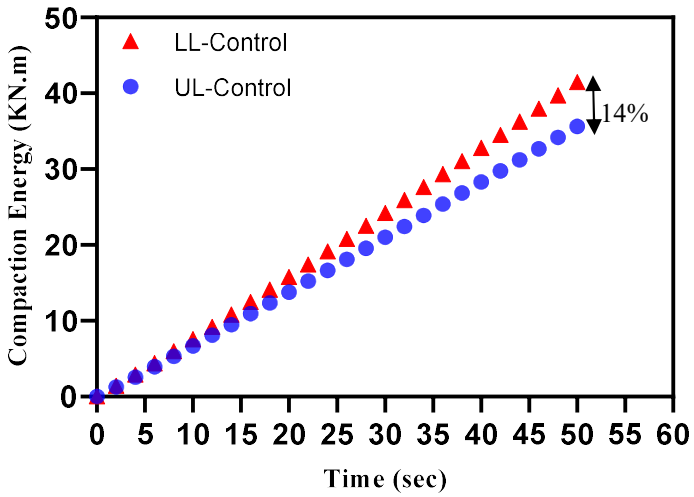

(c) RCC with LL and UL gradation comparison

Figure 4.5 Compaction energy with time representation (Reprinted from Issa and Zollinger 2021).

Figure 4.5 (a) and (b) shows the cumulative energy required to compact the 4500 g RCC specimens with different mixes. In Figure 4.5 (a), the cumulative energy with time is presented for LL aggregate gradation control specimens compared to the specimens with the 25% Fly Ash and water reducer. To be accurate in this comparison,

the maximum density achieved by the control specimen was used to allocate the associated cumulative energy required for all specimens. As shown in the figure, the control specimens required 25 gyration (or 50 seconds) to achieve a density of 98%, while specimens with 25% fly ash and water reducer required 16 gyration (or 32 seconds) to achieve the same level of compaction. These results show that additives can play a significant role in the compactibility of an LL aggregate gradation. The same comparison was made for the UL aggregate gradation specimens in Figure 4.5 (b). As shown in the figure, the control specimens required 25 gyrations to achieve 98% of density, followed by the specimen with 25% fly ash, which achieved the same level of density after 22 gyrations, and finally, the specimens with the water reducer achieved the same level of density in 15 gyrations. In the UL aggregate gradation case, results show that additives also affect the compactibility of a UL RCC. However, the effect of the water reducer is much higher than the effect of adding 25% fly ash, which can be explained by the high percentage of fines already present in the UL aggregate gradation. Furthermore, a comparison of the energy level between the UL and LL aggregate control mixes is represented in Figure 4.5 (c). As shown in the figure, specimens with LL aggregate require higher energy at each gyration level. The difference in energy level between the two aggregate gradation mixes increased with time until it reached 14% at 25 gyrations (50 seconds). This can be explained by the difference in fineness modulus between UL and LL aggregate gradation. The fineness modulus of UL aggregate gradation is 4.14 while it is 5.35 for LL aggregate gradation, which means that UL aggregate gradation is finer than LL aggregate gradation and consequently requires

lower energy to achieve a specific density level. As the specified density increases, the difference in required energy level between UL and LL aggregate gradations increases.

4.6.3. Assessment of density and energy of thicker RCC specimens

Determining the damping coefficient of different RCC mixtures in the previous step allows the assessment of thicker RCC specimens using the SGC. Mass of 4500 grams remained constant to prepare for SGC specimens and to compare behavior between different specimens. This mass is associated with 105.41 mm (4.15 inch) thickness at maximum dry density for specimens with UL aggregate gradation and 112.44 mm (4.43 inch) at maximum dry density for specimens with LL aggregate gradation. The damping coefficient found for each mix is constant and can be used to assess the density and energy required to compact greater thicknesses. In order to accomplish this assessment, the displacement equation was used to fit the data for greater thicknesses with their associated masses. In the displacement equation, all factors are known except the amplitude, which changes with different thicknesses. Under constant compaction effort, as thickness increases, the amplitude decreases. Four thicknesses of each RCC mix were used in this assessment. Considered thicknesses and their masses are listed in Table 4.3 below.

Table 4.3 Studied thicknesses and associated mass (Reprinted from Issa and Zollinger 2021).

Thickness- mm (inch)	LL aggregate gradation		UL aggregate gradation	
	Mass- Kg (Ib)	Amplitude-mm (inch)	Mass- Kg (Ib)	Amplitude-mm (inch)
127 (5)	5.09 (11.22)	4.38 (0.172)	5.41 (11.93)	3.44 (0.135)
177.8 (7)	7.12 (15.71)	3.45 (0.136)	7.58 (16.70)	2.75 (0.108)
228.6 (9)	9.16 (20.19)	2.87 (0.113)	9.74 (21.48)	2.31 (0.091)
304.8 (12)	12.21 (26.93)	2.33 (0.092)	12.99 (28.64)	1.89 (0.074)

The density of RCC specimens at 25 gyrations, considering the thicknesses listed in Table 4.3, was estimated using the displacement equation and its associated volume change. Figure 4.6 (a) and (b) shows the density after 25 gyrations for LL aggregate gradation and UL aggregate gradation mixes. In both cases, the density decreases with an increase in thickness. However, the rate of change in specimens with the LL aggregate gradation is higher than specimens with the UL aggregate gradation. For instance, the density of the LL aggregate gradation mix of 127 mm (5 inches) specimens with no additives is 95.15%, and the density of 304.8 mm (12 inches) specimen with the same mix is 87.5% compared to 96.87% and 92.0% for the same thicknesses of RCC with the UL aggregate gradation. This indicates that specimens with the UL aggregate gradations have more compactibility than specimens with LL aggregate after the same gyration number. Also, in Figure 4.6 (a) for the LL aggregate gradation case, specimens with additives have a higher density than the control specimens at all thicknesses. This

can be noticed in the specimen with 25% fly ash, which manifests the greatest density in all studied thicknesses. This indicates the importance of additives in the LL aggregate gradation. On the other hand, additives in specimens with the UL aggregate gradations have a lower impact in general, and specimens with water reducers achieved the greatest density of all studied thicknesses. As shown in Figure 4.6 (b), the effect of fly ash increases as thickness increases. This can be noticed by comparing the density of the control specimens to the specimens with 25% fly ash over different thicknesses.

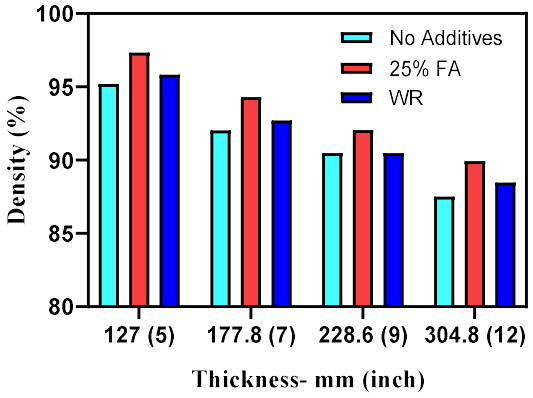

(a) RCC with LL aggregate gradation

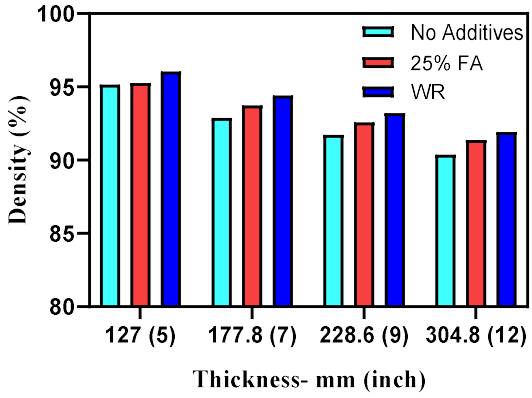

(b) RCC with UL aggregate gradation

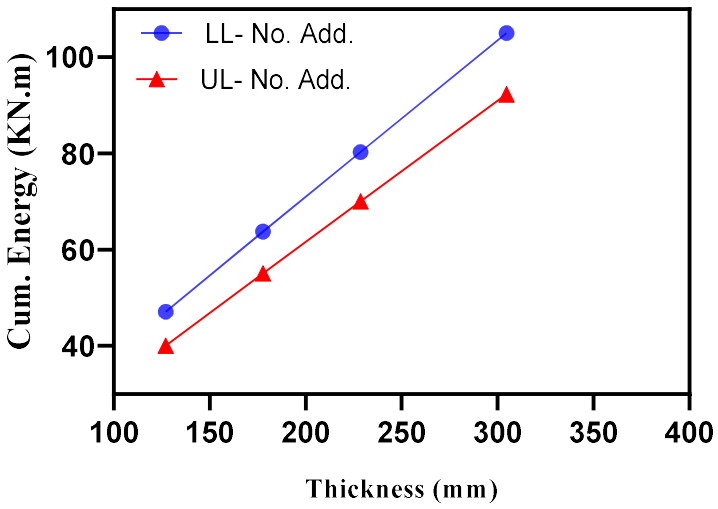

(c) RCC with LL and UL gradation-Energy level comparison at 25 gyration

Figure 4.6 Compaction energy with thickness comparison (Reprinted from Issa and Zollinger 2021).

The cumulative energy was also calculated for all specimen thicknesses with LL and UL aggregate gradations. The methodology discussed earlier was implemented to estimate the energy level for different RCC specimens' thicknesses at 25 gyrations. The cumulative energy at 25 gyration comparison between LL and UL aggregate gradation is made for different specimen thicknesses. As shown in Figure 4.6 (c), UL aggregate gradation required a lower energy level at 25 gyrations than specimens with LL aggregate gradation for all thicknesses. Despite the density being higher for specimens with UL aggregate gradation than specimens with LL aggregate gradations at higher thicknesses, the difference between the energy level increases as RCC specimen thickness increases. This difference starts at 5.6 KN.m when the thickness is 127 mm (5 inches) and increases to 9.7 KN.m when the thickness is 304.8 mm (12 inches).

4.7. Conclusions

A new methodology to estimate the energy applied by the SGC to compact RCC specimens is developed and proposed in this paper. The developed methodology revealed the following points about aggregate gradation and admixture use on the compactibility of RCC specimens:

1. The new methodology depends on the damping coefficient of different RCC mixes. A damping coefficient is a material property that indicates how efficiently a material absorbs energy. In RCC, the damping coefficient is low and ranges from 0.899 to 1.25 Kg/sec. These values represent the damping coefficient of the material itself, not the surrounding medium, as defined in the general application of vibrational mechanics. The damping coefficient is higher in specimens with UL aggregate gradation than specimens with LL aggregate gradation, which means that specimens with UL aggregate gradation have a higher capacity of absorbing energy and therefore obtain greater initial densities at a lower compacting effort.
2. The new methodology makes it possible to calculate the energy required to obtain the densities of RCC specimens as a percent of the maximum dry density by calculating the volume change of the RCC specimens. In all cases, the energy required to compact RCC specimens is greater in LL aggregate gradations than UL aggregate gradations, while the maximum dry density of UL aggregate gradations is much higher. The main reason for this observation is that UL aggregate gradation has a lower fineness modulus and higher surface area than

LL aggregate gradation, which requires less energy level to obtain a specific density level.

3. The fly ash and water reducer additives used in both aggregate gradation mixes showed a significant impact on the compactibility of RCC in terms of density and energy level. Specimens with additives achieved higher densities than specimens with no additives at the same gyration number and consequently required a lower energy level to achieve those densities. Additives had a greater impact on LL aggregate gradation specimens than UL aggregate gradation. In specimens with the LL aggregate gradation, both additives showed the same impact, with 25% fly ash being slightly more effective than water reducers. This can be related to the fact that fly ash has a more spherical shape than cement and requires less water, which enhances the compactibility of RCC mixes. On the other side, the water reducer has a greater impact on the specimen with UL aggregate gradation than the 25% fly ash.
4. The new methodology was used to calculate the cumulative energy and density of various RCC thicknesses after 25 gyrations. Specimen height study shows that UL aggregate gradation absorbs energy much more efficiently than LL aggregate gradation. This can be bolstered by the fact that the density of thicker specimens is greater in UL aggregate gradation mixes than LL aggregate gradation mixes. The energy level also increases as specimen thickness increases. This subsequently increases the difference in the energy level between LL and UL aggregate gradation specimens.

Modeling the displacement of the SGC effort and estimating the energy level of RCC specimens' compaction provides a new technique for RCC mix design optimization based on the placement thickness and density requirements. This effort can be developed by studying the effects of aggregate characteristics, such as smoothness and angularity, on the compactibility of RCC specimens, relating the density and its required energy with the field compaction procedure to systemize compaction effort, and suggesting a compaction protocol for different RCC mixes and thicknesses.

4.8. References

Issa IM, Zollinger DG. Modelling compactibility of RCC specimens using the asphalt gyratory compactor. Construction and Building Materials. 2021 Dec 6;310:125271.

Hazaree, C.V., Ceylan, H., Taylor, P., Gopalakrishnan, K., Wang, K., and Bektas, F. Use of Chemical Admixtures in Roller Compacted Concrete for Pavements. SN3243, Portland Cement Association, 2010, 54 pages

Khayat, K. H., Libre, N., A., Wu, Z. Roller Compacted Concrete for Rapid Pavement Construction. Report No. cmr 19-003, Missouri Department of Transportation, Construction and Materials Division, Jefferson City, MO, 2019.

LaHucik, R. J., Roesler, R. J. Material Constituents and Proportioning for Roller-Compacted Concrete Mechanical Properties. Report No. FHWA-ICT-18-014, Illinois Department of Transportation, Bureau of Research, Springfield, IL, 2018.

Juvas, K. J. Experiences in measuring rheological properties of concrete having workability from high-slump to low-slump. RILEM Colloquim on properties of fresh concrete, Hanover, West Germany, Chapman and Hall, 1990.

Kappi, A. and Nordenswan, E. Workability of No-Slump Concrete. Concrete International, USA, ACI, 29 (3): 37-41, 2007.

Paakkinen, I. Intensive Compaction Tester Device for testing the compactibility of No-Slump Concrete. Nordic concrete research report No.5: 109-116, 1986.

Amer, N., Delatte, N., and Storey, C. Using Gyratory Compaction to Investigate Density and Mechanical Properties of Roller-Compacted Concrete. Paper No. 03-3120 Transportation Research Record, Washington, DC, 2003.

Amer, N., Storey, C., and Delatte, N. Effect of Density on Mechanical Properties and Durability of Roller Compacted Concrete. SN2940, Portland Cement Association, Skokie, Illinois, USA, 61 pages, 2007.

Cominsky, R., R. B. Leahy, and E. T. Harrigan, "Level One Mixture Design: Materials Selection, Compaction and Conditioning." (SHRP-A-408). Strategic Highway Research Program, National Research Council, Washington, DC, 1994.

American Association of State Highway and Transportation Officials, "Standard Specifications for Transportation Materials and Methods of Sampling and Testing," ed. 21, Washington, DC, 2001.

Prowell, B. D., Brown, E. R.,Huner, M. Evaluation of the Internal Angle of Gyration of Superpave Gyratory Compactors in Alabama. NCAT Report 03-04, Alabama Department of Transportation, Montgomery, Alabama, 2003.

Kleppner, D., and Kolenkow R. An Introduction to Mechanics. McGraw-Hill, 1973.

ACI, 2005. “Guide for Consolidation of Concrete.” ACI 309R-05, Farmington Hills, Michigan

5. CHARACTERIZATION OF TRANSPORT PROPERTIES IN ROLLER COMPACTED CONCRETE BY INCORPORATING RCPT AND TDR

5.1. Introduction

The durability of concrete depends on its ability to resist the ingress of oxygen and moisture with deleterious materials. A quick and acceptable way to measure the permeability of concrete specimens includes using the Rapid Chloride Permeability Test ASTM C12022 and AASHTO T 227. The original procedure was presented by (Whiting 1981) to allow evaluating the permeability of concrete mixture to NaCl in bridge structure quickly as it pertains to the corrosion of reinforcements. Previous efforts evaluated the permeability by long-term bonding and measuring of either water and chloride solution with depth (Levitt 1973; Figg 1973; Cook 1951; Ruettger et al. 1935). Development of long-term testing was established in AASHTO T259 "Standard Method of Test for Resistance of Concrete to Chloride Ion Penetration" or so-called Salt Ponding Test and in the NordTest NTBuild 443 (i.e., Bulk Diffusion Test). The long-term testing, although it requires time, it presents an accurate estimate for the permeability of concrete specimen to NaCl by the actual measurement of the NaCl solution content with time. The RCPT test was a development of many research studies that concerned about the transport of chloride ions in a saturated concrete specimen by ionic diffusion as a predominant situation of the crack-free concrete specimens (Berman and Chiken 1974; Kondo et al. 1974; Clear 1976).

The Rapid Chloride Permeability Test or ASTM C1202 "Standard Test Method for Electrical Indication of Concrete's Ability to Resist Chloride Ion Penetration"

provides a qualitative measure of the permeability in concrete. This test method consists of monitoring the amount of electrical current passed through 2-in. (51-mm) thick slices of 4-in. (102-mm) nominal diameter cores or cylinders of saturated concrete during a 6-h period. A potential difference of 60 V dc is maintained across the ends of the specimen, one of which is immersed in a 3 % Sodium Chloride (NaCl) solution, the other in a 0.3N sodium hydroxide (NaOH) solution. The potential source is connected to the negative terminal in the NaCl solution and the positive terminal in the NaOH solution, which initiates the migration of the negatively charged ions toward the positive terminal and results in a current that mainly depends on the pore structure. The total charge passed over 6 hours' time, in coulombs (C), is then related to the resistance of the specimen to chloride ion penetration qualitatively using Table 5.1 to be related to the resistance of the specimen to chloride ion penetration. Table 5.1 provides a qualitative relationship between the results of this test and the chloride ion penetrability of concrete.

Table 5.1 Concrete permeability classification of ASTM C1202

Charge Passed (coulombs)	**Chloride Ion Penetrability**	**Typical Concrete Type**
> 4000	High	High w/c ratio (> 0.6)
2000 – 4000	Moderate	Moderate w-c ratio (0.40 to 0.50)
1000 – 2000	Low	Low w/c ratio (< 0.40)
100 – 1000	Very Low	Latex-modified concrete, internally sealed concrete
< 100	Negligible	Polymer-impregnated concrete, polymer concrete

The ASTM C1202 provides multiple benefits such as the simpleness and convenience of test and setup and procedure as well as the easiness of interpreting the results data, which make it relatively quick and preferred for quality control. However, it actually measures the electrical conductance rather than the real ingress of chloride ions. This paper presents a methodology to determine the amount of the solution over the time of the RCPT test by incorporating TDR measurements to interpret the dielectric constant and subsequently estimate the solution content. Furthermore, it uses the measured solution volumetrics with time to estimate the transport coefficients (i.e., diffusion and permeability) of RCC specimens. The paper also establishes a linear relationship between the solution volumetric with the charged passed.

5.2. Research Significance

The durability of concrete can be defined as the capability of the material by itself to keep the properties it originally possessed when initially placed over a certain period; durable concrete is concrete that in the particular environment of service resists the processes associated with a given environment that tend to cause it to disintegrate particularly in cases where a certain amount of maintenance may be lacking during its service life. A multitude of factors affects the durability of concrete either directly or indirectly. Some may be physical, while others may be inherent to the properties of a specific mix design. Transport properties (i.e., permeability and diffusivity) of concrete are believed to be the most important characteristic of concrete that affects its durability.

Decreased transport properties improve concrete's resistance to re-saturation, sulfate and other chemical attacks, and chloride ion penetration. Achieving a low

transport property of concrete normally requires the use of a low w/cm coupled with adequate moist curing. Concrete transport properties influence durability because it controls the rate of moisture ingress, which could contain an aggressive chemical, enters concrete and moves from point to point. The principal result of the intrusion of an element into concrete is the corrosion of the reinforcing steel, which is popular in bridge structures and concrete pavements containing reinforcing steel. Once this occurs, the integrity of the concrete will begin to disintegrate; the lifespan is reduced, and the general safety of the public could even be threatened.

In RCC, ingress of deleterious materials affects the rate of alkali-aggregate reaction and freeze-thaw damages. The RCPT provides an accelerated technique to evaluate the permeability of RCC specimens by estimating the charge passed through saturated specimens. However, it does not quantify the amount of NaCl solution actually ingresses during the test. Therefore, this paper proposes a methodology for quantifying the volumetric content of chloride solution with time. This is significant information that can be used to evaluate the transport properties of concrete. It also provides a prominent input to estimate the remaining service life of infrastructure. In this paper, the transport properties for RCC specimens are estimated by integrating the RCPT test with the TDR measurements for different aggregate gradations and additives.

5.3. Research Approach

In this effort, a methodology to quantify the solution volumetrics in the RCPT and relate it to the passed charges is developed. The test setup was modified to allow obtaining TDR traces. The TDR measurements were then interpreted to estimate the

dielectric constant of RCC samples, which can be used to calculate the volumetric solution content. The volumetric solution content was estimated at different times during the test to facilitate determining the diffusion coefficient and permeability coefficient of RCC samples, as well as developing a relationship between the volumetric solution and the charge passed.

The basic concept in this effort is to measure the voltage vs. time traces using the TDR whilst conducting the RCPT. A new TDR interpretation methodology proposed by Issa et al. 2021 allows fitting the voltage traces to estimate the electrical properties of RCC specimens. The new interpretation methodology uses disposable probes to facilitate taking the measurements after the concrete hardens. In this paper, the voltage traces were used in two main steps:

1. Fitting the TDR traces and estimating the dielectric constant at different times during the RCPT test
2. Estimate the volumetric of the solution associated with the dielectric constant using a self-consistent model

5.3.1. Fitting TDR traces

The composite dielectric constant is determined by fitting the transmission line equation to the voltage vs. time trace response obtained from the TDR. Fitting the TDR traces using the transmission line equation removes systematic errors such as assuming the unity of RCC mixture magnetic permeability or the noise produced from the probe orientation, length, and spacing. This equation accurately reflects the actual physics of wave transmission through a dielectric medium and determines the dielectric constant of

the surrounding medium, considering other electrical properties such as conductivity and reflectivity. The developed transmission line equation is detailed in Issa et al. 2021. The main equation can be expressed as:

$$v(t) = \left(e^{-\frac{\sigma t}{2\varepsilon\sqrt{\varepsilon_0}}} + \Gamma_L * (1 - e^{-ct}) \right) \quad (5\text{-}1)$$

Where v(t) is the relative instantaneous voltage in terms of time travel of microwave, σ is the material conductivity (S/m), t is time in seconds, ε is the dielectric constant of the composite material (i.e., RCC), ε_0 is the electric permittivity of free space and equals to $\frac{1}{36\pi} \times 10^{-9}$ F/m, Γ_L is the reflection coefficient, and c is a calibration coefficient.

5.3.2. Composite Dielectric Solution

The composite dielectric solution can be established in two steps and includes the following:

1. Measure the oven-dry reference dielectric constant and estimate associated volumetrics using the self-consistent model
2. Use the oven-dry volumetric contents to estimate the volumetric water content for the dielectric measured during the test

5.3.2.1. Oven-dry reference volumetrics and dielectric

The main step in determining the dry volumetric contents in RCC samples is eliminating the moisture in the samples by oven-drying. The reference dry dielectric constant can then be estimated by fitting the voltage reflection from a TDR measurement. The dielectric constant can be used to estimate the volumetric of voids,

the dielectric of solids, and the volumetric of solids by the self-consistent model. The self-consistent model has been used previously to estimate the volumetrics of the individual concrete components (Lee et al., 2008). It assumes that the composite dielectric constants (ε_c) of a composite material such as concrete vary relative to the individual volume fraction and dielectric of every component. Therefore, a generalization of the self-consistent model can be represented by:

$$\sum_{i=1}^{n} v_i \left(\frac{\varepsilon_i - \varepsilon}{\varepsilon_i + 2\varepsilon} \right) = 0 \qquad (5\text{-}2)$$

Where n is the number of components in a composite material, v_i is the volume fraction of component i ($\sum v_i = 1.0$), ε_i is the dielectric constant of component i, ε is the measured composite dielectric constant

The general equation (i.e., Eq.(6-2)) can be written to represent the dry RCC specimen as follows:

$$\theta_s \frac{\varepsilon_s - \varepsilon}{\varepsilon_s + 2\varepsilon} + \theta_{void} \frac{\varepsilon_{void} - \varepsilon}{\varepsilon_{void} + 2\varepsilon} = 0 \qquad (5\text{-}3)$$

Where θ_s and θ_{void} are the volume fractions of solids and voids, respectively. ε is the measured composite dielectric constant, ε_s, ε_{void} are the dielectric constants of solids and voids, respectively. The dielectric constant of the void can be taken as 1.0. Therefore, the unknowns in Eq. (5-3) are θ_s, θ_{void}, and $\boldsymbol{\varepsilon_s}$.

Eq. (5-3) can be solved by the System Identification (SID) method. The SID method iterates around the measured composite dielectric constant (ε) to produce the unknown values of θ_s, θ_{void}, and ε_s and compare the resulting values at each iteration

with the measured dielectric constant (ε). The SID method conducts the least square method for two parameters at once. Therefore, it uses matrix analysis for iteration until it stops whenever the change vector [β] is less than 0.05. The detailed procedure of the matrix analysis and related equations are discussed in reference (Lee et al., 2008). Once the change vector reaches less than 0.05, another restraint is checked prior to execution as follow:

$$\theta_s + \theta_{void} = 1.0 \qquad (5\text{-}4)$$

5.3.2.2. Finding the volumetric of solution

The dry volumetrics found from the first step can be further used to estimate the NaCl solution volumetric content with time. The measured dry dielectric constant can serve as a reference point for later measurements. The difference between the new dielectric constant obtained during the test from TDR measurements and the dry dielectric constant of oven-dry samples represents the volumetric of the solution at the location of the probes. To relate the dielectric constant difference with the volumetric of the solution, the complex refractive index model (CRIM) can be employed (Lezama 2007). The CRIM model assumes that a linear addition of individual dielectric characteristics is sufficient to estimate the composite dielectric of composite material (specifically for soil), as shown in Eq.(5-5). Therefore, recalculating the composite dielectric (i.e., the measured dielectric) using the estimated dry volumetric of solids and voids is required. The main point of recalculating the composite dielectric constant using the CRIM model is to incrementally consider the volumetric solution and draw a

relationship between the difference in composite dielectric constant and the NaCl solution volumetric content.

$$\varepsilon^a = \sum_i^n \theta_i \, \varepsilon_i^a \qquad (5\text{-}5)$$

Where ε is the calculated dielectric constant, a is a power regression coefficient can be assumed 0.5 (for granular material), θ_i is the individual volumetric of considered constituents, and ε_i is the individual dielectric of considered constituents.

In this test, the volumetrics of solid and air of dry concrete specimens remains constant throughout the test. Therefore, the difference in recalculated dielectric constants can be related to the volumetric of the solution using the following equation:

$$\theta_{sol.} = \frac{\Delta\varepsilon^{0.5}}{\varepsilon_{sol.}^{0.5}} \qquad (5\text{-}6)$$

Where $\theta_{sol.}$ Is the volumetric content of NaCl solution in the sample at probes location (1 inch from the surface of the sample), and $\Delta\varepsilon^{0.5}$ is the difference between the square root of recalculated dielectric constants. This difference increased incrementally to calculate the associated solution volumetric content. A 0.01 incremental change in volumetric of NaCl solution content was then drawn with the difference in the recalculated dielectric to establish a relationship. It is worth noting that the measured dry dielectric for RCC specimens ranged between 3 and 4 depending on the density of the compacted specimen and the constituents of the RCC mix. The relationship was established based on a dry dielectric constant of 4. Figure 5.1 shows the established linear relationship with an R-squared of 1.0, while Eq. (5-7) can be used for the

calculation of NaCl solution volumetric content based on the difference in dielectric constant.

$$\theta_{sol.} = 0.02421*\Delta\varepsilon + 0.0051 \qquad (5\text{-}7)$$

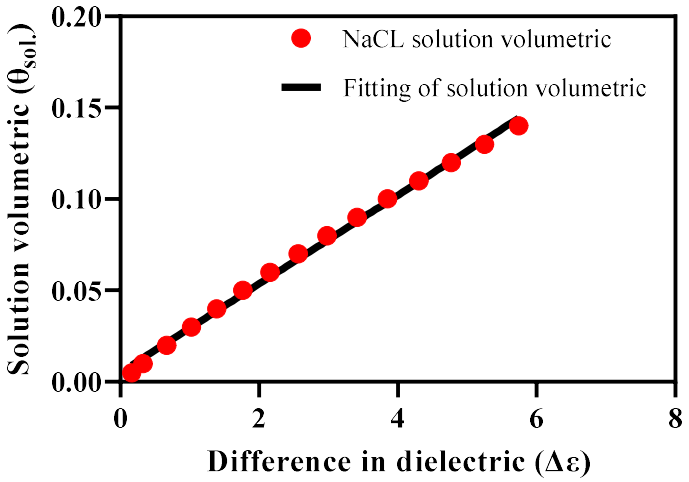

Figure 5.1 Difference in dielectric vs. Solution volumetric content

5.4. Experimental program

The main objective of the experimental program is to provide preliminary data on the proposed methodology. The testing program was designed to evaluate different factors affecting the permeability of the RCC specimens. The primary factor in this testing program is the aggregate gradation, while the second factor is using additives such as fly ash and water reducers. The fly ash and water reducers were incorporated in this study to provide replicate results for the same aggregate gradation and evaluate the effect of additives on the transport properties of RCC specimens.

5.4.1. Mix design

The soil compaction design method was employed for the mix design of RCC mixtures. Four aggregate grades were used in this study: No. 56 limestones, C rock, and F rock, as well as river sand. Coarse and intermediate aggregate types were sieved into their specific sieve size except for the river sand. Two aggregate gradations were then formed from these aggregate grades. The aggregate gradations were representative of the specified lower and upper limit aggregate gradation established in the soil compaction mix design Figure 5.2. The blended aggregate gradation was optimized by comparing with lower and upper specifications considering a maximum aggregate size of 1 inch for both gradations. The initial RCC mix designs were developed to establish the required moisture-density relationships for both aggregate gradations. Based on commonplace practice, an initial cement content was assumed as 450 Ib/yd3, while the specific gravities for cement and combined aggregate were taken as 3.15 and 2.63, respectively. The initial mix designs to establish the moisture-density curve are shown in Table 5.2 RCC mix design. Tex-113-E proctor test procedure using the 6-inch diameter mold was followed to determine the optimum moisture content at the maximum dry density of the mix. For the lower limit aggregate blend, a range of moisture of 4%, 6%, 8%, 9% of the dry material weight was used to determine that the optimum moisture content is 6.1% and the associated maximum dry density is 142.6 Ib/ft3. On the other hand, a range of moisture, 4%, 5.5%, 7%, and 8.5 %, was used for the upper limit aggregate gradation to determine the optimum moisture content of 7.2% and an associated dry density of 145.4 Ib/ft3. Based on the optimum moisture content found from the proctor test, the initial material quantities were re-proportioned for one yard or 27 ft3, as shown in Table 1. For

each aggregate gradation mix, one specimen was mixed by replacing 25% of the type I cement with a Class F fly ash. Another specimen was mixed with a Type F water reducer at a dosage of 390 ml/100 Kg of cement. These variations were used to replicate test results relative to the same aggregate gradation as well as investigate the effect of additives on the transport properties of RCC mixes.

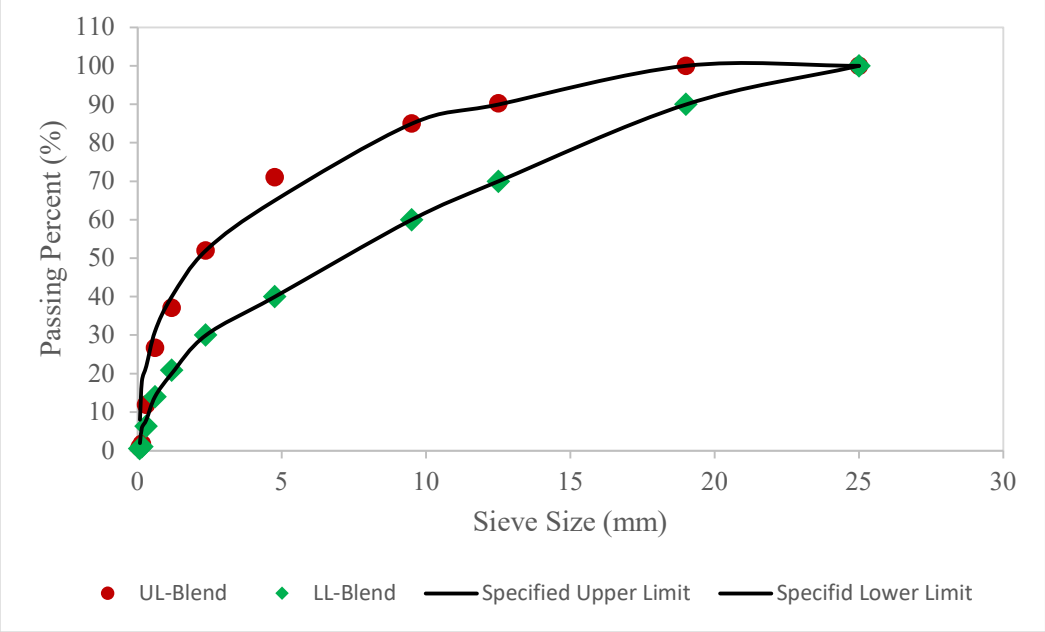

Figure 5.2 Upper and lower limit of aggregate gradation specification of RCC

Table 5.2 RCC mix design

RCC Constituents	Initial Mix Design (Ib/yd^3)	Final Mix Design (Ib/yd^3)

	Lower limit	Upper limit	Lower limit	Upper limit
Cement	450	450	479	461
Combined Dry Aggregate wt.	3300	3300	3513	3355
Mixing water	205.8	270	219	286

5.4.2. Specimen preparation and test setup

ASTM C1435 was employed to prepare 6 RCC cylinder specimens with dimensions of 101.6 X 203.2 mm. The plastic cylinders were previously prepared for insertion of the two metal probes at 1.0 inches spacing by drilling holes into the plastic cylinders at 101.6 mm from the exposed surface. The holes were duck taped prior to compaction of the RCC specimens to prevent water leakage during compaction. After compacting the RCC material specimens, two 89 mm disposable metal probes were inserted through the taped holes in the plastic specimens at mid-height (i.e., at 101.6 mm). To ensure the straightness of metal probes, an insertion path prior to placement of the probes was drilled with a small bit size. 25.4 mm of the probes were kept exposed to connect the female alligator clips, which are attached to the coaxial cable for taking TDR measurements. After 24 hrs, the plastic forms were removed and kept in the moisture room at 100 % RH and 20ºC for 28 days. Afterward, the RCPT test specimens were prepared by cutting the cylinder around the metal probes (i.e., 25.4 mm from probes at each side). The prepared specimens were then oven-dried for 24 hours under 100 C temperature to remove all moisture (Chen et al., 2011). Prior to placing the specimens in

the RCPT test, a TDR measurement was taken to establish the dry sample characteristics, especially the composite dielectric constant. In order to facilitate the TDR measurements, the metal probes were placed facing upward and away from any solution. Figure 5.3 shows the test setup of using TDR with the RCPT test. Once the ASTM C1202 Rapid Chloride Permeability test setup was completed, the RCPT test was run at 20 Volts. Originally, this test was conducted at 60 Volts, but the lower limit aggregate gradation specimens had too little resistance from the ion transfer, which caused exceeding the test equipment's amperage of 500 mA and stopping the test. A similar problem was faced at 40 Volts but after a long time into the test. Therefore, 20 Volts was considered appropriate to study the permeability in RCC specimens. At approximately every hour, the RCPT test was stopped to take TDR measurements to estimate the volumetric of the solution ingress with time.

Coaxial Cable to

Proove'it RCPT

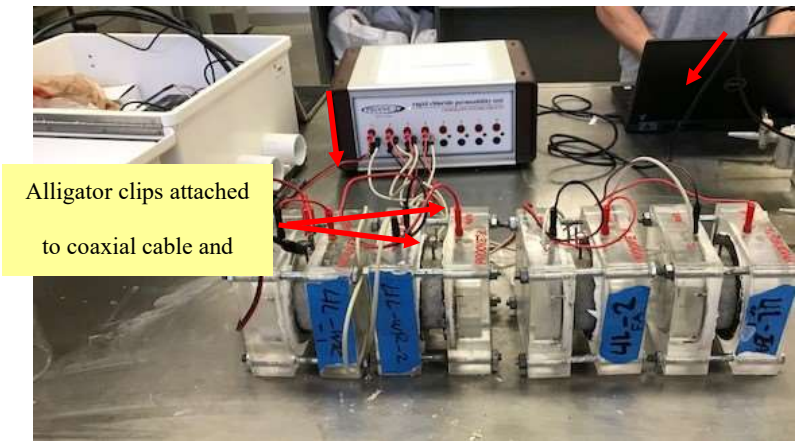

Figure 5.3 Test setup

5.5. Results and Discussion

In this study, RCC specimens with two aggregate gradations and two additives were investigated. Determining the solution volumetric condition with time along with the output of the RCPT test allows studying i) the diffusivity and permeability of RCC specimens and ii) the relationship between the volumetric solution content and the charge passed. The interpretation of the ASTM C1202 in this paper provides a quantitative measurement, which can help to set approximate but accurate values for the NaCL solution volumetric content and its relationship with time. Figure 5.4 shows the volumetric of NaCl solution with time for both aggregate gradations. It shows that the control specimen has higher volumetric values throughout the RCPT test time, indicating higher transport properties compared to specimens with additives. It is worth noting that in RCC, the compaction effort variability plays a significant role in reducing the volumetric of voids inside the specimen and hence affects the specimen's ability to allow ingress of more moisture. Therefore, a specimen with fly ash shows comparable solution

volumetric content in the case of LL aggregate gradation but not in UL aggregate gradation. This figure, along with RCPT inputs such as applied voltage and charge passed, serves as the basis for quantifying the transport properties of RCC specimens.

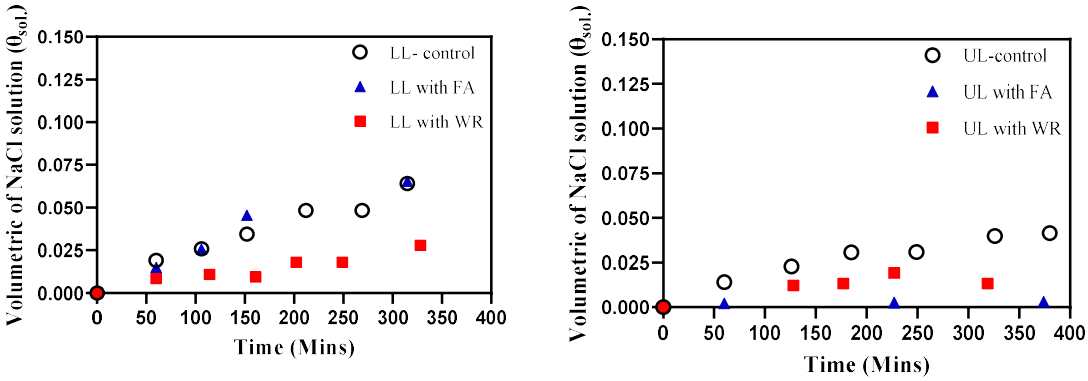

(a) LL aggregate gradation (b) UL aggregate gradation

Figure 5.4 Volumetric content of NaCl solution with time for LL and UL aggregate gradation

5.5.1. Diffusion of NaCl solution

The RCPT test is assumed to follow the one-dimension diffusion of moisture in concrete, which can be expressed using Fick's second law.

$$\frac{\partial \theta}{\partial t} = D \frac{\partial^2 \theta}{\partial x^2} \qquad (5\text{-}8)$$

Fick's second law solution depends on boundary conditions. The following solution of Fick's second law is incorporated in the RCPT is based on the chloride concentration (Germann Ins. 2014). As the boundary conditions remain constant, the same Fick's law solution can be used. The chloride concentration is replaced by the volumetric content as follows:

$$\theta(x,t) = \theta_s - (\theta_s - \theta_i)\,\mathrm{erf}\left(\frac{x}{2\sqrt{Dt}}\right) \qquad (5\text{-}9)$$

Where θ(x,t) is the volumetric content of solution at depth x and time t, θs is the volumetric content of the solution at the surface, θ_i is the initial concentration of the solution, which equals 0; x is the distance of the measurement; erf is the error function, and D is the diffusion coefficient in m^2/sec.

The volumetric at the surface θ_s can be considered equal to 1 because the solution at both terminals of RCPT test cells was kept at the same level of solution throughout the test. The initial concentration θ_i is equal to zero because the specimens were completely oven-dried before the test. Therefore, Eq. (5-9) can be rewritten as:

$$\mathrm{erf}\left(\frac{x}{2\sqrt{Dt}}\right) = 1 - \theta(x,t) \qquad (5\text{-}10)$$

Eq. (5-10) can be solved by numerical approximation to estimate $z = \frac{x}{2\sqrt{Dt}}$ in the error function. Eq.(5-10) can be written in terms of the diffusion coefficient in m^2/sec as follows:

$$\mathrm{D} = \frac{x^2}{4\,z^2 t} \qquad (5\text{-}11)$$

Figure 5.5 presents the calculated diffusion coefficient of both aggregate gradations with different additives. As shown in Figure 5.5, the diffusion coefficient for both aggregate gradations has slight differences. The difference in diffusion coefficient is clearly presented within the same aggregate gradation with different additives. In both cases, the control specimens have the highest diffusion with time coefficients compared to specimens with fly ash or water

reducer. Also, specimens with a water reducer have the lowest diffusion coefficient over the test time. The slight difference in diffusion coefficient between the aggregate gradation can be explained by the compaction density of the RCC specimen. This means that UL aggregate gradation had a lower compaction effort or achieved lower compaction density compared to its maximum dry density. Achieving the maximum dry density can also be the reason behind the lowest diffusion coefficient of RCC specimens with water reducer, as it was found to increase the compactibility of RCC (Issa and Zollinger).

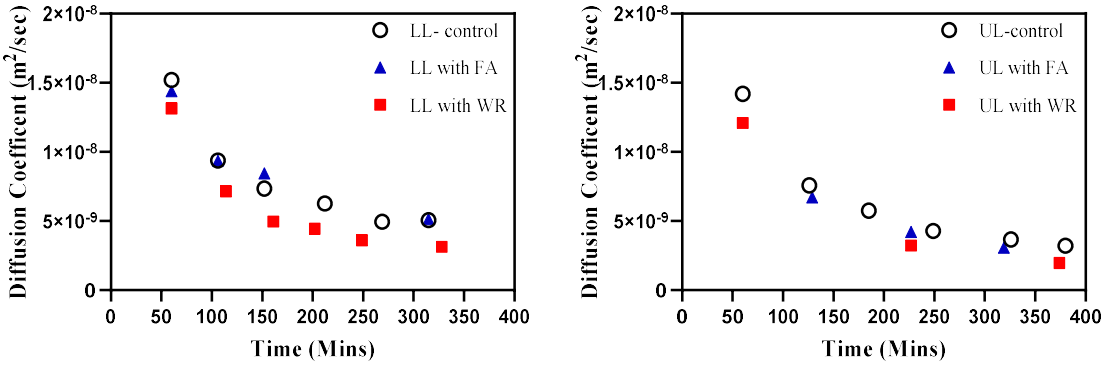

(a) LL aggregate gradation (b) UL aggregate gradation

Figure 5.5 Diffusion coefficient with time for LL and UL aggregate gradation

5.5.2. The permeability coefficient of the RCC mix

The coefficient of permeability can be calculated using Darcy's law. Eq. (5-12) was originally proposed in reference (Soongswang et al. 1988) based on the net inflow rate, and Darcy law was incorporated in this paper to estimate the permeability coefficients for LL and UL aggregate gradation RCC specimens.

$$K = \rho \frac{H}{P} \frac{Q}{A} \qquad (5\text{-}12)$$

Where K is the permeability coefficient in m/sec, ρ is the density of the 3% NaCl solution and equals to 1026.8 kg/m^3 (Simion et al. 2015), H is the height of specimen in m, P is the water pressure in N (Kg.m/sec^2), Q is the net flow rate in m^3/sec, and A is the cross-sectional area of the specimen in m^2.

Two parameters are unknown in this equation, flow rate and pressure. Flow rate can be found by taking the slope of the volumetric solution content (m^3) and time in sec. Pressure, on the other hand, requires utilizing the voltage applied on the cross-section of the specimens. Euler's equation of unsteady flow can be used to determine the pressure. Assuming the potential energy in both cells is equal, Euler's equation can be expressed in terms of kinetic energy as follow:

$$P_2 - P_1 = \Delta P = \Delta x * \rho * a_x \qquad (5\text{-}13)$$

Where ΔP is the difference in pressure between the two cells due to the voltage application, Δx is the distance between the two cells or the height of the specimen, ρ is the density of the solution and equals 1026.8 kg/m^3, and a_x is the local acceleration of fluid in the x-direction.

The acceleration of the fluid in the specimen can be found by estimating the velocity and time relationship. To establish this relationship, the kinetic energy due to the electrical charge should equal the kinetic energy of the moving mass. The mass here is represented by the volumetric solution content with time. The kinetic energy equivalency is expressed as follows:

$$\frac{q(t) * V}{v_s} = \frac{1}{2} m(t) * v^2 \qquad (5\text{-}14)$$

Where q (t) is the adjusted charge passed with time in Coulombs, V is the applied voltage which equals 20 V, v_s is the volume of the specimen, m(t) is the volumetric mass of the solution with time in Kg/m^3, v is the velocity in m/s. Eq. (5-14) can further be simplified in terms of velocity with time as:

$$v(t) = \sqrt{\frac{2\, q(t) * V}{m(t) * v_s}} \qquad (5\text{-}15)$$

In Eq (5-15), velocity can be calculated for each q and m value, which facilitates drawing a velocity vs. time relationship. Figure 5.6 shows the velocity vs. time relationship for LL and UL aggregate gradation. As shown in the figure, the slope (i.e., the acceleration) is the same for both aggregate gradations, which reflects the constant voltage current applied during the test. Taking the first derivative of each equation yields a constant acceleration of 0.0305 m/sec^2. This acceleration can consequently be used in Euler's equation to estimate a pressure of 1.59 N associated with the constant voltage of 20 V.

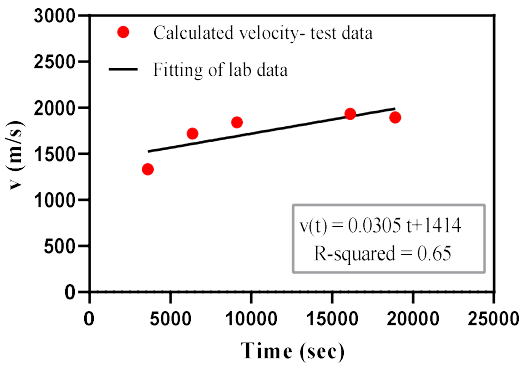

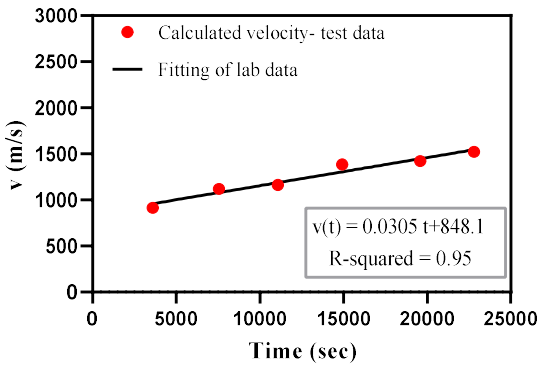

(a) LL aggregate gradation (b) UL aggregate gradation

Figure 5.6 Velocity vs. Time relationship for control LL and UL aggregate gradation samples

By determining the pressure, Eq. (5-12) was used to estimate the permeability coefficients for each tested specimen. Figure 5.7 shows the permeability coefficient of each specimen and summarize the difference in permeability between the two-aggregate gradation. As shown, the permeability coefficient for each aggregate gradation is in the magnitude of 10^{-6}. This indicates either the permeability nature of RCC specimens or/and the improper compaction effort of RCC specimens. It also explains the inability to perform the test at a higher voltage due to the high current reading. However, based on the results, it is clear the difference between LL and UL aggregate gradations is significant. The LL aggregate gradation specimens have three times higher permeability coefficients compared to the UL aggregate gradation.

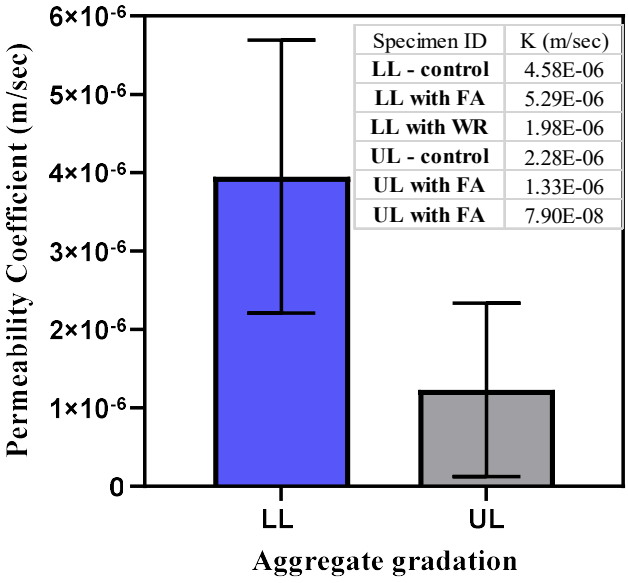

Figure 5.7 Permeability coefficient for LL and UL aggregate gradation

5.5.3. Charge Passed vs. Volumetric Content of Solution

Figure 5.8 shows the fitting of the Proove'it output for the cumulative adjusted charge passed in the control LL and UL specimens. The cumulative number of charges passed was used in this work because the machine was stopped and re-run whenever the TDR measurement was taken. As shown in Figure 5.8, the relationship between the charge passed, and the volumetric content of the solution is linear. The main difference between the two specimens is exhibited in the value of the charge passed, where UL aggregate gradation has a much lower charge passed over the course of the test while LL aggregate gradation has almost three times as much charge passed by the end of the test. Table 5.3 shows the slope and y-intercept for each tested specimen. These equations can be used to evaluate the permeability of tested specimens as well as calculate the amount of solution associated with critical permeability levels established in ASTM C1202.

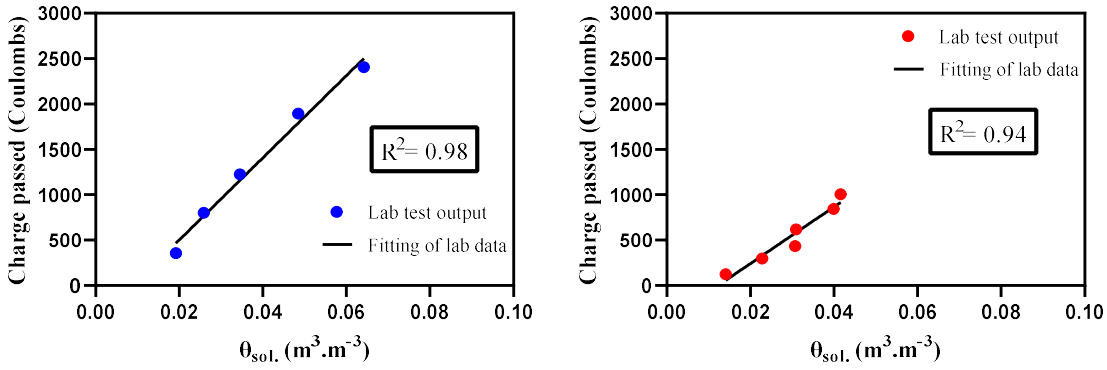

(a) LL aggregate gradation (b) UL aggregate gradation

Figure 5.8 Volumetric content of NaCL solution vs. charge passed relationship for LL and UL aggregate gradation- Control Specimens

Table 5.3 Linear fitting parameters for charge passed vs. volumetric content of solution relationship

Specimen	Slope	Y-intercept	R-squared
LL-control	45272	-404	0.98
LL with FA	16625	-168.2	0.94
LL with WR	45641	-186.4	0.91
UL - control	31123	-379.7	0.94
UL with FA	3421	-28.01	0.95
UL with WR	135709	-273.9	0.99

5.6. Conclusions

This effort proposes a new methodology to quantify the volumetric content of NaCl solution ingress in the RCPT. It suggests using TDR traces to obtain dielectric constant and subsequently estimate the volumetric content of NaCl solution. The volumetric content with time was successfully used to relate the charge passed with the volumetric content of NaCl solution as well as estimate the diffusion and permeability coefficients of RCC specimens. The experimental program used two aggregate gradations reflecting the lower and upper limits of specified RCC aggregate gradation. Fly ash and water reducer additives were used in each aggregate gradation to provide replicability and repeatability of test results and validate the proposed methodology. It was found that RCC has diffusion coefficients in the order of 10^{-8} (m^2/sec), while the permeability coefficients are in the order of 10^{-6} (m^2/sec). In general, the diffusion coefficients have a slight difference between the two-aggregate gradation, with LL

aggregate gradation being higher than UL aggregate gradation. This may be related to the level of compaction effort and associated density of tested specimens. On the other hand, permeability coefficients for LL aggregate gradation are three times higher than UL aggregate gradation. Regardless of the aggregate gradation, the control specimen (i.e., RCC specimen with no additives) has higher transport properties values than the specimen with additives.

5.7. References

Whiting D. Rapid determination of the chloride permeability of concrete. Final Report Portland Cement Association. 1981 Aug.

Berman HA, Chaiken B. TECHNIQUES FOR RETARDING THE PENETRATION OF DEICERS INTO CEMENT PASTE AND MORTAR. Public Roads. 1974 Jun;38(1).

Kondo R, Satake M, Ushiyama H. Diffusion of various ions in hardened Portland cement. InThe 28th General Meeting, The Cement Association of Japan, Tokyo 1974 May (pp. 41-43).

Clear KC. Time-to-corrosion of reinforcing steel in concrete slabs. Volume 3: Performance after 830 daily salt applications. 1976 Apr.

Levitt M. Non-destructive testing of concrete by the initial surface absorption method. In Non-destructive testing of concrete and timber 1970 (pp. 23-26). Thomas Telford Publishing.

Figg JW. Methods of measuring the air and water permeability of concrete. Magazine of Concrete Research. 1973 Dec;25(85):213-9.

Ruettgers A, Vidal EN. An investigation of the permeability of mass concrete with particular reference to Boulder Dam. InJournal Proceedings 1935 Mar 1 (Vol. 31, No. 3, pp. 382-416).

Cook HK. Permeability tests of lean mass concrete. *Proc., ASTM,* Vol. 51, 1951

Luping T, Sörensen HE. Evaluation of the rapid test methods for measuring the chloride diffusion coefficients of concrete. Nordtest project 1388-98. 1998.

AASHTO T 277, "Standard Test Method for Electrical Indication of Concrete's Ability to Resist Chloride," American Association of State Highway and Transportation Officials, Washington, DC, 2007, 12 pp.

ASTM C1202-12, "Standard Test Method for Electrical Indication of Concrete's Ability to Resist Chloride Ion Penetration," ASTM International, West Conshohocken, PA, 2012, 8 pp.

Issa IM, Zollinger D, Onifade I., Lytton R, "A Laboratory Approach to Determine RCC Mixture Electrical Characteristics Using a New TDR Interpretation Method". Under consideration, Transportation Research Records, 2021.

Lee SI, Zollinger DG, Lytton RL. Determining moisture content of soil layers with time domain reflectometry and micromechanics. Transportation research record. 2008 Jan;2053(1):30-8.

Avelar Lezama I. Preliminary non-destructive assessment of moisture content, hydration, and dielectric properties of Portland cement concrete (Doctoral dissertation, Texas A&M University).

Chen HJ, Tang CW, Peng HS. Feasibility of utilizing oven-drying test to estimate the durability performance of concrete. Computers & Concrete. 2011 Aug 1;8(4):389-99.

GERMANN INSTRUMENTS. NDT Systems: Bridging NDT Theory and Practice. GERMANN INSTRUMENTS. Catalog NDT, 2014

Issa, MI, Zollinger D., "Modelling Compactibility of RCC Specimens Using the Asphalt Gyratory Compactor". Under review, Construction and building materials, 2021

SooNGSWANG PR, Tia M, Bloomquist DG, Meletiou C, Sessions LM. Efficient test setup for determining the water-permeability of concrete. Transportation research record. 1988;1204:77-82.

Simion AI, Grigoraş CG, Roşu AM, Gavrilă L. Mathematical modelling of density and viscosity of nacl aqueous solutions. Journal of Agroalimentary Processes and Technologies. 2015;21(1):41-52.

6. USING PAVESCAN GPR DATA TO ASSESS FRESH AND HARDENED AIRFIELD CONCRETE PAVEMENTS

6.1. Introduction

GPR provides a non-destructive methodology to assess concrete pavement conditions (Alongi et al. 1982). The main benefit of using the GPR system in evaluating pavement stems from its continuity and flexibility in collecting data. Many researchers use GPR to evaluate pavement surface thickness and to evaluate the physical characteristics of the subsurface materials by collecting continuous pavement profiles (Scullion 1992). In most studies, the air-launched GPR is used as a non-disruptive and time-saving NDT tool to map and assess the overall integrity of the asphalt roadways and determine rehabilitation requirements (Saarenketo and Scullion 2000; Jol 2009; Goulias and Scott 2015; Hong and Chen 2016). The use of GPR in concrete can be hampered by the aggregate size and shape, which affects reflectivity due to the physical properties of the cement-based materials (Guillemoteau et al. 2012; Rasol et al. 2020). This can affect the permittivity of the material and reduce the quality of measurements. Also, since concrete is a non-magnetic material with a relative magnetic permeability of one, the main factor that affects the permittivity of concrete is the moisture content in the concrete pores, which differs with depth. This, along with the absence of a methodology to assess the GPR data for concrete pavements, reduces the reliability of using GPR to characterize concrete materials.

Air-launched GPRs like the PaveScan avoids permittivity variations with depth in concrete pavements by measuring dielectric data only for the top surface of the paved materials. Originally designed to control and assure the quality of asphalt placement, it has been adapted to evaluate only the top surface of concrete pavement, eliminating the need to deal with deeper moisture variations. The relative permittivity of concrete typically varies from about 6 for naturally dry concrete to 12 for saturated concrete (Soutsos et al. 2001, Davis et al. 2003). From the naturally dry surface dielectric reference, the existing concrete surface can be characterized to quantify the distress types and determine the existence of moisture volumetrics inside the concrete pores. The fresh concrete surface can also be evaluated by estimating the volumetrics of water, solids, and air. In both cases, a System Identification (SID) solution (Lytton 1989) is incorporated. However, the state of the concrete material requires different solution procedures. This paper presents different solutions to characterize fresh and hardened airfield concrete pavements using GPR dielectric measurements.

6.2. Research Approach

In this paper, a methodology to characterize the condition of fresh and hardened concrete pavement is proposed. Dielectric data was gathered from a freshly placed concrete pavement section and a hardened concrete pavement section in an airfield in El Paso to develop a methodology to accurately validate the curing effectiveness of a freshly placed concrete pavement as well as to quantify the condition of the pavement surface. To achieve these goals, the following steps are presented in this work:

1. Develop a solution for the dielectric constant to estimate the water, solid, and air voids in fresh concrete.
2. Use the dielectric obtained from the GPR to quantify the volumetric content of the dry surface (i.e., solid and air).
3. Interpret the solutions for fresh and hardened concrete surfaces.

6.2.1. Fresh Concrete Surface Solution

The PaveScan system provides the dielectric constant of the top concrete surface (i.e., the top one inch of the pavement). Using this dielectric can be beneficial, especially as a general means of estimating the volumetric of solid, water, and voids in the fresh concrete. The self-consistent model has been used previously to estimate the volumetrics of the individual concrete components (Lee et al. 2008). The self-consistent model assumes that the composite dielectric constants (ε_c) of a composite material such as concrete vary relative to the individual volume fraction and dielectric of every component. Therefore, a generalization of the self-consistent model can be represented by:

$$\sum_{i=1}^{n} v_i \left(\frac{\varepsilon_i - \varepsilon}{\varepsilon_i + 2\varepsilon} \right) = 0 \qquad (6\text{-}1)$$

Where n is the number of components in a composite material, v_i is the volume fraction of component i ($\sum v_i = 1.0$), ε_i is the dielectric constant of component i, ε is the measured composite dielectric constant

The above equation solves for the individual dielectric constant and volumetrics of each component. In reference (Lee et al. 2008), the dielectric constant is calculated for

each individual concrete constituent (i.e., aggregate, hydrated cement, and unreacted cement) and then uses the calculated dielectrics to estimate the volumetrics of individual components. In this paper, a similar concept is facilitated to identify the volumetrics of fresh concrete surfaces. One difference is presented here by considering three main components in the mix, which are solids (including aggregate, hydrated, and unreacted cement), water, and air.

$$\theta_s \frac{\varepsilon_s - \varepsilon}{\varepsilon_s + 2\varepsilon} + \theta_w \frac{\varepsilon_w - \varepsilon}{\varepsilon_w + 2\varepsilon} + \theta_{Air} \frac{\varepsilon_{air} - \varepsilon}{\varepsilon_{air} + 2\varepsilon} = 0 \qquad (6\text{-}2)$$

Where, θ_s, θ_w, θ_{Air} the volume fractions of solids, water, and air, respectively. ε is the measured composite dielectric constant, ε_s, ε_w, ε_{air} are the dielectric constants of solids, water, and air, respectively. The dielectric constant of air can be taken as 1.0, while the dielectric of water can be assumed at 80. The volume fractions of fresh concrete constituents are either time dependents, such as water and air voids, or fixed as aggregate. The unknowns in Eq.(6-2)(6-2) are θ_w, θ_{Air}, ε_s . The θ_{Air} can be replaced by incorporating the fact that $\sum \theta_i = 1$. Eq. (6-2) can be further simplified as:

$$\theta_s \frac{\varepsilon_s - \varepsilon}{\varepsilon_s + 2\varepsilon} + \theta_w \frac{\varepsilon_w - \varepsilon}{\varepsilon_w + 2\varepsilon} + (1 - \theta_s - \theta_w) \frac{\varepsilon_{air} - \varepsilon}{\varepsilon_{air} + 2\varepsilon} = 0 \qquad (6\text{-}3)$$

The above equation can be solved by the System Identification (SID) method detailed in (Lee et al. 2008). The main concept of the SID method is the iteration around the composite dielectric constant (ε_c) to produce the unknown values (θ_w, ε_s). The

measured volume fractions at each iteration are compared with the measured dielectric constant (ε). The measured dielectric constant here corresponds to the dielectric constant found from the GPR data, while the composite dielectric constant is the dielectric produced at each iteration. In that sense, the SID method conducts the least square method for two parameters at once. Therefore, it used matrix analysis for iteration until it stops whenever the change vector [β] is less than 0.05. The detailed procedure of the matrix analysis and related equations are discussed in reference (Lee et al. 2008). In this paper, an additional constraint was added to the procedure concerning the volumetrics summation. Once the change vector reaches less than 0.05, the following equation will be checked before providing the final solution:

$$\theta_s + \theta_w + \theta_{Air} = 1.0 \qquad (6\text{-}4)$$

The volumetrics of water, solids, and air from the fresh concrete solution can be used to calculate the fresh unit weight as shown in Eq.(6-5). The volumetrics of water can be used to evaluate the moisture evaporation in the newly placed concrete pavement. Knowing the volumetrics of water with time can also be incorporated to develop a relationship that can be used to evaluate the curing effectiveness.

$$\gamma_{FC} = (\theta_s + \theta_w) * G_s * \gamma_w \qquad (6\text{-}5)$$

Where γ_{FC} is the wet unit weight of concrete surface, θ_s is the volumetric of the solids, θ_w is the volumetric of the water and G_s is the specific gravity of the concrete mix measured in the lab using ASTM C 1688, and γ_w is the unit weight of water and equals 62.4 Ib/ft^3.

6.2.2. Dry Concrete Surface Solution

For the dry concrete surface solution, the GPR can be used to evaluate to the first order the surface condition of concrete pavement. Knowing the dielectric constant with distance, the volumetric of voids, the dielectric, and the volumetric of solids can be obtained using the self-consistent model discussed earlier. However, Eq.(6-2) can further be simplified by omitting the moisture component as follows:

$$\theta_s \frac{\varepsilon_s - \varepsilon}{\varepsilon_s + 2\varepsilon} + \theta_{void} \frac{\varepsilon_{void} - \varepsilon}{\varepsilon_{void} + 2\varepsilon} = 0 \qquad (6\text{-}6)$$

Where θ_s and θ_{void} are the volume fractions of solids and voids, respectively. ε is the measured composite dielectric constant, ε_s, ε_{void} are the dielectric constants of solids and voids, respectively. The dielectric constant of the void can be taken as 1.0. Therefore, the unknowns in Eq. (6-6) are θ_s, θ_{void}, and $\boldsymbol{\varepsilon_s}$.

Eq. (6-6) can be solved by the System Identification (SID) method. The SID method iterates around the measured composite dielectric constant (ε) to produce the unknown values of θ_s, θ_{void}, and ε_s and compare the resulting values at each iteration with the measured dielectric constant (ε). The measured dielectric constant here corresponds to the dielectric constant found from the GPR data collection, while the composite dielectric constant is the calculated dielectric at each iteration. Once the change vector reaches less than 0.05, another restraint is checked as follow:

$$\theta_s + \theta_{void} = 1.0 \qquad (6\text{-}7)$$

The dielectric constants obtained from the GPR were used to determine the void and solid volume fractions for each dielectric constant. The volume fractions can be used to estimate the dry unit weight of the concrete surface by the following equation:

$$\gamma_{CS} = (\theta_s) * G_s * \gamma_w \quad (6\text{-}8)$$

Where γ_{CS} is the dry unit weight of concrete surface, θ_s is the volumetric of the solids, and G_s is the specific gravity of the concrete mix measured in the lab using ASTM C 1688, and γ_w is the unit weight of water and equals 62.4 Ib/ft^3.

6.3. Results and Discussion

In this study, dielectric constants were collected with GPR over a concrete pavement surface in Fort Bliss, El Paso. Two sections were considered in this study. The first section is a freshly poured concrete pavement, and the second is a two-years-old pavement section. The GPR data were collected for the fresh concrete at the edge of the pavement once the concrete was placed and cured for four days to conclude about the effectiveness of the curing. The data were also collected in the middle of a 2-years old pavement lane to evaluate the condition of the existing pavement surface. It was found that the main distress in the existing pavement surface is the cracking or/and scaling both in low severity levels.

6.3.1. Fresh Concrete Surface- Dielectric Solution

The wet surface solution is used to determine the effect of curing on a freshly placed concrete pavement. The solution for this case is dedicated to the water content, which has a high dielectric constant. In this part, Eq.(6-3) is used to calculate the dielectric of solids and the volumetrics of the water, air, and solid at the edge of the placed pavement over four days. The collected data was determined for the same pavement during the first three days, while the fourth data set was taken from a different section (placed four days earlier) with the same mix design. In this analysis, the first 100

ft of the pavement was considered. As shown in Figure 6.1(a), the dielectric constant ranges from around 15 on the first day to around seven on the fourth day. In Figure 6.1(b), the volumetric of water represents the total water volumetric, including the chemically and physically bounded water as well as the free water. The volumetric of water tends to replicate the dielectric constant in Figure 6.1(a) because water is the most significant constituent in the fresh concrete mix due to its high dielectric constant compared to other constituents. Figure 6.1 (c) shows the variation of wet unit weight with time. The wet unit weight was found by calculating the summation of solid and water volumetrics, which can be multiplied by the bulk specific gravity of the concrete mix and the unit weight of water to find the unit weight. As shown in the figure, the fresh unit weight starts at 146 Ib/ft^3 level on the first day and drops to 141 Ib/ft^3 level by the fourth day, which indicates the loss of water content due to hydration and the gradual formation of hydrated cement products.

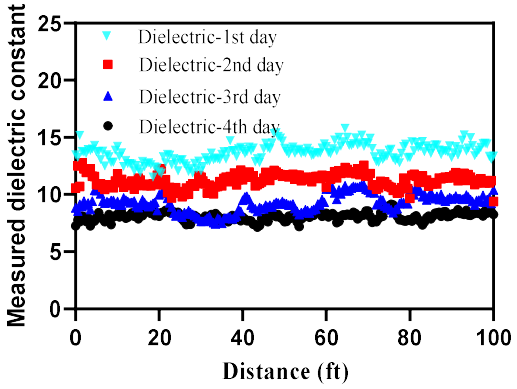

(a) The measured dielectric constant for 100 ft section

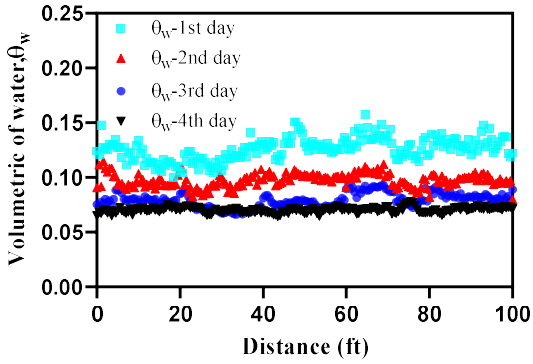

(b) Estimated water volumetrics for 100 ft section

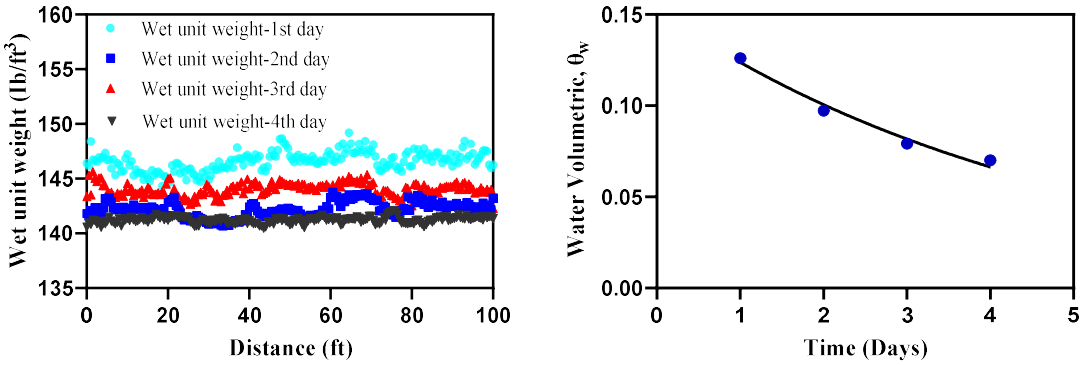

(c) Estimated wet unit weight for 100 ft section

(d) Water reduction vs. time relationship

Figure 6.1 Measured GPR dielectric and related characteristics in the wet concrete surface

Figure 6.1(d) exhibits the relationship between the average water volumetrics with time for the fresh concrete pavement. It shows the average water volumetrics for each day and the fitting of these averages to result in the nonlinear relationship that characterizes the water reduction in a cured pavement surface. Eq. (6-9) shows the relationship between the volumetric of water and time. This relationship can be used to either evaluate the curing quality or/and estimate the reduction of water volumetric at a later age. The water reduction with time can help model the shrinkage in fresh concrete, which is essential to understanding the long-term behavior of concrete pavement.

$$\theta_w = A * e^{-K*t} \qquad (6\text{-}9)$$

Where θ_w is the volumetric of water with time, A is an unknown parameter related to the initial volumetric of water in the concrete mix considering the water loss prior to placement, K is a fitting coefficient depending on the efficiency of the curing

compound, and t is the time in days. In this specific case, A equals 0.1523, K equals 0.2076, with R-squared equals 0.98.

6.3.2. Dry Concrete Surface-Dielectric Solution

The dry concrete surface solution requires first identifying the volumetrics of solid and voids. This solution assumes that the surface of the pavement is naturally dry where the water content does not exist and that dielectric measurements include only solids and voids. It is reported that the naturally dry concrete has a dielectric of around 6 (Davis et al. 2003), which can be assumed as the reference of the dry concrete surface solution. These assumptions are adopted in the existing concrete surface because i) they represent the typical status of a hardened concrete surface, and ii) they help quantify the GPR dielectric by eliminating the water volumetrics.

Figure 6.2 shows the dielectric constant from GPR for a 100 ft section in the longitudinal direction. As shown in Figure 6.2 (a), the measured dielectric constant ranges between 6 and 6.5 with few points lower than 6 to 5. These values present a typical dielectric constant for a dry concrete surface. The sudden decrease in the dielectric at the joints (every 20 ft) or within the slab indicates the existence of "distress" at that specific reading. In general, dielectrics tend to fluctuate at the edge of slabs. Possible reasons for this observation can be:

1. The dielectric is an average of the PaveScan sensor area. Each individual dielectric constant presented in Figure 6.2 is the average of a 19.625 $inch^2$ sensor. Near the transverse joints of the concrete slab, the area of the averaged dielectric

includes concrete and the void of the joint, which has a dielectric of 1 compared to hardened concrete, which can range between 6 to 7.

2. The joints of the slab tend to have more distress due to the environmental stresses (i.e., curling and warping of slabs due to periodic expansion and contraction of slabs) and the inefficiency of joint sealant. These distresses can be represented by voids volumetrics. Having a significantly higher than average dielectric constant means that the voids at the edge are partially filled with water while having a lower-than-average dielectric indicates a joint with air voids.

The dielectric constants were used in the SID solution to calculate the solid and void volumetric for the 100 ft section. Figure 6.2 (b) shows that the solid and void volumetrics is almost constant throughout the analyzed section. It is worth noting that the solid (the blue dots) is constant even with the existence of water inside the air spaces in a hardened concrete surface. On the other hand, the void volumetric (the red dots) represents the air voids inside the concrete as well as the possible material loss in the surface due to cracking or/and scaling.

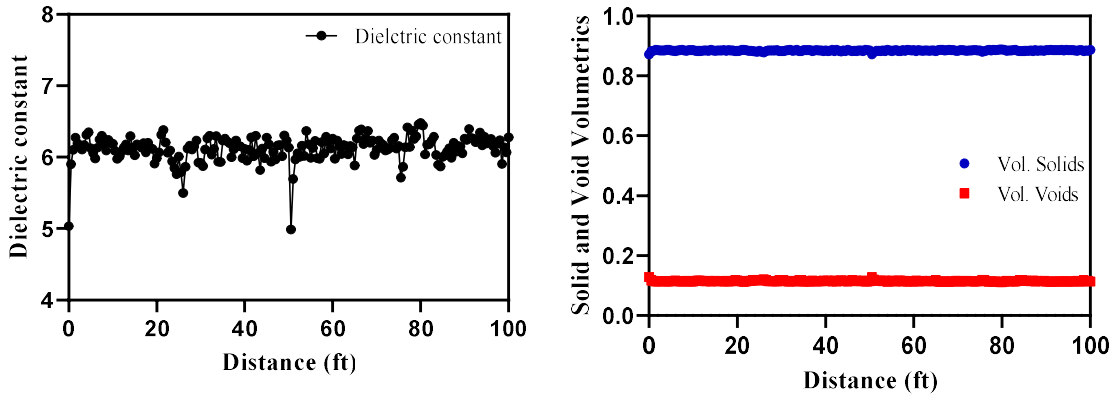

(a) The measured dielectric in the longitudinal direction- 100 ft section

(b) Estimated volumetrics of solids and voids in the longitudinal direction- 100 ft section

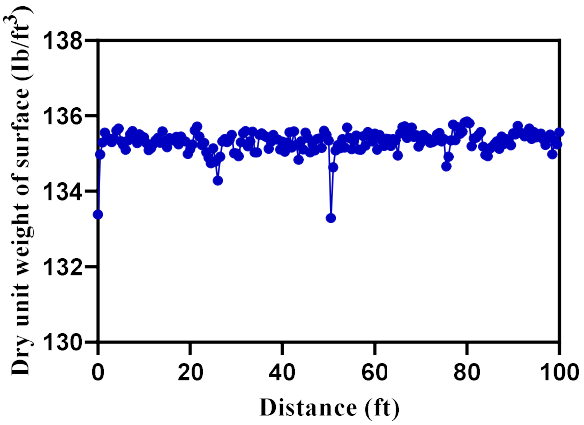

1

(c) Estimated surface dry unit weight - 100 ft section

Figure 6.2 Measured GPR dielectric and related characteristics- dry concrete surface

The calculated solid and voids volumetrics can further be incorporated to estimate the dry unit weight Using Eq.(6-8). Figure 6.2 (c) shows the unit weight-based for the same run. The specific gravity of placed concrete was 2.45, and the unit weight of water was taken as 62.4 Ib/ft^3.

2.1.Consideration of Water in a Dry Surface Solution

In this paper, the dry surface solution of concrete assumes no water content, which allows an accurate determination of the total volumetric of solids and voids. To validate this consideration, the volumetric of water can be estimated using Eq. (6-2).

Using the SID solution for different dielectric values ranging from 2 to 12, Figure 6.3 (a) shows the volumetrics of solids considering the water and void. It is clearly shown that the volumetric of solid is almost constant, especially in the range 2 to 12. This indicates that the dielectric constant change is dominated by the volumetric of water, which has a dielectric of 80. However, the dry surface solution of hardened concrete shows that dielectric increases as the solids increase. The constant dielectric estimation from the wet surface solution also shows that the combined water and air content is constant to around 15% of the total volume fraction, which indicates the dependence of wet surface solution to the water content even at a low dielectric constant. On the other hand, the dry surface solution shows that the low composite dielectric constant is associated with the high void content, while the high composite dielectric constant is related to the low volume of voids and the high volume of solids. In the hardened concrete surface, external water fills out the existing voids. The existing voids depend on many factors, such as material quality, surface finishing, and the loss of material. Considering these differences, it is more reliable to use the dry surface solution even when water exists as it is an actual representation of the volumetric of voids in a naturally hardened concrete surface.

The dry solution does not mean eliminating the existence of water. Instead, the existence of water can be evaluated by estimating the effect of water volumetric on the composite dielectric. The dry volumetric of the void can be used to estimate the total amount of water the surface can hold. To do that, the complex refractive index model

(CRIM) can be used (Lezama 2007). The CRIM model assumes that a linear addition of individual dielectric characteristics is sufficient to estimate the composite dielectric of composite material, as shown in Eq.(6-10). However, it was developed for soil material. Therefore, re-calculating the composite dielectric (i.e., the measured dielectric) using the estimated dry volumetric of solids and voids is required. The main point of re-calculating the composite dielectric constant using the CRIM model is to incrementally consider the volumetric of water and draw a relationship between the difference in composite dielectric constant with the water volumetric in the field. Figure 6.3 (b) shows the difference in the composite dielectric of different volumetrics of water at a composite dielectric of 6. In Figure 6.3 (b), considering only a minimum water volumetric of 0.025 and above is associated with one of the dielectric constants that make up the composite dielectric constants. This means that as long as the measured dielectric constant from GPR is within one dielectric constant from a dry surface dielectric, water volumetric can be negligible in the voids of the hardened concrete surface.

$$\varepsilon^a = \sum_{i}^{n} \theta_i \, \varepsilon_i^a \qquad (6\text{-}10)$$

Where ε is the calculated dielectric constant, a is a power regression coefficient can be assumed 0.5 (for granular material), θ_i is the individual volumetric of considered constituents, and ε_i is the individual dielectric of considered constituents.

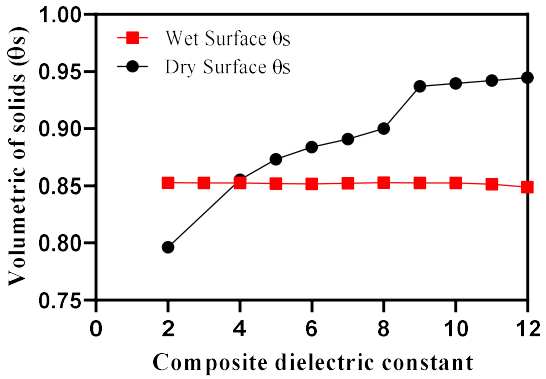

(a) Volumetric of solids from wet and dry surface solutions

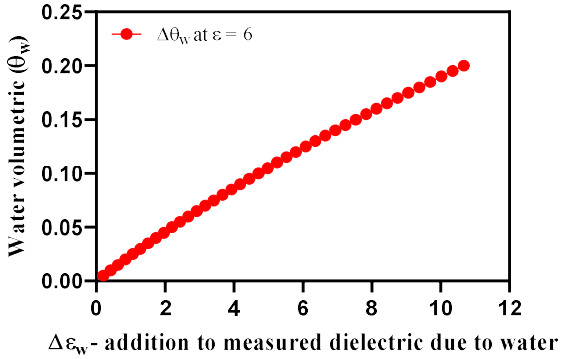

(b) The difference in composite dielectric constant relative to different volumetric of water at composite dielectric of 6

Figure 6.3 Water volumetrics in the dry concrete surface

6.4. Conclusions

This paper develops a new procedure to interpret GPR data for fresh and hardened concrete pavement surfaces. The PaveScan RDM system is extensively used for quality assurance/quality control (QA/QC) of Asphalt concrete pavement surface to check the density. In this paper, the dielectric data was used to evaluate the condition of fresh and hardened airport concrete pavement surface by assessing the effectiveness of the curing in the freshly placed concrete pavement as well as presenting a methodology to evaluate the condition of existing pavement surface by quantifying the scaling and crack width distresses as an example. The following summarizes the finding of this paper.

1. The dielectric GPR data collected from an existing pavement range between 5 and 6 matches the dielectric of the naturally dry concrete surface found in the literature.
2. The GPR dielectric constant can be effectively used to evaluate the surface of concrete pavement. The measured dielectric constants using GPR are associated with the surface layer (the top 1 inch), which can help to evaluate the effect of curing in fresh concrete pavement and estimate the distresses of an existing pavement. This paper provides a procedure to evaluate the volumetrics of solid, water, and voids in fresh concrete as well as solids and voids for hardened concrete.
3. The measured dielectric constant at joints tends to be higher or lower than the average of the collected dielectric. This increase or decrease can be validated through the condition of the concrete in terms of void volumetric, the existence of water, and the quality of densification.
4. The GPR dielectric solution of fresh concrete was successfully used to evaluate the effectiveness of curing after placement. The GPR data shows that the reduction of water volumetric in the surface of the concrete decrease with time and follow an exponential trend. A relationship can be established between the water volumetric and time to estimate water volumetric and estimate the hydration process of placed concrete.

Using GPR to evaluate fresh and hardened concrete pavement conditions can be a flexible and accurate method of quality control for rigid pavements in the field. Besides

evaluating the curing effectiveness and distress quantification, GPR data also can be used to make maintenance and rehabilitation plans. This effort may be further used to study the shrinkage in fresh concrete prior to the application of load and estimate the long-term performance of the pavement. It may also be developed to predict the time needed before an overlay by investigating the relationship between scaling density and the associated scaling thickness. These methods may also be used to assess the condition of joints and to develop timely maintenance and rehabilitation plans.

6.5. References

Alongi, A. V., Cantor, T. R., Kneeter C. P., and Alongi, A. J. (1982). " Concrete evaluation by radar theoretical analysis. " *Transportation Research Record* 853, Transportation Research Board, National Research Council, Washington, D.C., 31-37.

Scullion, T., Lau, C., and Chen, Y. (1992). "Implementation of the Texas ground penetrading radar system." *Report No. FHWA/TX-92/1233-1,* Texas Department of Transportation, Austin, Texas.

T. Saarenketo, T. Scullion, Road evaluation with ground penetrating radar, J. Appl. Geophys. (2000) 119–138, http://dx.doi.org/10.1016/S0926-9851(99) 00052-X.

H.M. Jol, Ground Penetrating Radar Theory and Applications, Elsevier, 2009.

D. Goulias, M.L. Scott, Effective Implementation of Ground Penetrating Radar (GPR) for Condition Assessment & Monitoring of Critical Infrastructure Components of Bridges and Highways, 2015, p. 183.

F. Hong, D. Chen, Evaluation of asphalt overlay permanent deformation based on ground-penetrating radar technology, J. Test. Eval. 44 (2016) 20130241, http://dx.doi.org/10.1520/JTE20130241.

Guillemoteau, J., Bano, M., and Dujardin, J. R, (2012). Influence of grain size, shape and compaction on georadar waves: examples of aeolian dunes. Geophysical Journal International, 190 (3), 1455–1463. doi:10.1111/j. 1365-246X.2012.05577.x.

Rasol et al. 2020.NDT assessment of rigid pavement damages with ground penetrating radar: laboratory and field tests

Soutsos MN, Bungey JH, Millard SG, Shaw MR & Patterson A, "Dielectric properties of concrete and their influence on radar testing", NDT&E International, Vol. 34, 2001, pp 419-425.

J Davis, Y Huang, SG Millard, JH Bungey .”Determination of dielectric properties of insitu concrete at radar frequencies”, Non-Destructive Testing in Civil Engineering (NDT-CE), Vol.8, 2003

Lytton, R. L. Backcalculation of Pavement Layer Properties. In Symposium on Nondestructive Testing of Pavements and Backcalculation of Moduli, Special Technical Publication 1026 (A. J. Bush III and G. Y. Baladi, eds.), ASTM, Philadelphia, Pa., 1989, pp. 7–38

Lee, S., D. G. Zollinger, and R. L. Lytton. Determining Moisture Content of Soil Layers with Time Domain Reflectometry and Micromechanics. In Transportation Research Record: Journal of the Transportation Research Board, No. 2053,

Transportation Research Board of the National Academies, Washington D.C., 2008, pp. 30-38.

Avelar Lezama I. Preliminary Non-Destructive Assessment of Moisture Content, Hydration and Dielectric Properties of Portland Cement Concrete. MS thesis, Texas A&M University, College Station, 2005.

7. A FRAMEWORK TO EVALUATE SHORT- AND LONG-TERM PERFORMANCE OF RCC PAVEMENTS UNDER TRAFFIC LOADS[3]

7.1. Introduction

RCC pavements are prone to issues related to workability, density, and built-in set because of the absence of standards that adequately characterize the mixture consistency before placement operations take place. Issues such as built-in set, in-place density, joint stiffness, and the potential for pavement blow-up can limit the applicability of RCC pavements in a high-speed roadway. Multiple factors affect RCC durability either directly and/or indirectly. The major factors are inherently related to the properties of the RCC mix design and its properties. Therefore, it is significant to research RCC mixture and characterize its behavior under different environments to propose adequate recommendations that can be used in newly designed and constructed RCC pavements. This understanding of RCC pavement behavior can be vital for the popularity and applicability of RCC mixtures in a wider range of routes. In order to achieve this goal, the short- and long-term performance of RCC pavement is vital to evaluate the real effect of RCC's issues on pavement condition under service.

RCC pavement, like concrete pavements, is prone to suffer from environmental and mechanical factors that accelerate the damage of the RCC pavement. Concrete pavements exhibit fatigue failures, including transverse, longitudinal, and corner

---

[3] Part of this paper is preprinted with permission from "Developing a Distress-Based Traffic Equivalency to Efficiently Evaluate the Effect of Traffic Loads on Pavement Performance" by Issa M. Issa and Dan G. Zollinger, 2021, International Journal of Pavement Engineering, pp. 1-9, Copyright [2021] by International Journal of Pavement Engineering. https://doi.org/10.1080/10298436.2021.1952411

cracking, due to the repeated environmental changes under traffic loading (Hiller and Roesler 2005, Ceylan et al. 2016). An additional factor that increases the complexity of understanding the RCC pavements is the level of compaction, which affects the mechanical properties of the RCC (Nader et al. 2003; Nader et al. 2008). Combining the effect of the environmental and mechanical loads with the mechanical properties of the RCC mix seems to be a complicated task to accomplish. Recognizing the importance of environmental load on the performance of the concrete pavements, many practices model the curl and warp behavior under traffic loads (ARA 2004, AASHTO 2008). However, the main issue is with the accurate evaluation of the mechanical properties of RCC specimens, which basically depends on the level of compaction and, most importantly, on the way RCC specimens are fabricated to test their mechanical properties. ASTM C 1435 "Standard Practice for Molding Roller-Compacted Concrete in Cylinder Molds Using a Vibrating Hammer" indicates that vibratory compaction should be applied for each layer of RCC until mortar forms a ring around the total perimeter of the tamping plate or the compaction should be stopped after 20 sec. In that sense, the compaction effort of RCC is subjective, depends on experience, and produces non-uniform compacted specimens, which lead to density variation and subsequently mechanical properties variations.

Nader et al. 2003 studied the mechanical properties of uniformly compacted RCC specimens by using the Asphalt gyratory compactor. Issa and Zollinger 2021 proposed a methodology to evaluate the workability of the RCC in terms of compactibility, which can be used to estimate the energy and level of compaction for

different RCC mixes. Combining both efforts help evaluate the tensile strength of uniformly compacted RCC specimens with time, which can give important input to evaluate the effect of level of compaction on the short- and long-term performance of the RCC pavement.

In this study, a newly developed traffic model proposed in Issa and Zollinger 2021 was used to combine the environmental and mechanical loads along with the mechanical properties of RCC specimens to investigate the effect of all three combined factors on the development of fatigue damage. The traffic model involves the environmental load as constant tensile stress throughout the analysis period, which can reflect the stress variation due to the temperature and moisture gradient as well as existing residual stresses due to material shrinkage. The traffic model also incorporates a model that represents the tensile strength test results to evaluate the effect of compaction level on the performance of the RCC pavement at an early age.

7.2. Research Approach

In this paper, the effect of traffic loads on RCC pavements is characterized through a distress-based equivalency framework to calculate the fatigue ESALs related to the actual damages presented in RCC pavements. This characterization was accomplished via the following tasks:

1. Estimate the tensile strength development at early RCC age (i.e., up to 28 days).
2. Incorporate a neural network tool to automate the stress calculation at critical pavement locations.

3. Consider the tensile strength development to evaluate the damage at an early age and the tensile strength aging to evaluate the long-term performance.

The framework includes testing the RCC specimens for tensile strength. It is well known that the mechanical properties depend mainly on the degree of compaction of the specimens. Therefore, a methodology is consulted in this paper to measure the tensile strength at an early age with time relative to the degree of compaction of RCC specimens (Nader 2003). The long-term age tensile strength (i.e., after 28 days) is evaluated by the aging model presented in the Pavement Mechanistic-Empirical (ME) (ARA 2004).

The short-term performance of RCC pavement is assessed by first establishing a repeatable procedure to measure the tensile strength at different times. The procedure used in this paper incorporates the Asphalt gyratory compactor to achieve a specific compaction effort. The compacted specimens were then tested under splitting tensile strength at different ages up to 28 days. The framework uses the development of tensile strength in the 28 days period to estimate the damage at an early age. In the short-term performance, the traffic equivalency provides the fatigue ESALs per day for 28 days. The long-term performance uses the 28-days tensile strength as a starting point to calculate the fatigue ESALs on a yearly basis. The 28-day tensile strength is also used in a Pavement ME aging model to consider the changes in tensile strength over the analysis period.

It is important for the framework to calculate the stresses of the pavement based on the thickness of the pavement surface. Many stresses can be considered critical for the RCC pavement. Therefore, the location and magnitude of the stresses are evaluated using the finite element program ISLAB 2000 to calculate the stresses for two main loading schemes (i.e., at the edge mid-span and at the joint edge location). The stresses are then automated for different slab thicknesses and joint spacing using the built-in neural network algorithm in MATLAB. The framework provides the ESALs calculations for each stress location so it can be used to determine the damages at critical locations. The allowable fatigue repetitions for RCC specimens are still to be established. However, the fatigue allowable repetition used in the conventional concrete pavement can serve as a starting point for the damage calculations of RCC pavement. The framework allows input of the material properties of the RCC, specifically the tensile strength as a power function. It also allows using different pavement thicknesses, joint spacings, and traffic information as a single input of Average Daily Traffic (ADT) or detailed traffic data including the axle group percent per vehicle classifications $\%AT_{SA}$, $\%AT_{TA,}$ and $\%AT_{Tri,}$ The percent of a truck per vehicle classification and, The axle distribution for each axle group. After inputting this information, the tensile strength properties with time are linked to the ESALs calculations to output the fatigue ESALs at four main pavement locations, discussed later.

7.3. Traffic Model

The traffic model used in this paper is described in detail in (Issa and Zollinger 2021), which considers the distribution and the variance of bin axle weight of the traffic data. The traffic distribution model is expressed by the probability density (%f) and accumulative functions (%F). The traffic model connects the two functions to define relevant traffic factors and relationships. %f and %F functions are presented in terms of the loaded radius with the tire load and inflation pressure. The model computes the number of distress-equivalent 18-kip single axles (ESALs) from a single input of average daily traffic (ADT). It takes the ADT value and calculates predefined axle distribution inputs. The axle distribution is then used to evaluate the incremental increase of weight bin and associated ESALs.

The model computes the number of distress-equivalent 18-kip single axles (ESALs) from inputs of LTPP, or any traffic data elaborated later. In Figure 7.1, three limit ranges refer to the range of truckloads in the load distribution as follows:

- Lower Limit: Lowest truckload
- Upper Limit: legal truckload
- Maximum Limit: Maximum truckload

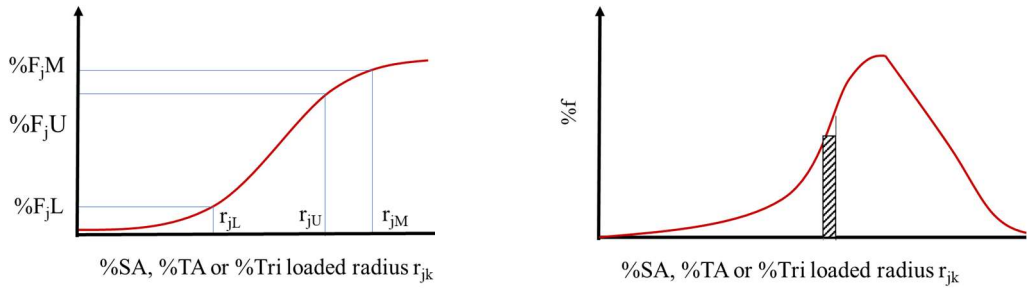

Figure 7.1 Traffic distribution model (Reprinted from Issa and Zollinger 2021).

The average daily truck traffic is found from:

$$ADTT = ADT \cdot \%Trucks \qquad (7\text{-}1)$$

To calculate the ESALs, the truck loading equivalency calculations need to be computed with respect to the mechanism associated with a given distress type. These calculations, shown in Eq.(7-2) below, can be done for any time interval but typically are done on a yearly basis. The term ESALs in the past has been related to pavement roughness or ride. However, distress-based ESAL will be related to a specific distress type such as erosion/faulting, which typically occurs immediately along with the slab/subbase interface. Therefore, Eq. (7-2) can be used to calculate any distress-based ESALs by using the correct form for the EAF_j, and ELF_k.

$$ESAL_i = ADT \cdot \sum_{k=1}^{39} \sum_{j=1}^{3} \left(\left(\%F_{jk+1} - \%F_{jk} \right) \cdot \%AT_j \cdot EAF_j \right) \cdot ELF_k \,.\, GF \qquad (7\text{-}2)$$

Where $\%F_{jk}$ is the accumulative load distribution for j (axle Type = 3) and k (number of bin weights for each axle type), $\%AT_j$ is the percent of axle type (j = 1 to 3), EAF_j is the equivalent axle factor for j, ELF_k is the equivalent load factor with respect to

the single axle, GF is the growth factor which used to calculate the AADTT increase each year and can be identified as no growth, compound or linear.

Using the accumulative function, the equation for the accumulative load distribution ($\%F_{jk}$) can be defined as:

$$\%F_{jk} = a + b\frac{1}{Ln(r_{jk})} + c\frac{1}{r_{jk}}\ , \quad \text{for } r_{jk} > r_L \tag{7-3}$$

$$or$$

$$\%F_{jk} = \left(\frac{P_{jk} - P_{min}}{P_L - P_{min}} \cdot \%F_L\right)\ , \text{ for } r_{jk} \leq r_L \quad 2 \tag{7-4}$$

Where $\%F_{jk}$ is the percent less than the j (axle Type = 3) and k (number of bin weights for each axle type), a, b, and c are coefficients determined from the regression of the load distribution data subsequently explained. r_{jk} is the loaded radius for j and k. r_L is the loaded radius of the minimum axle load in the traffic mix. P_{jk} is the axle load of j and k, P_{min} is the minimum axle load in the traffic mix, P_L is the axle load lower limit of truck loading, $\%F_L$ is the percent less than the lower axle limit, and r_L is the loaded tire radius of the lower axle limit.

The fitting coefficients can be found using the following equations:

$$a_j = \%F_{jL} - b_j\frac{1}{Ln(r_{iL})} - c_j\frac{1}{r_{iL}} \tag{7-5}$$

$$b_j = \frac{\%F_{j(M-L)} - c_{j0}\%F_{j(U-L)}}{a_{j0} - b_{j0}c_{j0}} \tag{7-6}$$

$$c_j = \frac{\%F_{j(U-L)} - b_j b_{j0}}{\frac{1}{r_{jU}} - \frac{1}{r_{jL}}} \tag{7-7}$$

$$a_{j0} = \frac{1}{Ln(r_{jM})} - \frac{1}{Ln(r_{jL})} \tag{7-8}$$

$$b_{j0} = \frac{1}{Ln(r_{jU})} - \frac{1}{Ln(r_{jL})} \tag{7-9}$$

$$c_{j0} = \frac{\frac{1}{(r_{jM})} - \frac{1}{(r_{jL})}}{\frac{1}{(r_{jU})} - \frac{1}{(r_{jL})}} \tag{7-10}$$

$$\%F_{j(M-L)} = \%F_{jM} - \%F_{jL} \tag{7-11}$$

$$\%F_{j(U-L)} = \%F_{jU} - \%F_{jL} \tag{7-12}$$

The shaded area in the density diagram, Figure 7.1, is the incremental change in load distribution with loaded radius, and the difference between any two consecutive weight bins can be calculated as follows:

$$\Delta\%F_j = \left(\%F_{j+1} - \%F_j\right) \tag{7-13}$$

This difference should be taken for any two consecutive loaded radius or weight bins of each axle type. This is useful in the computation of ESAL, where the parameter $\%F_{kl}$ considers traffic load distribution variability between sections.

The proposed traffic model can use different traffic mix details. For the sake of generally evaluating the performance of RCC pavements, a typical axle number and

percent shown in Table 7.1 is used. It is worth noting that to characterize the probability and accumulative functions, a lower, the upper, and maximum truckload should be input. These values can be aligned with the state's legal traffic load to evaluate the effect of overweight traffic fractions on RCC pavement performance. In this paper, the following legal limits were used in all analyses; Single axle: 20,000 Ibs, Tandem axle: 34,000 Ibs, and Tridem axle: 42,000 Ibs.

Table 7.1 Number and ($\%AT_k$) of Different Axles per Truck.

Vehicle Classification (TC)	Number of single axles per truck	Number of Tandem axles per truck	Number of Tridem axles per truck	$\%AT_{SA}$	$\%AT_{TA}$	$\%AT_{Trid}$
4	1.62	0.39	0.00	80.6%	19.4%	0.0%
5	2.00	0.00	0.00	100.0%	0.0%	0.0%
6	1.02	0.99	0.00	50.7%	49.3%	0.0%
7	1.00	0.26	0.83	47.8%	12.4%	39.7%
8	2.38	0.67	0.00	78.0%	22.0%	0.0%
9	1.13	1.93	0.00	36.9%	63.1%	0.0%
10	1.19	1.09	0.89	37.5%	34.4%	28.1%
11	4.29	0.26	0.06	93.1%	5.6%	1.3%
12	3.52	1.14	0.06	74.6%	24.2%	1.3%
13	2.15	2.13	0.35	46.4%	46.0%	7.6%

7.4. Neural Network for Stress Calculations

To automate the calculation of the stresses in rigid pavements, the neural network in MATLAB was used to predict the load-induced stress as a function of the key slab and load parameters. Before using the neural network tool, stresses at different slab locations were calculated for an unbonded pavement structure of different parameters using the ISLAB 2000 finite element program. The analyses were conducted for many

cases based on i) 2 to 20 feet joint spacing range at 2 ft intervals, ii) 6-to-16-inch slab thickness range at 2-inch intervals, and iii) joint load transfer efficiency (LTE) of 1,15, 40, 65, 90, 99 percent

Figure 7.2 shows the analyzed pavement structure. Table 7.2 shows the inputs for the material of the Portland cement concrete (PCC) and the cement-treated base (CTB) throughout the analysis.

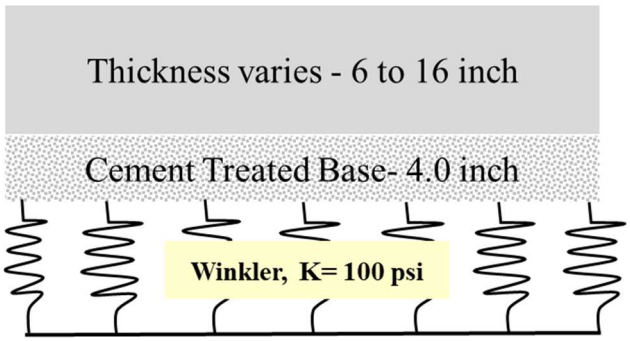

Figure 7.2 ISLAB 2000- pavement structure cross-section

Table 7.2 PCC slab and CTB materials properties

Layer	Parameter	Range
PCC slab	Modulus of elasticity (psi)	5.0×106
	Unit weight(lbs/inch3)	0.0876
	Poisson's ratio	0.15
	Coefficient of thermal expansion (ε/°F)	5.35×10-6
CTB	Modulus of elasticity (psi)	1.0×106
	Unit weight(lbs/inch3)	0.0831
	Poisson's ratio	0.20
	Coefficient of thermal expansion (ε/°F)	4.0×10-6
	Thickness (inch)	4.0

The 18 kips single axle load with a dual tire and defaulted 120 psi tire pressure were used. The configuration of the AASHTO 2002 design was incorporated by i) Average axle width was used 8.5 ft for a typical truck. This distance can be defined as the distance between two outside edges of an axle, and ii) Typical dual tire spacing was taken 12 inches for trucks. Two load positions were studied, which are at the transverse joint and at the mid-slab between two-transverse joints.

For each case, four types of stresses were produced from the ISLAB 2000 analysis. These stresses are the maximum or critical stresses developed in a concrete slab. The critical stresses are the bottom-top transverse crack (SLB), the top longitudinal crack (STT), the bottom longitudinal stress (STB), and the corner stress (SLT). Figure 7.3 shows the considered stress locations. The critical stress was used to calculate the equivalent axle factor (EAF) as well as the equivalent load factor (ELF) shown in Table 7.3. A built-in Shallow Neural Network in Matlab was used to model the stresses based on specific inputs. This neural network fits data by training a two-layer feed-forward network with a sigmoid transfer function hidden layer and a linear transfer function output layer. The number of neurons in the hidden layer is set to 10 by default; however, it can be increased based on the network training results. The Levenberg-Marquardt algorithm is the default algorithm in this toolbox for training data, and the model's performance is measured by the mean squared error. Once the dataset has been trained, it will continue until the validation error fails to converge for six iterations, indicating that the training data has been verified and can be used to predict with high confidence. To estimate stresses using the neural network algorithm, only joint spacing and radius of

relative stiffness are required. The load transfer efficiency is another input that can change, but it was taken 100 in the presented analysis.

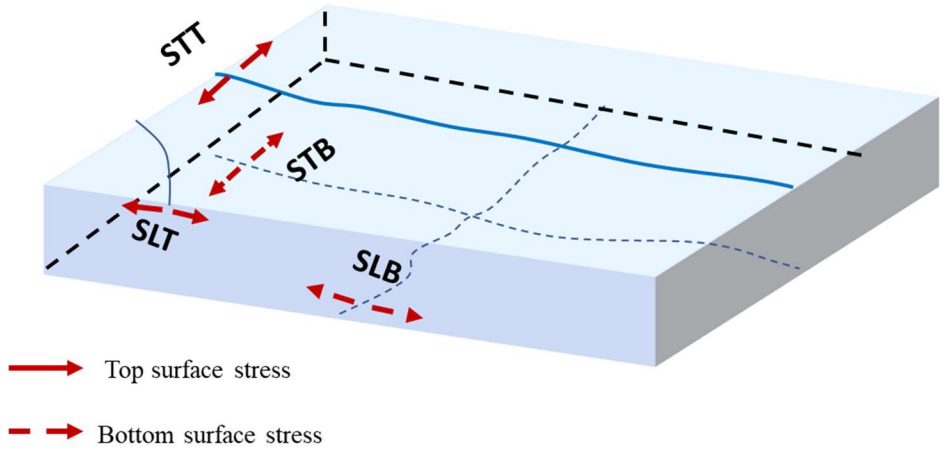

Figure 7.3 Typical ISLAB 2000 stress outputs

Table 7.3 Traffic Equivalency Factors (Adapted from Issa and Zollinger 2021)

Equivalency Factor	Fatigue-based Damage	Erosion-based Damage
ELF	SA: $10^{-17.61(R_{18kip\ load} - R_{load})}$ TA: $10^{-17.61(R_{36kip\ load} - R_{load})}$ TR: $10^{-17.61(R_{54kip\ load} - R_{load})}$	SA: $10^{-2.470(R_{18kip\ load} - R_{load})}$ TA: $10^{-2.470(R_{36kip\ load} - R_{load})}$ TR: $10^{-2.470(R_{54kip\ load} - R_{load})}$
EAF	SA: 1 TA: $10^{-17.61(R_{SA} - R_{TA})}$ TR: $10^{-17.61(R_{SA} - R_{TR})}$	SA: 1 TA: $10^{-2.470(R_{SA} - R_{TA})}$ TR: $10^{-2.470(R_{SA} - R_{TR})}$

7.5. Tensile Strength of RCC Specimens

The tensile strength of RCC specimens is dictated by the compaction degree of the RCC specimen. ASTM C1435 provides a procedure to fabricate RCC specimens which includes using a vibratory compactor to compact specimens in 5 layers for the

6x12 inch specimen or 3 layers for 4x8 inch specimens. The specification and duration of vibratory compaction are limited to achieving the full compaction. The ASTM provides subjective measures to judge achieving the required compaction level. The use of the Superpave gyratory compactor presents an effective tool to control the compactibility of RCC specimens (Nader et al. 2003, Issa and Zollinger 2021; Shabani et al. 2021). Using the Superpave gyratory compactor for RCC requires compacting the RCC material in a smaller size compared to the ASTM C1435 specimens. However, modification factors can be used to estimate the equivalent standard tensile strength. In this paper, 4500 grams of RCC mix is used to fabricate the tensile strength specimens. Using the mentioned weight of the RCC mix results in fabricated specimens of 6 inches in diameter and height of 4.15 to 4.9 inches, depending on the compactibility of the RCC mix (Issa and Zollinger 2021). Based on a previous study on compactibility by Issa and Zollinger 2021, 25 gyrations of asphalt gyratory compaction are enough to produce the nearest specimen height associated with the maximum dry density of the RCC mix. After testing the specimens, the maximum load resulting in the splitting tensile strength test will be used to calculate the tensile strength of the specimens with different heights and associated compaction levels.

7.5.1. Material and specimen preparation

In this work, the upper and lower specified RCC aggregate gradation is considered. The RCC mix design requires using the soil compaction design method, which requires initiating trial mixes at different water percentages to evaluate the maximum dry density and optimum moisture content. The mix design and procedure

outlined in (Issa and Zollinger 2021) are incorporated to measure tensile strength at 1, 3, 7, 14, 21, and 28 days. For the lower limit (LL) aggregate blend, the optimum moisture content is 5.4 %, and the associated maximum dry density is 137.2 lb/ft^3 (2197.73 Kg/m^3). For the upper limit (UL) aggregate gradation, the optimum moisture content is 6.3 %, and the associated dry density of 146.1 lb/ft^3 (2340.30 Kg/m^3).

Two samples per tensile strength testing day were fabricated. For each sample, 4500 grams (9.92 Ibs) of the mixed material was used to fill out the compaction cylinder in order to get a sample thickness of around 4 inches. A total of 12 specimens per aggregate gradation were fabricated for 25 gyrations. After specimen fabrication, the specimens were placed in a 100% RH curing room.

7.5.2. Specimen's testing

Two specimens at each testing day were tested for splitting tensile strength, as shown in Figure 7.4. The ASTM C496/C496M – 17 "Standard Test Method for Splitting Tensile Strength of Cylindrical Concrete Specimens" was followed in this paper to measure the tensile strength of RCC specimens. The splitting tensile strength was considered because the maximum load and specimen dimensions are used in Eq.(7-14) to determine the tensile strength of the RCC of any specimen height.

Figure 7.4 Splitting tensile strength test setup

$$T = \frac{2P}{\pi l d} \qquad (7\text{-}14)$$

Where T is the splitting tensile strength in psi, P is the maximum applied load indicated by the testing machine (Ibf), l is the length or height of the specimen in inches, and d is the diameter of the specimen in inches.

The equation provides the ability to approximate the tensile strength associated with different heights. As RCC materials properties depend on the level of compaction, which subsequently depends on the thickness of the compacted specimens. The maximum load results of the splitting tensile strength test of the fabricated specimens (i.e., for 25 gyrations) can be further used to estimate the tensile strength associated with lower compaction or higher compaction levels. In this paper, the tensile strength of three

compaction levels was investigated. The levels are 90%, 95%, and 100%. The compaction levels are represented with different thicknesses, which is associated with the maximum dry unit weight for the LL and UL RCC mix designs. Therefore, specimen heights of 4.40, 4.65, and 4.90 inches are associated with 100%, 95%, and 90% of LL aggregate gradation, while specimen heights of 4.15, 4.40, and 4.60 are associated with the same compaction levels for the UL aggregate gradation. The calculated values were also adjusted for the aspect ratio of the 6 x 12-inch standard cylinder. A general relationship for the size effect of test specimen on tensile splitting strength is incorporated to standardize the tensile strength of lesser RCC thickness specimens (Kadlecek et al. 2002*)*. The test results for evaluated compaction levels considering the 6 x 12-inch standard cylinder are presented in Figure 7.5.

.

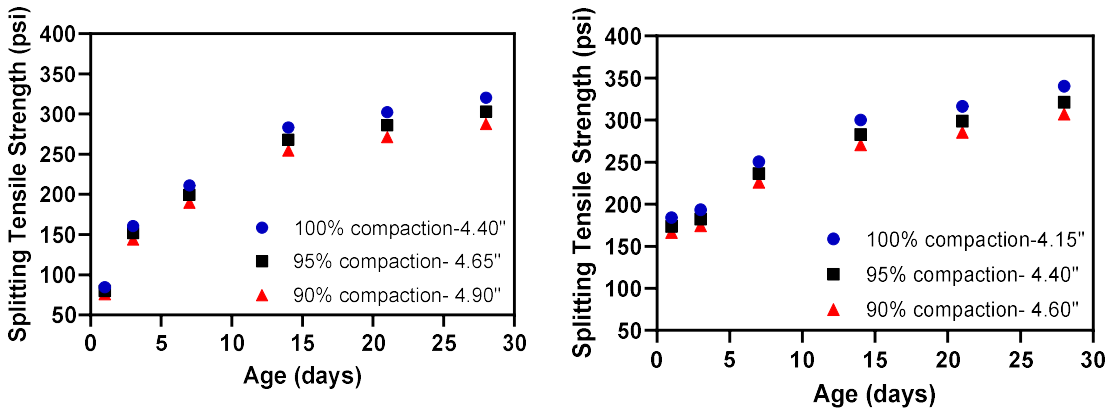

(a) LL aggregate gradation (b) UL aggregate gradation

Figure 7.5 Splitting tensile strength of LL and UL aggregate gradation RCC specimens.

The splitting tensile strength exhibits a power function with time, which means that the test results can be generalized by a power function, presented in eq. (**7-15**), which can help calculate the splitting tensile strength every day up to 28 days. Table 7.4 shows the fitting coefficients for each aggregate gradation and compaction level.

$$T_i = A * t^B \quad (7\text{-}15)$$

Where T is the splitting tensile strength at day i, A is a fitting coefficient, t is the age in days and B is a fitting coefficient.

Table 7.4 Model fitting coefficients for splitting tensile strength calculations

Fitting Coefficient/ compaction level	LL aggregate gradation			UL aggregate gradation		
	90%	95%	100%	90%	95%	100%
A	83.95	88.46	93.49	155.18	162.24	172.01
B	0.395	0.395	0.395	0.20	0.20	0.20
R^2	0.97	0.97	0.97	0.97	0.97	0.97

The splitting tensile model is used in the framework to evaluate the change of tensile strength of the ESALs calculation. Using the developed model in calculations of ESALs, an assumption is that the tensile strength is increasing for 28 days, even under traffic loadings. However, the framework provides the ability to change the tensile strength model coefficients to consider the development of the tensile strength in the field.

7.6. Case study

The developed framework was used to mainly evaluate the performance of different aggregate gradations of RCC mixes. Additionally, secondary parameters were also considered to investigate their effects on different aggregate gradations. The secondary parameters are:

1. The compaction levels. The tensile strength curves were developed for three levels of compaction. The compaction levels are 90%, 95%, and 100%.
2. The environmental stresses. The built-in and cyclic environmental stresses were incorporated into the framework as existing tensile stress. Stresses of 20 psi, 40 psi, 60 psi, and 100 psi were assumed as existing stresses during traffic load application.
3. Pavement thicknesses. The pavement performance was evaluated for 5-, 7-, and 10-inch RCC sections

Figure 7.6 shows the cross-section assumed for the case study and the general inputs used. In this study, predefined traffic distribution is used where only ADT is required. Figure 7.7 shows the predefined traffic load distribution for SA, TA, and Tri axle distribution. For comparison purposes, the legal load was assumed to equal 20,000 Ibs for the SA axle, 34000 for the TA axle, and 42000 for the Tri axle.

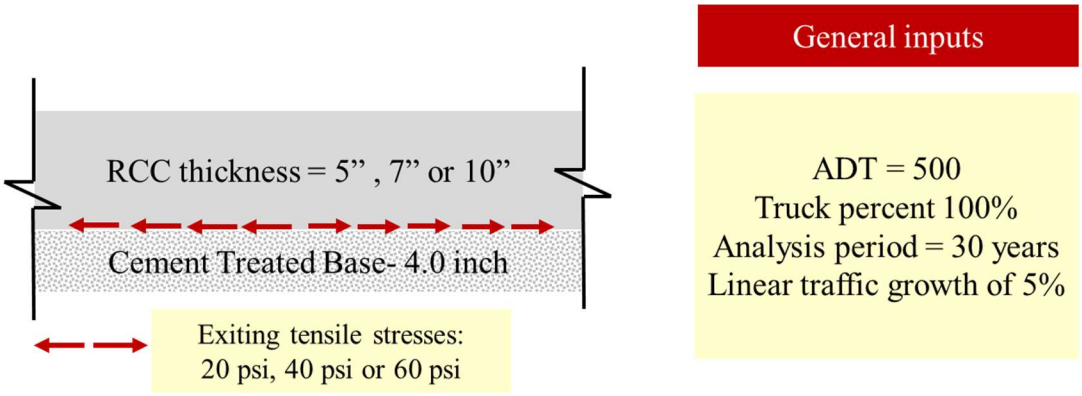

Figure 7.6 Pavement cross-section and general inputs

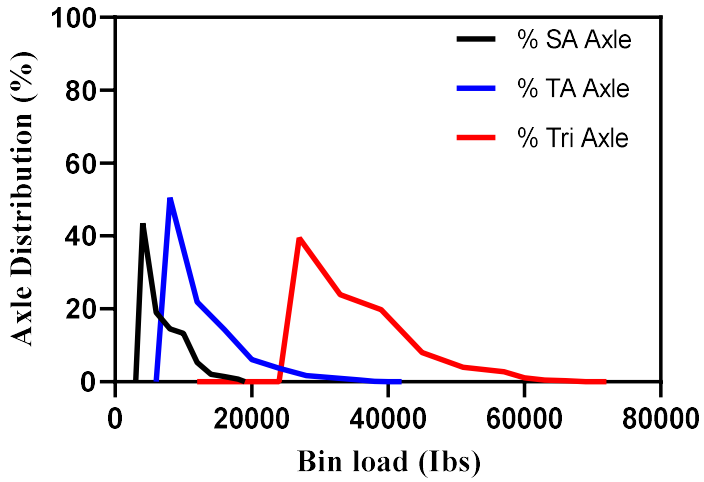

Figure 7.7 Defaulted traffic distribution

The ESALs for different thickness of RCC pavement was calculated at different locations of the pavement. Figure 7.8 shows the ESALs calculation at all critical pavement locations for the 5-inch RCC pavement thickness, with 100% compaction and 0 tensile stress for upper limit aggregate gradation. The results are shown for yearly increments (i.e., for 30 years analysis period). The ESALs calculations for the LL aggregate gradation are approximately the same as the UL aggregate gradation.

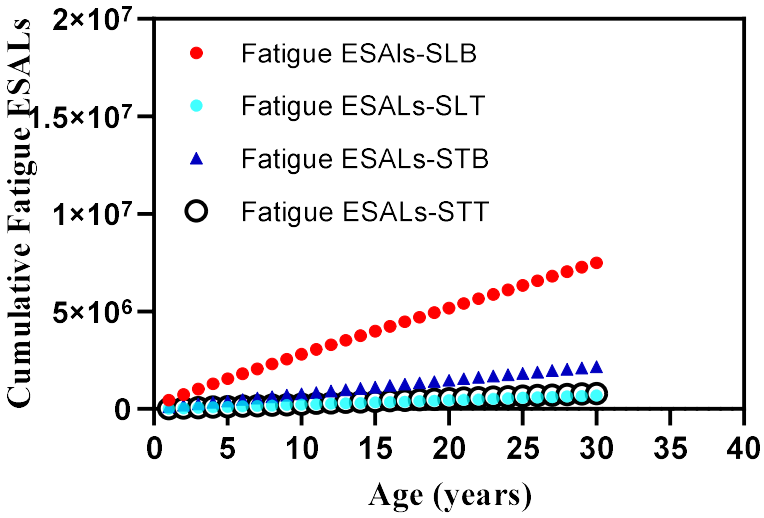

Figure 7.8 ESALs calculations at critical stress locations- upper limit aggregate gradation mix

As shown in Figure 7.8, the ESALs associated with the bottom-up crack are significantly higher than the ESALs associated with other stress locations. Therefore, it is acceptable to consider only the ESALs of the bottom-up cracking (i.e., SLB) to evaluate the performance of RCC pavement. In order to facilitate the comparison between different factors, the allowable fatigue load repetition was used to calculate the damage for different pavement conditions. Knowing the ESALs at a different age, the allowable repetition fatigue load presented for rigid pavement in the mechanistic-empirical design method (ARA 2004) can be used to calculate the damage through the miner's equation of damage. Eq.(7-16) and Eq. (7-17) :

$$D_i = \frac{n_i}{N_f} \tag{7-16}$$

$$N_f = 10^{C_1 * \left(\frac{MR}{\sigma + \sigma_r}\right)^{C_2} + 0.4371} \tag{7-17}$$

Where D_i is the damage at age t, n_i is the ESALs at age t, and N_f is the allowable fatigue repetitions (i.e., ESALs at failure), MOR is the modulus of rapture, σ is the stress, σ_r is the residual environmental stress. c1 and c2 are national calibration coefficients and equals 2 and 1.22, respectively

Based on the damage calculations, Figure 7.9 shows the damage calculated for the 5-inch LL and UL aggregate gradation pavement with 0 curling set stress and 100 % compaction level for the long-term performance.

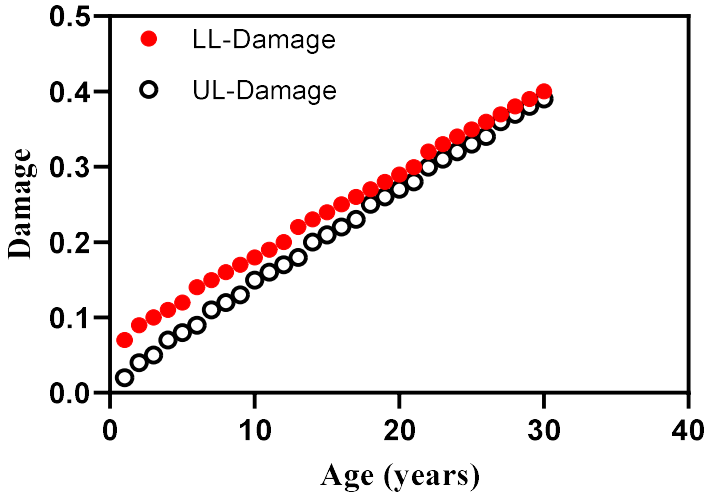

Figure 7.9 Long term damage calculations for pavements with UL and LL aggregate gradation, 5-inch thickness, 100% compaction level, and zero built-in curling stress

7.6.1. Effect of pavement thickness and aggregate gradation

In this study, three thicknesses were studied under the same traffic loading. The short-term damage (i.e., until 28 days) and long-term damage (i.e., for 30 years analysis period) was calculated in the pavement with different thicknesses. Figure 7.10 (a) shows

the short-term damage of the pavement with different thicknesses at built-in curling stress of 0 and 100 % compaction. As shown in the figure, the short-term pavement performance depends on the aggregate gradation. The damage is in the order of 10^{-2}, while the damage of 5-inch pavements with LL aggregate gradation is approximately 8 times higher than damage in 5- inch pavements with UL aggregate gradation. Figure 7.10 (b) and (c) show the long-term damage calculations for 7- and 10-inches pavement thicknesses, respectively. As shown in the figures, the damages for 7- and 10-inches pavement thickness with different aggregate gradations are almost the same with slight differences over the analysis period. Considering both short- and long-term performances of pavements with different thicknesses, the main difference in short- and long-term pavement performance is presented only in 5-inch pavement thickness. As shown in Figure 7.9, the aggregate gradation affects the long-term performance of the 5-inch pavement, specifically in the early years of the analysis period, but then reaches a comparable damage value by the end of the analysis period (i.e., at 30 years). In the case of 7- and 10-inch pavement, the damages are not significantly different in the short and long term, which can indicate either the ability of pavement thickness to reduce the impact of aggregate gradation on pavement performance or the inability of considered ADT and associated traffic distribution to induce expected damages.

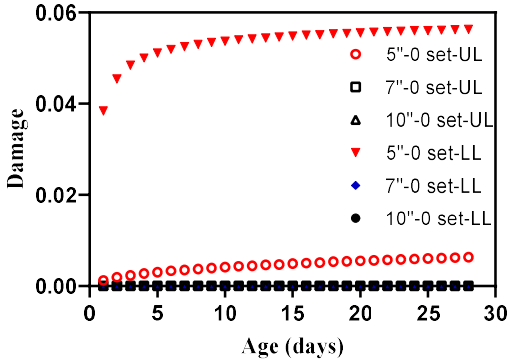

(a) Short term damage per thickness

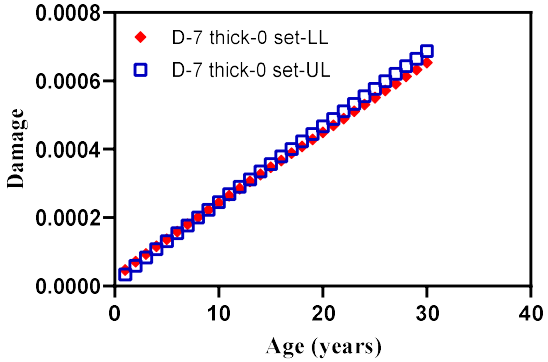

(b) Long term damage for 7-inch pavement thickness and different aggregate gradation

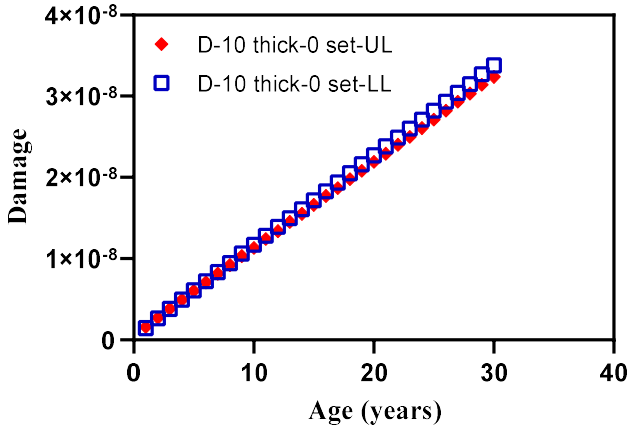

(c) Long term damage for 10-inch pavement thickness and different aggregate gradation

Figure 7.10 Short- and long-term damage calculations for LL and UL aggregate gradation, 100% compaction level, and zero built-in curling stress

7.6.2. Effect of Compaction level

The compaction of RCC specimens affects their mechanical properties. In this paper, the tensile strength of the RCC specimen was estimated by compacting the RCC specimens using the Asphalt gyratory compactor for a specific level to control the amount of energy applied and hence control the compaction level. The specific level

(within 90% to 100% compaction effort) of compaction and its associated tensile strength was employed to estimate the tensile strength of the RCC specimens in cases of 90%, 95%, and 100% compaction levels. Based on the lab results, the tensile strength tends to follow a power function for the first 28 days. Although it does not reflect the real tensile strength in the field, the idea of incorporating the tensile strength trend as a function in the developed framework provides a flexibility to use any other functions to represent the tensile strength change at an early age (i.e., 28 days) of RCC pavement. For the sake of comparison, this work uses the results obtained from the lab, which indicate an increase in the tensile strength for the first 28 days.

Using the tensile strength function that represents the early age of the RCC specimens, the performance of the RCC pavement in the short term is facilitated and can be studied by estimating the ESALs and their associated fatigue damage. Figure 7.11 shows the damage calculation for different LL RCC pavement thicknesses subjected to different compaction levels. The compaction level of 95% was assumed to represent the mean of the three damage calculations at each age. The error bars represent the damage of the 90% (the higher value) and 100% (the lower value) compaction levels, respectively. As shown in the figure, the error bar ranges are higher in the pavement with a thickness of 5 inches than in pavements with 7 or 10 inches. Also, the error bar ranges decrease as the thickness of the studied RCC pavement increases. This indicates that the damage is not sensitive to the tensile strength variation at higher RCC thicknesses. When comparing the three figures, only the 5-inch RCC pavement thickness shows significant damage compared to the 7 and 10 inches RCC pavement

thickness. As shown in the figure, the damage in the 7-inch pavement thickness is in order of 10^{-5} while it is in the order of 10^{-10} for the pavement with 10-inch thickness with similar materials and compaction level.

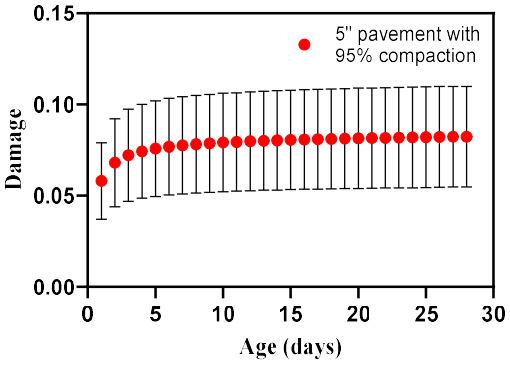

(a) Short term damage for 5-inch pavement at different compaction effort

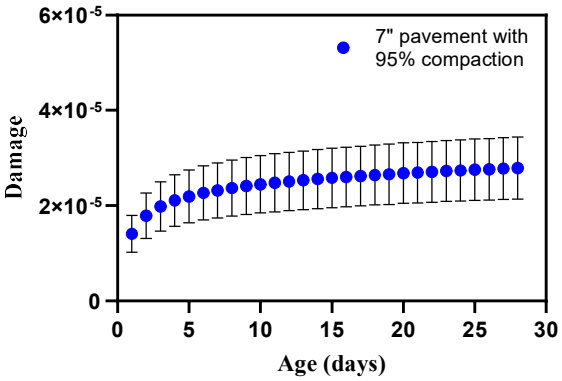

(b) Short term damage for 7-inch pavement at different compaction effort

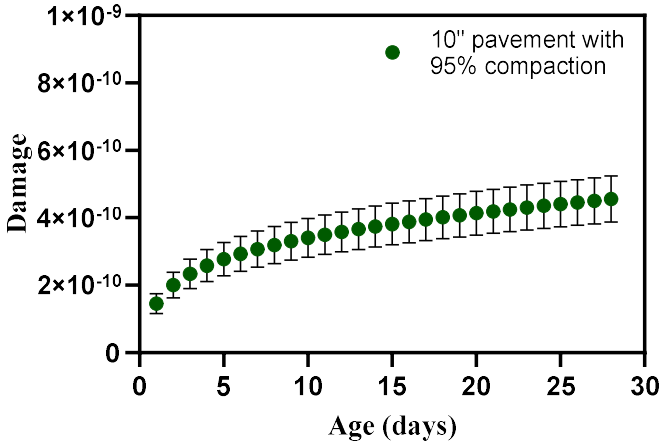

(c) Short term damage for 10-inch pavement at different compaction effort

Figure 7.11 Damage associated with the level of compaction at an early age- LL RCC pavement

7.6.3. Effect of environmental stresses

The environmental stress represents the early age residual stress in the concrete pavement after casting the concrete due to shrinkage of concrete materials. Unlike conventional concrete, RCC is not a saturated mix by means voids are not filled with water prior to and after placement (Issa et al. 2021). These characteristics of the RCC are the source of its dryness which imposes the requirement for compaction to achieve mechanical properties. However, it can be beneficial to reduce the built-in residual tensile stresses developed in the RCC pavement after placement. Environmental stress also includes the temperature and humidity gradient variations throughout the day and the seasons. The effect of environmental stresses (i.e., residual and fluctuating tensile stresses) developed throughout the life of the pavement was evaluated in this paper. It is known that environmental stresses vary in correspondence to weather conditions. However, it can vary within a specific range, especially if there is no special condition(s) that allow the pavement to achieve the theoretical 0 set gradient. Therefore, the built-in residual tensile stresses considered here can be dealt with as the minimum of the environmental tensile stress at any given time. A constant value of environmental stresses was added to the framework to evaluate the effect of existing tensile stresses on the performance of the RCC pavement. Three values were considered besides the 0 psi, which are 20 psi, 40 psi, and 100 psi.

Table 7.5 shows the calculation of damages at the mid-bottom of the concrete slab at 1 day (the age when the pavement is open to traffic), 28 days (the 28 days tensile strength of RCC specimen, which marks the start of the long-term performance), and 30 years (the end of the analysis period). All calculations were made for specimens with

100% compaction level. As shown in the table, residual stresses have a significant impact on the performance of the RCC pavement, especially for RCC pavement with a 5-inch thickness. The damage goes to infinity (i.e., D > 1.0) in 5-inch pavement thicknesses at 30 years, no matter what the aggregate gradation is. On the other side, the UL aggregate gradation mix reduces the effect of residual stresses, which can be seen in the 7-inch RCC pavements where damage reaches 0.1807 after 30 years and a minimum of 100 residual stress. At the specific traffic input studied in this paper, the thickness plays the main factor in reducing the effect of studied residual stresses. This can be shown in all 10-inch RCC pavements. However, aggregate gradation still makes a difference in damage development. Damage for LL aggregate gradation, 10-inch RCC pavement at 30 years is almost ten times higher than UL aggregate gradation, 10-inch RCC pavement.

Table 7.5 Damages associated with different residual tensile stresses

LL aggregate gradation with 100% compaction level									
Residual tensile Stress (psi)	5-inch RCC pavement			7-inch RCC pavement			10-inch RCC pavement		
	1 day	28 day	30 yrs	1 day	28 day	30 yrs	1 day	28 day	30 yrs
0	0.0384	0.056	0.403	1.0E-05	2.2E-05	6.5E-04	1.15E-10	3.8E-10	3.2E-08
20	0.4809	0.653	∞	2.0E-04	3.6E-04	6.5E-03	2.67E-08	7.01E-08	3.7E-06
40	∞	∞	∞	2.9E-03	4.5E-03	4.9E-02	2.2E-06	4.7E-06	0.00015
100	∞	∞	∞	∞	∞	∞	0.0069	0.0117	0.1840
UL aggregate gradation with 100% compaction level									
Residual tensile Stress (psi)	5-inch RCC pavement			7-inch RCC pavement			10-inch RCC pavement		
	1 day	28 day	30 yrs	1 day	28 day	30 yrs	1 day	28 day	30 yrs
0	0.0012	0.006	0.393	7.9E-07	6.0E-06	6.8E-04	1.7E-11	1.9E-10	3.4E-08
20	0.011	0.050	∞	1.1E-05	7.4E-05	6.8E-03	3.0E-09	2.7E-08	3.9E-06
40	0.083	0.333	∞	1.1E-04	6.7E-04	4.9E-02	1.8E-07	1.4E-06	0.00016
100	∞	∞	∞	0.00121	4.7E-03	0.1807	0.0012	0.0059	0.0371

7.6.4. The combined effect of compaction level and residual stress

Environmental stresses combined with mechanical stresses provide an accurate approximation to the performance of the short and long-term RCC pavement. Considering both stresses, the proposed framework model the mechanical properties of the RCC at an early age by testing the tensile strength of RCC specimens. The tensile strength of the specimen depends mainly on the compaction level. Therefore, studying the compaction level with the residual stresses under traffic loading can present the most accurate performance for short and long-term RCC pavement. Table 7.6 and Table 7.7 show the damage calculations when combining the residual environmental stresses,

traffic loads, and mechanical properties of RCC specimens. The tables show the damage after 1 day to indicate the performance of the early age RCC pavements, while damage at 30 years is represented to show the long-term performance of different RCC pavement thicknesses. As shown in both tables, pavements with 0 residual stresses exhibit good performance in early age and long term regardless of the thickness and compaction levels of the RCC pavement. The combined effect of residual stresses and compaction level is prevalent in both cases, with the pavement with LL aggregate gradation exhibiting much more damage compared with the pavement with UL aggregate gradation. At an early age, the damage for the pavement with LL aggregate gradation is close or reaches 1.0 once the residual stress is 20 psi, while the damage is in the range of 0.1 to 0.15 at residual stress of 40 psi for the pavement with UL aggregate gradation.

The long-term performance, the damage reaches infinity for 5-inch pavement at any residual stress value above zero regardless of the aggregate gradation. Aggregate gradation and compaction effort play a role in pavements with higher thicknesses. 7-inch Pavements with LL aggregate gradation show the damage of infinity once the residual stress is 100 psi regardless of the compaction level, while damage in pavements with UL aggregate gradation depends on the level of compaction. The damage reaches infinity when compaction effort is 95% or 90% only, not when compaction level is 100%. The thickness again plays a significant role in lessening the effect of the mechanical properties and the considered environmental stresses. 10-inch thickness pavements show reasonable damage calculations after 30 years. The damages at 30 years show comparable values for the LL and UL aggregate gradation, which support the effect of

thickness in reducing the effect of the mechanical properties of the pavement. On the other hand, thickness has a lower impact on pavement performance than aggregate gradation. The pavements with 100% compaction effort show lower damages compared to other compaction levels, while 90 % and 95 % compaction efforts show slight differences in damage calculations.

Table 7.6 Damage Calculations considering mechanical properties, environmental and traffic stresses- LL aggregate gradation

Damage @ 1 day					
Thickness (inches)	**compaction level (%)**	**Residual stress (psi)**			
		0	**20**	**40**	**100**
5	100	0.0384	0.4809	∞	∞
	95	0.0557	0.7214	∞	∞
	90	0.0801	∞	∞	∞
7	100	1.04E-05	2.04E-04	2.90E-03	∞
	95	1.38E-05	2.79E-04	4.11E-03	∞
	90	1.81E-05	3.79E-04	5.76E-03	∞
10	100	1.15E-10	2.7E-08	2.2E-06	0.00685
	95	1.48E-10	3.4E-08	3.8E-06	0.05313
	90	1.73E-10	4.3E-08	3.8E-06	0.07658
Damage @ 30 years					
Thickness (inches)	**compaction level (%)**	**Residual stress (psi)**			
		0	**20**	**40**	**100**
5	100	0.4034	∞	∞	∞
	95	0.4789	∞	∞	∞
	90	0.5698	∞	∞	∞
7	100	6.54E-04	6.58E-03	4.92E-02	∞
	95	7.24E-04	7.43E-03	5.70E-02	∞
	90	8.01E-04	8.40E-03	6.61E-02	∞
10	100	3.24E-08	3.8E-06	1.57E-04	0.184
	95	3.48E-08	4.1E-06	1.91E-04	0.45264
	90	3.67E-08	4.4E-06	1.91E-04	0.53899

Table 7.7 Damage Calculations considering mechanical properties, environmental and traffic stresses- UL aggregate gradation

Damage @ 1 day					
Thickness (inches)	compaction level (%)	Residual stress (psi)			
		0	20	40	100
5	100	0.0012	0.0113	0.084	∞
	95	0.0016	0.0154	0.117	∞
	90	0.0020	0.0195	0.152	∞
7	100	7.98E-07	1.14E-05	1.18E-04	0.0012
	95	9.83E-07	1.44E-05	1.54E-04	0.053
	90	1.16E-06	1.73E-05	1.89E-04	0.0022
10	100	1.76E-11	2.99E-09	1.80E-07	0.0012
	95	2.05E-11	3.56E-09	2.21E-07	0.0015
	90	2.31E-11	4.095E-09	2.58E-07	0.002
Damage @ 30 years					
Thickness (inches)	compaction level (%)	Residual stress (psi)			
		0	20	40	100
5	100	0.393	∞	∞	∞
	95	0.459	∞	∞	∞
	90	0.518	∞	∞	∞
7	100	6.87E-04	6.85E-03	0.050	0.181
	95	7.64E-04	7.75E-03	0.0575	∞
	90	8.31E-04	8.55E-03	0.0643	∞
10	100	3.38E-08	3.94E-06	1.65E-04	0.371
	95	3.61E-08	4.30E-06	1.83E-04	0.433
	90	3.81E-08	4.60E-06	1.99E-04	0.489

7.7. Conclusions

This paper proposes a framework to evaluate the short- and long-term performance of RCC pavement. The framework studies the short-term performance of RCC pavement by modeling the tensile strength variation in the first 28 days. The framework allows modeling the tensile strength by providing the equation that represents the tensile strength with age. A power relationship was used in this paper to evaluate the

change in tensile strength with time from lab data. This might not be the case for the pavement in the field. However, the framework allows using different relationships to reflect the field case scenario of tensile strength change at an early age.

The long-term performance of RCC pavement was evaluated by considering the compaction level (which affects the mechanical properties) and the environmental load under traffic loading. Environmental stresses and compaction levels significantly accelerate the damage of the RCC pavement, with the environmental stresses having more impact on damage calculations. Also, the aggregate gradation is a key factor affecting the performance of RCC pavement, especially for low RCC pavement thicknesses. The thickness of RCC pavement plays a significant role in reducing the environmental and traffic loadings damage regardless of the aggregate gradation. The thickness also reduces the impact of the compaction level. However, comparing pavement with different compaction levels under similar traffic volume can still show slight differences in RCC pavement damage in the long term. This difference can increase considering high traffic volume or different traffic characteristics.

7.8. References

Issa IM, Zollinger DG. Developing a distress-based traffic equivalency to efficiently evaluate the effect of traffic loads on pavement performance. International Journal of Pavement Engineering. 2021 Jul 15:1-9.

Hiller JE, Roesler JR. Determination of critical concrete pavement fatigue damage locations using influence lines. Journal of Transportation Engineering. 2005 Aug;131(8):599-607.

Ceylan H, Gopalakrishnan K, Kim S, Taylor P, Alhasan AA, Yang S. Impact of curling and warping on concrete pavement.

Amer N, Delatte N, Storey C. Using gyratory compaction to investigate density and mechanical properties of roller-compacted concrete. Transportation research record. 2003;1834(1):77-84.

Amer NH, Storey CS, Delatte NJ. Effect of density on mechanical properties and durability of roller compacted concrete. Portland Cement Association; 2008. Transportation Officials. Mechanistic-empirical pavement design guide: a manual of practice. AASHTO; 2008.

Issa IM, Zollinger DG. Modelling Compactibility of RCC Specimens Using the Asphalt Gyratory Compactor. 2021.

Issa IM, Zollinger DG. Developing a distress-based traffic equivalency to efficiently evaluate the effect of traffic loads on pavement performance. International Journal of Pavement Engineering. 2021 Jul 15:1-9.

Shabani R, Sengun E, Ozturk HI, Alam B, Yaman IO. Superpave Gyratory Compactor as an Alternative Design Method for Roller Compacted Concrete in the Laboratory. Journal of Materials in Civil Engineering. 2021 Jun 1;33(6):04021101.

Kadleček V, Modrý S. Size effect of test specimens on tensile splitting strength of concrete: general relation. Materials and Structures. 2002 Jan;35(1):28-34.

Issa IM, Zollinger DG, Onifade I, Lytton RL "Establish Moisture and Density Profiles In RCC Specimens at Early Age Using TDR Measurements"

ARA (2004). *Guide for Mechanistic-Empirical Design of New and Rehabilitated Pavement Structures*. Transportation Research Board, Washington, D.C.

8. CONCLUSIONS AND FUTURE RESEARCH

8.1. Overview

In 2017, annual federal spending on highways exceeded 45 billion dollars, with almost 50% of this spending directed for planning and executing maintenance and rehabilitation (M&R) plans (Transportation for America 2019). From 2009 and 2017, the percentage of poor condition roadways increase from 14 to 20 percent. On the other hand, and despite $21.4 billion/year of spending on repair between 2009 and 2017, roads in good condition increased only 2% from 36 to 38% (Transportation for America 2019). This can be explained by i) the unsustainability of the asphalt materials used to build roadways, which means that roads were built to be maintained, and ii) the lack of an understanding of the behavior of asphalt pavement to effectively evaluate their performances and develop an accurate M&R plan. In order to increase the pavement with good conditions in the future, concrete pavements should be used as they can last for a long time with minor maintenance activities. However, cost and construction procedures limit its use to specific applications or for projects with high traffic volume. RCC pavement provides the solution to replicate the performance of conventional concrete at a much cheaper cost and with a construction speed that can be compared to the asphalt pavement. However, understanding the RCC pavement behavior is still under study due to the lack of systematic procedures to evaluate the behavior at an early age, the quality control of RCC mixture before and after placement, and the limited understanding of its short- and long-term behavior under combined traffic and environmental conditions.

This study is concerned with developing procedures that can help assess the RCC materials and pavement. It developed a test configuration and interpretation method to use the TDR for RCC material characterization. Using the TDR measurements to estimate RCC properties such as the electrical properties, the density, and free water content with time are developed in this study.

The workability in terms of compactibility of RCC was modeled by considering different aggregate gradation and material additives. The model was also used to calculate the energy required to achieve specified density in the field of different RCC mixture thicknesses, aggregate gradation, and chemical additives.
Furthermore, the transport properties of RCC mixtures with different aggregate gradation and chemical additives were investigated. To achieve this goal, the ASTM standard of using the RCPT test was consulted. A modification is suggested by incorporating the TDR measurements along with the test to evaluate the actual NaCl solution ingress into an oven-dry RCC specimen. The solution ingress with time was a useful relationship that can be used to characterize the permeability and diffusivity coefficients of RCC specimens.

A PaveScan GPR system was used to evaluate the RCC pavement directly after placement. This methodology can be facilitated to estimate the in-place density and suggest further compactions in places where specified density is not achieved. The same instrument was used to evaluate the long-term performance of the concrete pavement by estimating the volumetrics of the surface and tying the measured volumetrics to the commonly existing distress type.

Last but not least, a framework to evaluate the short- and long-term performance of RCC pavement was developed. The development of this framework allows using the detailed traffic load characteristics to estimate the development of the fatigue damage in RCC pavement. The damage in this framework is considered in four critical locations of the RCC slab. The framework considers inputs about the tensile strength development during the first 28 days to estimate the damage in the short term, while the long-term performance is studied considering the tensile strength aging after the 28 days period. In both cases, the degree of compaction, aggregate gradation, and the existence of residual environment stress was combined with traffic loading to study the performance of RCC pavement.

8.2. Conclusions

The following summarizes the key findings based on the results of this study.

1. The TDR test configuration and interpretation method depend on fitting the voltage traces by the transmission line equation. This is a physical solution for the TDR traces that can eliminate the systematic error involved in using empirical models. Also, it can yield important electrical characteristics for the studied composite material. Properties such as conductivity, dielectric constant, and reflectivity can be used in further analysis to estimate important metrics such as the water content, the density of the material, and the ions' transfer and quantification. This procedure allows a wide range of conductive materials to serve as disposable TDR probes and obtain voltage traces for different composite materials.

2. The TDR traces are affected by the aggregate gradation. Upper limit aggregate gradation tends to preserve the moisture longer due to its high fine aggregate content, which reduces the void content compared to the lower limit aggregate gradation that contains a higher percentage of coarse aggregate, which allows faster water loss than upper limit aggregate gradation.
3. The TDR traces are also affected by the curing method. The curing effect is significant regardless of the aggregate gradation, but it is more prevalent in the lower limit aggregate gradation than the upper limit aggregate gradation. The effect of aggregate gradation and curing suggests designing RCC mixtures close to the upper limit aggregate gradation and placing the RCC pavement with a well-developed curing technique.
4. The volumetric content of total water shows that the RCC specimens have a drying front, meaning that water content is the lowest near the exposed surface at all measurement times. The upper limit aggregate gradation seems to hold moisture for a longer period than the lower limit aggregate gradation. Adding curing reduces falling moisture rate during the first 8 hours for the lower limit aggregate gradation while it eliminates the rapid moisture falling in the first 8 hours in the upper limit aggregate gradation, which can be significant to the RCC's early age mechanical properties.
5. The RCC specimens are unsaturated concrete mixes because a minimal amount of free water exists at all depths of the specimen after compaction. The water amount is not enough to fill the void content, which yields to unsaturated mix.

6. The curing and aggregate gradation facilitate producing a uniformly compacted RCC specimen. The effect of both factors is prevalent in RCC with Upper limit aggregate gradation than in RCC with lower limit aggregate gradation.
7. Using the Asphalt Gyratory Compactor helps estimate the damping coefficient of the RCC material to model the compactability of the RCC mixture. The damping coefficient in this study is a representation of the RCC material itself and the amount of energy it can hold. The damping coefficient is higher in specimens with upper limit aggregate gradation than specimens with LL aggregate gradation, which means that specimens with upper limit aggregate gradation have a higher capacity of absorbing energy and therefore obtain greater initial densities at a lower compacting effort.
8. The damping coefficient facilitates the calculation of energy required to obtain the densities of RCC specimens as a percent of the maximum dry density by calculating the volume change of the RCC specimens. In all cases, the energy required to compact RCC specimens is greater in lower limit aggregate gradations than upper limit aggregate gradations.
9. The fly ash and water reducer additives used in both aggregate gradation mixes showed a significant impact on the compactibility of RCC in terms of density and energy level. Specimens with additives achieved higher densities than specimens with no additives at the same gyration number and consequently required a lower energy level to achieve those densities.

10. The RCC specimens have diffusion coefficients in the order of 10^{-8} (m^2/sec), while the permeability coefficients are in the order of 10^{-6} (m^2/sec). In general, the diffusion coefficients of specimens with lower limit aggregate gradation are higher than specimens with upper limit aggregate gradation. This may be related to the level of compaction effort and associated density of tested specimens. On the other hand, permeability coefficients for specimens with lower limit aggregate gradation are three times higher than specimens with upper limit aggregate gradation. Regardless of the aggregate gradation, the control specimen (i.e., RCC specimen with no additives) has higher transport properties values than the specimen with additives.
11. The GPR dielectric constant can be effectively used to evaluate the surface of concrete pavement. The measured dielectric constants using GPR are associated with the surface layer (the top 1 inch), which can help to evaluate the effect of curing in fresh concrete pavement, the density of the concrete surface, and estimate the distresses of an existing pavement.
12. The short-term performance of RCC pavement can be studied f by modeling the tensile strength variation in the first 28 days. The proposed framework allows modeling the tensile strength by providing the equation that represents the tensile strength with age (28 days). Considering the variation in the tensile strength in the first 28 days and the associated damage, the long-term performance of RCC pavement can be evaluated by considering the compaction level (which considers the aggregate gradation and affects the mechanical properties) and the environmental load under traffic loading.

8.3. Future Research

The following are suggestions for future research to facilitate the characterization of the RCC specimens in the lab and predict their performance in the field:

1. Characteristics of the aggregates used in an RCC mixture have a significant effect on the shape of the moisture-density curve, which has an impact on mixture compactibility and finishability as well as the capability to optimize the effective placement of an RCC pavement. This suggests a need for a database that would be useful in the design and specification of 'constructible and cost effective' RCC pavement mixtures. Therefore, the need for research on aggregate characteristics such as angularity, shape, and texture that influence workability is warranted as a means to optimize RCC mixtures with respect to the available aggregate sources.
2. Along with RCC pavement characterization, the durability of joints in jointed concrete pavement, especially in the Midwest, is concerned as it has been a threat to the marketability of concrete pavements. Improving the joint sealant configuration and performance to reduce the tendency to trap water in the joint will allow minimizing the joint failure due to freeze-thaw durability as well as the development of recommendations on the proper application of joint sealant.
3. Evaluate the freshly placed RCC pavement to estimate the density variations with depth and relate it to the permeability and the quality of curing. This aspect includes developing a methodology to determine the dielectric of the RCC at different depths from the surface. It also has implications that involve determining the relationship between the permeability of RCC and the potential of moisture evaporation during

the hydration process, as well as the effect of curing quality to control moisture loss during the 1st drying cycle.

4. Investigate the method of construction by studying the relationship between vertical strain profiles and thermal and moisture properties of the RCC pavement. Also, evaluate the built-in set and shrinkage as well as the curling and warping stresses developed due to the temperature and humidity gradients.
5. Examine the relationship between the durability (freeze-thaw and abrasion resistance) of finishing aids and other RCC surface treatments and the RCC mixture characteristics and/or the type of surface treatment applied during finishing operations.
6. Investigate the curing compound types and rate of application to develop a curing protocol that can be applied on newly placed RCC pavement based on its location and ambient conditions (humidity and temperature).

8.4. References

Repair Priorities, Transportation for America and Taxpayers common sense., 2019. https://t4america.org/maps-tools/repair-priorities/